

INSTABILITY OF NATURAL CONVECTION FLOW
AROUND HORIZONTAL CYLINDERS

A THESIS

Presented to

The Faculty of the Division of Graduate
Studies and Research

By

Kadry A. F. Fathalah


In Partial Fulfillment
of the Requirements for the Degree
Doctor of Philosophy
in the School of Mechanical Engineering


Georgia Institute of Technology

August, 1976


INSTABILITY OF NATURAL CONVECTION FLOW
AROUND HORIZONTAL CYLINDERS


Approved:


K. Hassan, Chairman


L. H. Bangert

P. Durbetaki


P. V. Kadaba


W. O. Winer

Date approved by Chairman: 8-24-76

ACKNOWLEDGMENTS

Special thanks go to the thesis advisor Dr. Kamal Eldin Hassan for his generous contributions of time, and his useful advice, suggestions and discussions during all stages of the research. Thanks are also due the other members of the reading committee: Dr. L. H. Bangert, Dr. P. Durbetaki, Dr. P. V. Kadaba, and Dr. W. O. Winer.

The author is grateful to Dr. Stothe P. Kezios and the School of Mechanical Engineering of Georgia Institute of Technology for financial support of the research.

Thanks are also expressed for the encouragement and support given by the author's wife.

TABLE OF CONTENTS

	Page
ACKNOWLEDGMENTS	ii
LIST OF ILLUSTRATIONS	v
NOMENCLATURE	vii
SUMMARY	xii
Chapter	
I. INTRODUCTION	1
II. LITERATURE REVIEW	4
Analytic Work	
Experimental Work	
III. ANALYSIS	16
Derivation of the Differential Equations Governing Disturbances	
Order of Magnitude Analysis	
Substitution for Disturbance Quantities	
Method of Solution	
The Eigenvalue Problem	
The Asymptotic Solution	
Solution Within the Boundary Layer	
Computational Results	
IV. EXPERIMENTAL APPARATUS	45
Experimental Cylinder	
Hot Wire Probe	
Transverse Mechanism	
Heating Wire	
Enclosure	
Calibration of the Hot Wire Probe	
Temperature Calibration	
Velocity Calibration	
V. EXPERIMENTAL RESULTS	57

TABLE OF CONTENTS (Continued)

	Page
Steady State Measurements	
Local Temperature Measurements	
Velocity Measurements	
Determination of the Neutral Stability Curve	
Hot Wire Response to Small Oscillations	
Results of Stability Measurements	
VI. CONCLUSIONS	71
Proposed Further Work	
APPENDICES	
A. BASIC VELOCITY AND TEMPERATURE PROFILES	73
B. ORDER OF MAGNITUDE ANALYSIS OF TERMS OF THE DISTURBANCE EQUATION	79
C. SOLUTION OF THE ASYMPTOTIC EQUATIONS	83
D. DESIGN OF PROBE	86
E. CORRECTION OF VELOCITY MEASUREMENTS FOR LOCAL TEMPERATURE EFFECTS	91
F. ERROR IN EVALUATING POSITION ANGLES OF POINTS OF NEUTRAL STABILITY	96
G. CORRECTION OF THE DISTURBANCE TEMPERATURE AMPLITUDES FOR CHANGES OF BASIC VELOCITY U WITH STREAMWISE TRAVEL . . .	100
H. HEATING WIRE RESPONSE TO SINUSOIDAL ELECTRIC POWER INPUT	103
I. COMPUTER PROGRAM	107
BIBLIOGRAPHY	116
VITA	120

LIST OF ILLUSTRATIONS

Figure	Page
(2-1) Nachtsheims Neutral Stability Curves	6
(2-2) Calculated Disturbance Amplitude Contours	8
(2-3) Neutral Stability Curve for Flow Adjacent to a Vertical Uniformly Heated Plate	10
(2-4) Comparison Between Results of Haaland and Those of Nachtsheim	11
(3-1) Neutral Stability Curves for Natural Convection Around Horizontal Cylinders	33
(3-2) Neutral Stability Curves for Natural Convection Around Horizontal Cylinders in Air	34
(3-3) Comparison of the Present Results and those of Haaland	35
(3-4) Instability Curves for Horizontal Cylinders	36
(3-5) Instability Curves for Horizontal Cylinders	37
(3-6) Frequency Response of Natural Convection Flow Around Horizontal Cylinders	39
(3-7a) Amplification Rates for Disturbances of Different Frequencies	41
(3-7b) Amplification Rates for Disturbances of Different Frequencies	42
(3-8) Distribution Curve for the Amplitude Ratio \hat{A}/\hat{A}_N at a Position Angle $x^+ = 150^\circ$	43
(4-1) Plan of Cylinder Assembly	47
(4-2) Hot Wire Probe	48
(4-3) Probe Traversing Mechanism	50

LIST OF ILLUSTRATIONS (Continued)

	Page
(4-4) Temperature Calibration of Sensor	53
(4-5) Elevation of Velocity Calibration Apparatus	54
(4-6) Velocity Calibration of Sensor	55
(5-1) Basic Temperature Profiles	60
(5-2) Basic Velocity Profiles	62
(5-3) Temperature Response of Probe	65
(5-4) Relative Amplitude of Temperature Oscillations	67
(5-5) Appearance of Second Harmonics in the Hot Wire Response for Small Frequencies	68
(5-6) Neutral Stability Experimental Points, Compared to Present Analytic Results	70
(E-1) Dimensionless Velocity Calibration Curve and Its Straight Line Approximation	92
(E-2) Correction for Basic Velocity Due to Temperature Variations	95
(G-1) Correction for the Measured Amplitude of Oscillatory Temperature due to Variations in \bar{h}	102

NOMENCLATURE

English
Symbols

a	Thermal diffusivity, m^2/s .
\hat{A}	Area, cm^2 .
A_1, A_2, A_3	Coefficients of second order equation used in least square fitting.
A	Amplitude of an oscillatory quantity.
\bar{c}	Reduced wave velocity, cm.
c	Reduced wave velocity, cm, $c = \bar{c}/U^*$.
$\hat{c}_1, \dots, \hat{c}_8$	Coefficients of the assumed asymptotic solutions.
C_1, C_2, C_3, C_4	Coefficients of the asymptotic solutions.
C	Plate thermal capacity.
C_p	Specific heat, Ws/KgC .
d	Probe or heating wire diameter, μ .
D	Cylinder diameter, cm.
E	Anemometer or heating wire voltage, volt.
\bar{E}	Mean value of the wire voltage, volt.
\tilde{e}	Oscillatory voltage component, volt.
$F(\eta)$	Dimensionless normal component of basic velocity.
$f(x^+)$	Function defined by Hermann and by equation (A-18).
\hat{f}	Frequency, Hertz.
\mathcal{F}	Correction factor for \bar{E} , given by equation (E-7).
$g(x^+)$	Function defined by Hermann and by equation (A-19).

\hat{g}	Gravitation acceleration, cm^2/s .
G	Instability parameter, defined by $G = f(x^+) N_{Gr,r}^{1/4}$, dimensionless
h	Heat transfer coefficient, $\text{W}/\text{m}^2\text{C}$.
\bar{h}	Mean value of the heat transfer coefficient, $\text{W}/\text{m}^2\text{C}$.
\tilde{h}	Oscillatory part of the heat transfer coefficient, $\text{W}/\text{m}^2\text{C}$.
$H(\eta)$	Dimensionless basic temperature difference
k	Thermal conductivity, $\text{W}/\text{m C}$.
l	Variable distance on the wire sensor, measured from the wire support, mm.
L	Physical length, or wave length.
M	Frequency response parameter, defined by $M = 4h/\rho C_p d, s^{-1}$.
n	Normal distance from the cylinder, cm.
N_{Bi}	Biot number, defined by hd/k .
N_{Gr}	Grashof number, defined by $\hat{g}\beta\Delta T d^3/\nu^2$.
$N_{Gr,r}$	Grashof number defined by $\hat{g}\beta\Delta T r^3/\nu^2$.
N_{Nu}	Nusselt number, defined by hL/k .
N_{Pr}	Prandtl number
N_{Re}	Reynolds number, defined by ud/ν .
\hat{p}	Perimeter, cm.
p^*	Dynamic total pressure, $\text{Newton}/\text{cm}^2$.
P	Mean value of the dynamic pressure, $\text{Newton}/\text{cm}^2$.
\tilde{p}	Disturbance component of the pressure, $\text{Newton}/\text{cm}^2$
\hat{q}	Volumetric rate of heat generation, W/m^3 .
Q^*	Relative thermal capacity factor, defined by $Q^* = (\hat{C}/A)/\rho C_p \delta$.
\hat{r}	Radian coordinate.
r	Cylinder radius, cm.

R	Electric resistance, ohm.
S	Tangential distance over the circumference of the cylinder, measured from the lower stagnation point.
t	Time, S.
T	Temperature, C
u	Tangential velocity component, cm/s
U	Basic tangential velocity component, cm/s.
\tilde{u}	Disturbed tangential velocity component, cm/s.
$U^*(x^+)$	Function defined by $U^* = fg$
v	Normal velocity component, cm/s.
V	Basic normal velocity component, cm/s.
\tilde{v}	Disturbance normal velocity component, cm/s.
x	Position angle, measured from the lower stagnation radius, rad.
y	Reduced normal distance, $y = n/r$.
Greek Symbols	
$\bar{\alpha}$	Wave number, cm^{-1} .
α	Dimensionless wave number.
$\alpha_1, \alpha_2, \alpha_3, \alpha_4$	Correction factors for R_w , $(40 + R_w)$, k , v due to variation in temperature, dimensionless.
$\bar{\beta}$	Dimensionless frequency
β	Dimensionless frequency, $\beta = \bar{\beta} \delta / U^*$.
$\hat{\beta}$	Coefficient of thermal expansion C^{-1} .
$\hat{\gamma}_1, \dots, \hat{\gamma}_6$	Roots of auxiliary equations, equations (C-3 and 5).
$\gamma_1, \gamma_2, \gamma_3$	Roots of auxiliary equations, having negative real parts.
δ	Boundary layer thickness, dimensionless.
ϵ	Small error.

$\zeta, \bar{\zeta}$	Amplitude of temperature oscillations, $\zeta = \bar{\zeta}$, dimensionless.
$\zeta_I, \zeta_{II}, \zeta_{III}$	Asymptotic solutions for ζ .
η	Dimensionless normal distance.
θ	Temperature difference, C.
Θ	Basic temperature difference, C.
$\bar{\Theta}$	Temperature difference between the hot wire and the surrounding air, C.
$\tilde{\theta}$	Oscillatory temperature difference, C.
θ^*	Dimensionless temperature oscillations.
ν	Kinematic viscosity, m^2/s .
ξ	Dimensionless tangential distance, $\xi = x/\delta$.
ρ	Density Kg/m^3 .
σ	Reduced frequency, dimensionless
$\bar{\tau}$	Reduced time, $\bar{\tau} = t\nu/r^2$, dimensionless.
τ	Reduced time, $\tau = \bar{\tau}U^*/\tau\delta$, dimensionless.
$\bar{\phi}$	Amplitude of normal disturbance velocity, dimensionless
ϕ	Amplitude of normal disturbance velocity, $\phi = \bar{\phi}/\delta U^*$, dimensionless.
$\phi_I, \phi_{II}, \phi_{III}$	Asymptotic solutions for ϕ .
Φ	Position angle, defined by $\Phi = x - 90$, degrees.
ψ	Mean stream function, dimensionless.
$\tilde{\psi}$	Disturbance stream function, m^2/s .
ψ^*	Reduced disturbance stream function, $\psi^* = \psi^*/y$, dimensionless.
ω	Angular velocity, rad./s.
\approx	Of order of.

Superscripts

\sim	Disturbance quantity.
$'$	Differentiation with respect to η .
$+$	Designates the coordinates associated with a basic quantity.

Subscripts

a	Air.
A	Amplitude of a disturbance quantity.
c	Cylinder.
e	Edge of the boundary layer, or experimental value of.
i	Imaginary part.
m	Means.
N	Points of neutral stability.
n, \hat{r}, s, x, y	Differentiation with respect to these quantities.
0	At reference or calibration conditions.
r	Real part.
w	Wire.
∞	Far from the cylinder.

SUMMARY

The coupled Orr-Sommerfeld equations for natural convection flow around horizontal cylinders are derived and solved for air for Grashof numbers up to 4×10^9 , with the neutral stability curves determined. The favorite frequency band which the fluid amplifies most was found to vary, with variation of the total Grashof number, the cylinder radius, and the kinematic viscosity ν .

Experiments were carried out to check the analysis. A hot wire sensor was used to measure the basic temperature and velocity profiles. It was also used to detect temperature oscillations induced in the boundary layer. Neutral stability points were determined for different frequencies and found to agree well with the analytic results.

CHAPTER I

INTRODUCTION

The problem of natural convection is one of the oldest in heat transfer. Work was done to determine the local and average heat transfer coefficients, the temperature and velocity profiles, and to study the flow instability.

In the case of vertical and inclined plates, these three sides of the problem are well covered in literature. For horizontal cylinders, the only works available are those carried out to determine the velocity and temperature profiles, and the local and average heat transfer coefficients. Earliest experiments are those of Jodlbauer [42],* while the earliest analysis was that of Hermann [16]. More recent analyses were carried out using Blasius series by Chiang and Kaye [43], Saville and Churchill [44] and Lin and Chao [45]. This latter method did not improve on Hermann's results; however, it is more suited to some of the more complicated problems where the surface is non-isothermal, or of a more complicated geometry.

Instability of natural convection flow around horizontal cylinders does not seem to have been studied before, it is studied here both analytically and experimentally.

In the present analysis, the coupled Orr-Sommerfeld differential equations that govern small disturbances in velocity and temperature were derived, assuming the disturbances to be two-dimensional. These equations were solved by the method devised by Kaplan [22] and Mach [29]. The solution

*References are listed in the Bibliography.

revealed information about the behaviour of a disturbance of certain frequency as it travels streamwise. Points where the amplitude of a disturbance attains its minimum value were determined; they designate locations where the disturbances neither amplify nor dampen with infinitesimal streamwise travel. These are the neutral stability points and their locus at various frequencies is the neutral stability curve. The importance of this curve is that it gives locations beyond which instabilities would amplify. Before these locations, instabilities would be damped.

In the present study, neutral stability curves were determined for air and for values of total Grashof number $N_{Gr,r}$ up to 4×10^9 . The flow was found, as in the case of flow adjacent to a vertical plate, to be sensitive to a certain band of frequencies. The solution also gives the favorite frequency band that amplifies most and, hence, characterizes the flow instability.

In the present case, the favorite band of frequencies was found to depend on the value of the total Grashof number, the cylinder radius and the kinematic viscosity, whereas the favorite frequency band does not change along a flat plate, except with inclination.

Experiments were carried out to check the analytic results. A boundary layer type hot wire probe with a long wire sensor (8 mm length), specially designed for the present work, was used to measure both temperature and velocity. The probe was designed to minimize the error in temperature measurements due to conduction in wire supports, and to pick temperature and velocity fluctuations in the frequency range expected. Basic temperature and velocity profiles were measured and the results were found to agree well with previous theoretical and experimental data of Hermann [16]

and Jodlbauer [42].

To determine points of neutral stability, instabilities were generated by a heating wire placed in the boundary layer. This wire was used in conjunction with a function generator to induce sinusoidal temperature oscillations of controlled frequency and amplitude in the boundary layer. A neutral stability curve was thus obtained by measuring the temperature oscillations. The experimental results agreed well with those analytically obtained.

CHAPTER II

LITERATURE REVIEW

The Orr-Sommerfeld equations governing the amplification or damping of disturbances in flow fields have been solved for many flow situations, due to both forced and natural convection. The present problem, instability of natural convection flow around horizontal cylinders, has not been considered before. The following review, therefore, deals only with natural convection flows over vertical and inclined plates or cases pertinent to this problem.

Analytic Work

The coupled Orr-Sommerfeld equations for a buoyancy driven flow adjacent to a vertical plate were first derived by Plapp [32] and widely used thereafter in similar problems. He obtained a neutral stability curve; nevertheless, the agreement with the available data of onset of turbulence for such flow was considerably poor because of computational limitations and inadequacies in assumptions.

Szewczyk [39] used a series solution for the uncoupled equations, i.e. with temperature disturbances neglected, for natural convection from isothermal vertical flat plates. He assumed the velocity profile to be parabolic. The results obtained were higher than the known values for the onset of turbulence. Kurtz and Crandall [26] used a computer aided finite difference technique to obtain a solution for the uncoupled equations. They found values lower than those of Szewczyk.

Nachtsheim [30] seems to be the first to solve the coupled equations, i.e. with the temperature disturbances taken into consideration. He solved them in the region extending from the outer edge of the boundary layer into the unaffected fluid far from the plate. The equations in this region are linear differential equations with constant coefficients and are relatively easy to solve. This "asymptotic" solution of the Orr-Sommerfeld equations served as a boundary condition at the outer edge of the boundary layer. He then used this condition as a check for an iterative method where the coupled equations were solved within the boundary layer of an isothermal vertical plate using step-by-step integration starting from the plate. Nachtsheim obtained the neutral stability curves for air ($N_{Pr} = .733$) and water ($N_{Pr} = 6.7$). His results showed that instability starts much earlier than predicted by Szewczyk and by Kurtz and Crandall. Nachtsheim solution of the coupled equations gave results that differed considerably from those of the uncoupled equations as could be seen from Figure (2-1) which presents his results for the two cases.

Polymeropoulos and Gebhart [33] used Nachtsheim method to solve the uncoupled equations for a vertical plate of constant heat flux density. Their theoretical findings were in reasonable agreement with their experimental results [34] in which controlled velocity oscillations were introduced in the flow field.

Kaplan [22] introduced a new method for calculating points of neutral stability in isothermal flow. The method is similar to that of Nachtsheim except that integration starts from the outer edge of the boundary layer. This allowed him to use a two-dimensional search procedure whereas a six-dimensional search procedure is needed with Nachtsheim's method.

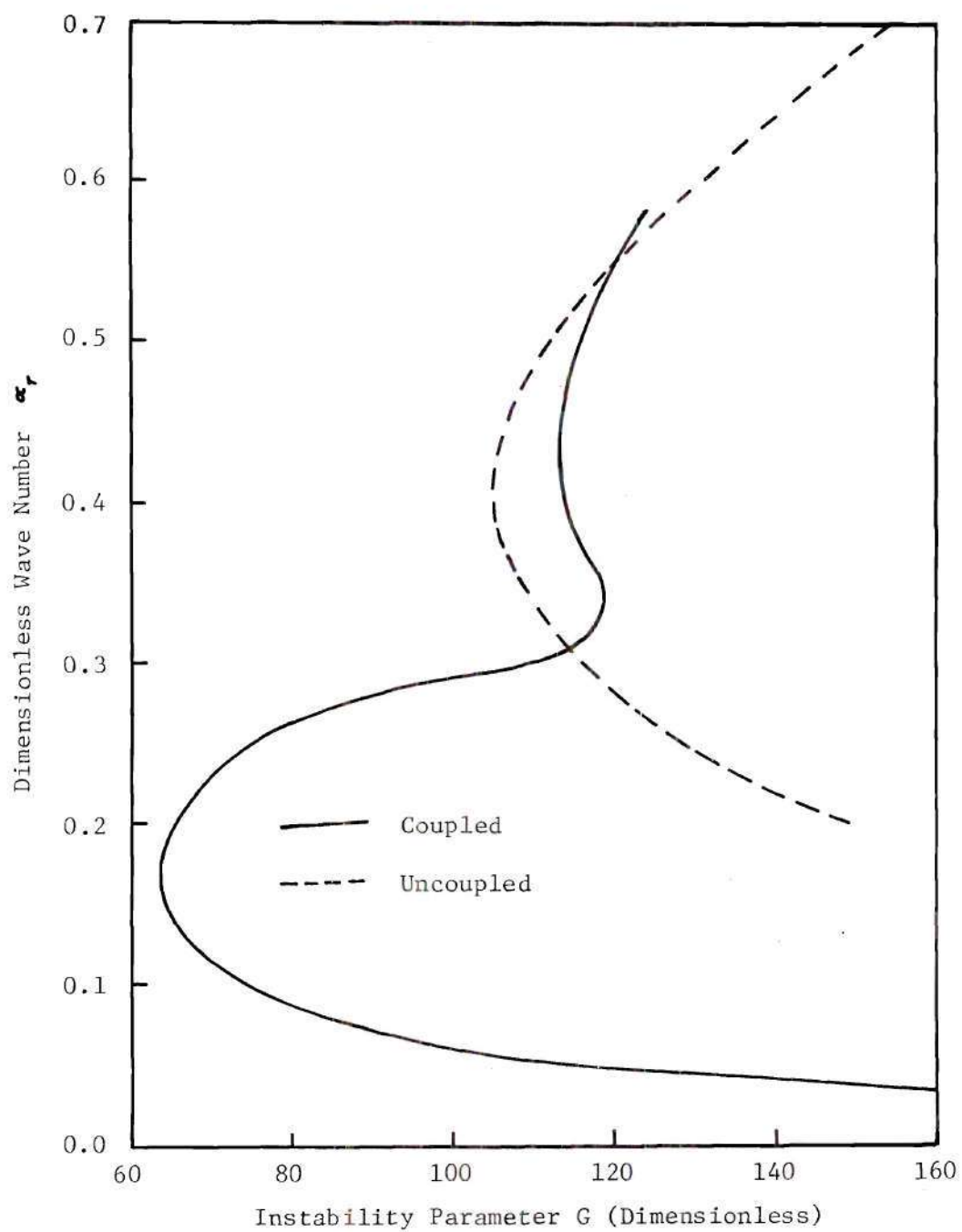


Figure 2-1 . Nachtsheim's Neutral Stability Curves for Air, $N_{Pr} = 0.733$.

Mach [29] extended this method to coupled equations in supersonic flow problems. As a result of these contributions later workers in natural convection were able to consider higher Grashof numbers with relative ease.

Knowles and Gebhart [24] presented a thorough study of the effects of coupling, of the fluid Prandtl number, and of the relative thermal capacity factor $Q^{*†}$ on neutral stability. Disturbance velocity and temperature profiles in the normal directions were also computed. Their phase angles were found to vary with the normal distance from the plate, and with the streamwise travel.

Dring and Gebhart [6] were the first to report the "frequency filtering phenomenon" for vertical flat plates in natural convection. This is best explained by Figure (2-2) as follows. The curves of this figure represent constant amplification (or damping) ratio. A disturbance with frequency \hat{f}_1 is the first to amplify; however, this would reach a low maximum. On the other hand, a disturbance of frequency \hat{f}_2 starts amplification further downstream but acquires the highest amplification rate. Thus, further along the plate, \hat{f}_2 dominates. Therefore \hat{f}_2 , and a small neighboring band, represent the favorite frequencies which would characterize the flow instability. Gebhart and Mahajan [46] correlated the available data of the characteristic frequency for natural convection flow over vertical flat plates, with Prandtl number.

$†Q^{*} = (\hat{C}/A)/\rho c \delta$. It designates the ratio between the thermal capacities of the plate and the fluid where (\hat{C}/A) is the plate thermal capacity per unit area, and δ is the boundary layer thickness.

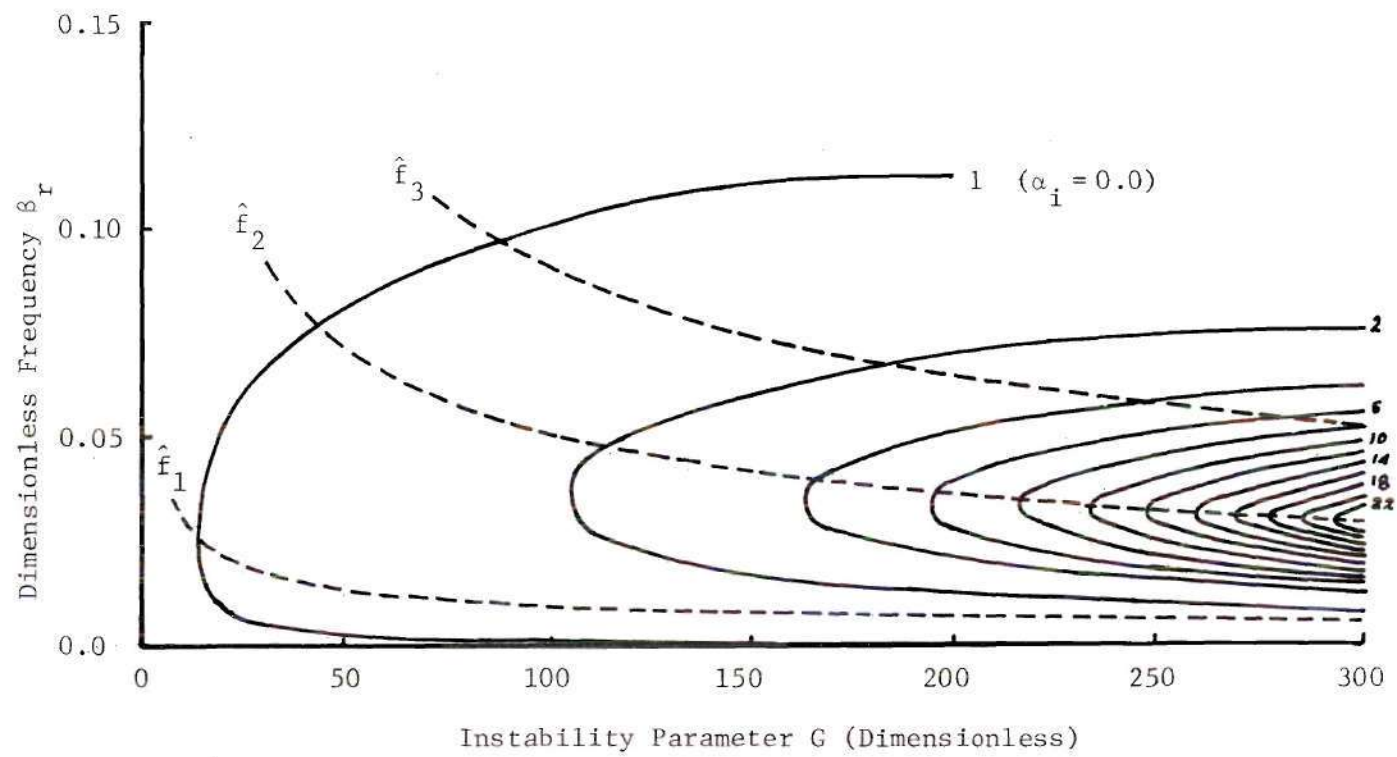


Figure 2-2 . Calculated Disturbance Amplitude Contours for Water,
 $N_{Pr} = 6.7$ (Dring and Gebhart [6]).

Hieber and Gebhart [17] extended the analysis to higher Grashof numbers in the vicinity of 10^{12} . They also discovered two modes of oscillations, one due to hydrodynamic instability and the other due to temperature coupling. For moderate and large values of Prandtl number, a loop appears in the neutral stability curve as a result of the merging of two unstable modes, Figure (2-3). The nose shape of Nachtsheim's curve is attributed to that.

A study of the effect of having a very large Prandtl number was carried out by Gill and Davy [13] for a double-infinite buoyancy layer, and by Hieber and Gebhart [18] for a vertical plate of constant heat flux density. The primary source of instability is shown to arise from the temperature coupling effect.

Haaland [14] included in the coupled Orr-Sommerfeld equations some terms that have been previously neglected; namely the derivatives with respect to the distance along the plate. His results showed the appreciable effect of these terms on the neutral stability curve as shown in Figure (2-4). Better agreement with experimental results was obtained. Haaland's solution was given for different inclination angles ranging from -45° to 45° with the vertical for water, and 0° and 30° for air.

Iyer and Kelley [20], and Khawita and Meroney [23] deduced the governing equations for small oscillations assuming longitudinal vortices that were discovered earlier in experiments by Sparrow and Husar [37]. They concluded that three dimensional vortices dominate the flow field for angles more than 17 degrees with the vertical, in agreement with Sparrow and Husar findings.

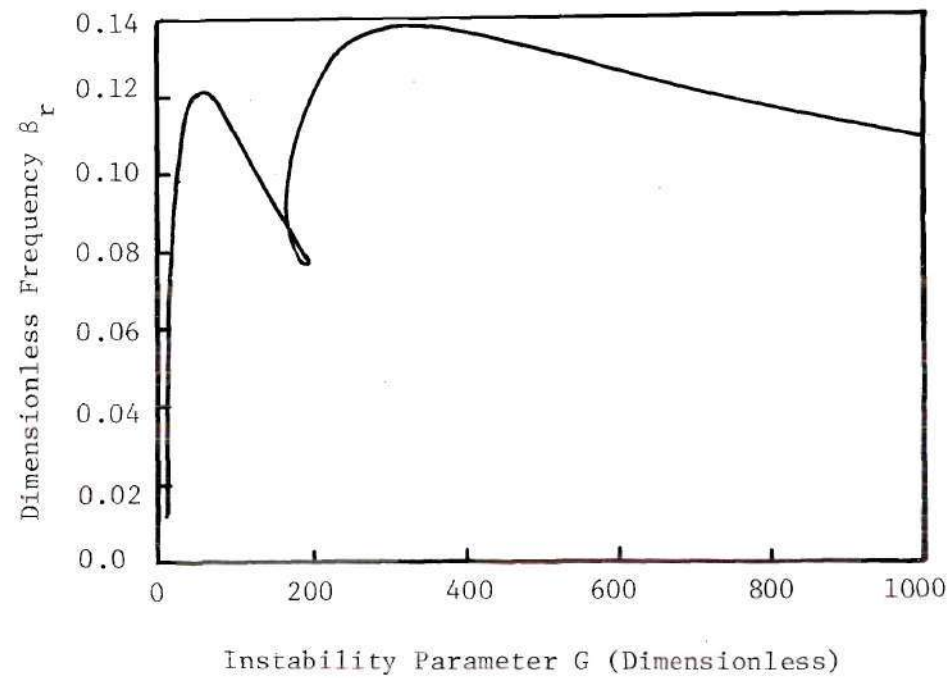


Figure 2-3 . Neutral Stability Curve for Flow Adjacent to a Vertical Uniformly Heated Plate in Air $N_{Pr} = 0.733$. (Hieber and Gebhart [17]).

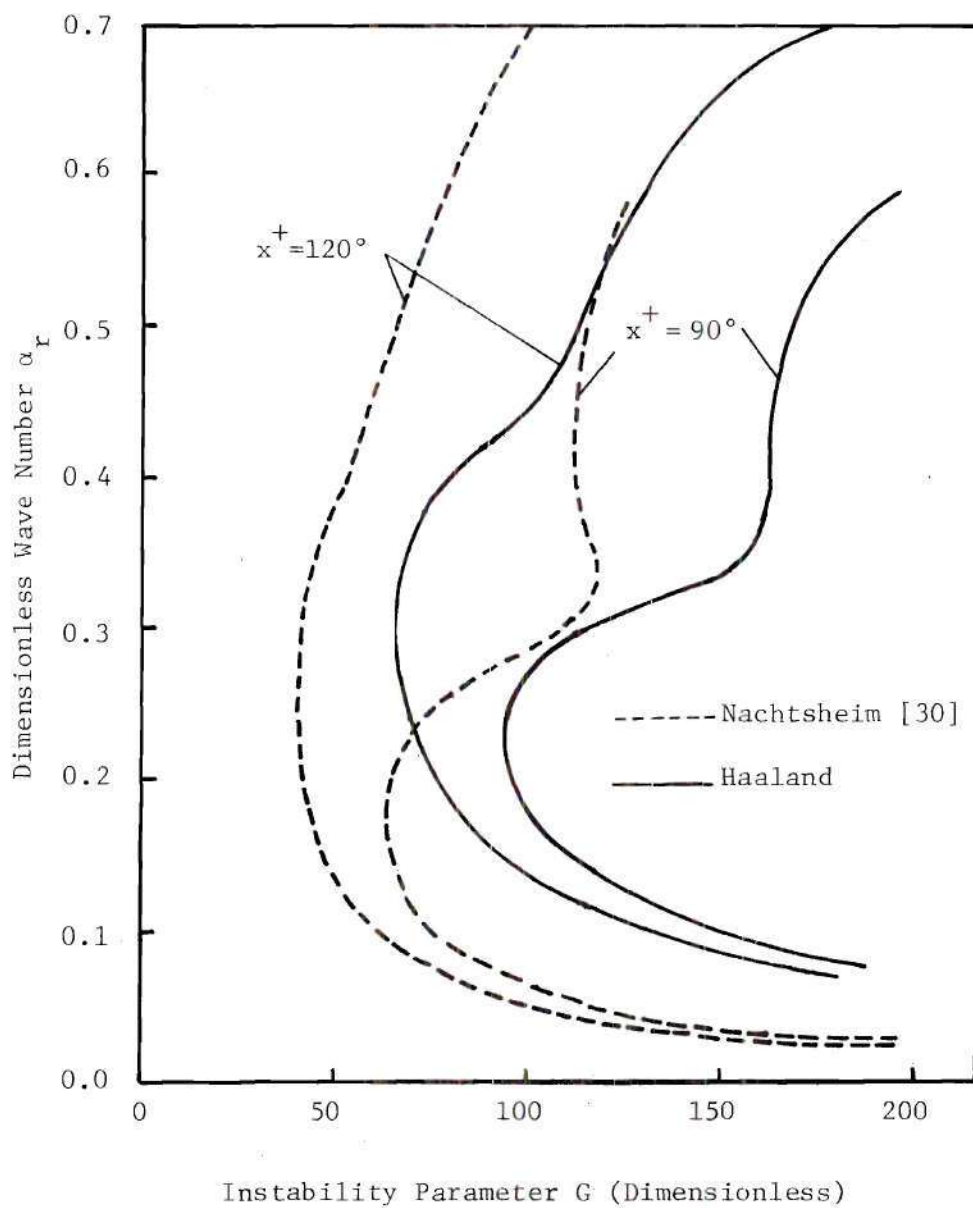


Figure 2.4 . Comparison Between Results of Haaland and Those of Nachtsheim (Haaland [14]).

Experimental Work

Experiments were carried out to study the randomly occurring disturbances, or to determine the response of the flow to induced oscillations of controlled amplitude and frequency.

The first successful experiment for introducing controlled oscillations in the boundary layer and measuring spatial rate of amplification seems to be that carried out by Schubauer and Skramstad [36] for forced flow over flat plate. A vibrating ribbon was used to oscillate the boundary layer, and two hot wire probes were used to detect the oscillatory velocity components together with their phase lag. Neutral stability curves and disturbance velocity profiles were determined and found in good agreement with the available analytical data.

In natural convection, Birch [2] used an electrically pulsed 0.001 inch diameter wire to introduce artificial disturbances in the boundary layer over a vertical isothermal plate in air. A Mach-Zehnder interferometer was used to detect these disturbances as they travelled downstream; the study was essentially qualitative in nature. Gartrell* [12] carried out a similar study; however, no direct comparison between the two investigations could be made.

Eckert, Hartnett and Irvine [9] employed smoke threads for the visualization of natural convection flow over a flat vertical plate in air. Two-dimensional waves appeared first with wave fronts essentially normal to the flow direction and parallel to the flat surface in the third direction. Vortices with axes in the flow direction were also observed; these

* Comments on Birch and Gartrell works are quoted from Polymeropoulos and Gebhart work [34].

latter longitudinal vortices indicate the presence of transverse effects in the process. Therefore, it is inferred that the disturbances were initially predominantly two-dimensional and that, at some stage, transverse effects become significant.

Czewczyk [39] used dye injection in water to observe instability waves arising from random disturbances. A double row of longitudinal vortices was noticed. His work was the first trial to compare theory with experiment, however, the comparison was inconclusive.

Colak-Antic^{*} [4,5] reported observations on the breakdown of two-dimensional waves which would then be replaced by three-dimensional disturbances in the flow of air and water over a vertical isothermal plate. An electrically pulsed wire was used to induce disturbances in the flow field. Most of the study was qualitative in nature; however, some data were obtained for air using a hot wire anemometer. Due to a lack of sensitivity of the hot wire system, the measurements were made in a region where disturbances had undergone considerable amplification.

It was not until the carefully controlled experiments of Polymeropoulos and Gebhart [34] that the agreement between the linear stability theory and experimental results for natural convection was demonstrated. With pressurized nitrogen as the fluid and a vibrating ribbon to induce controlled oscillations, a Mach-Zehnder interferometer was used to determine the neutral stability curve.

Knowles and Gebhart [25] used a hot-wire anemometer together with a Mach-Zehnder interferometer. Silicone oil (of Prandtl number 7.7) was used

^{*}Quoted by Knowles and Gebhart [25].

to limit the temperature difference needed to achieve the required values of Grashof number. The thermal boundary layer thickness was very small, and the overall influence of temperature variations on the hot wire readings was limited. The hot-wire was calibrated against the theoretical results previously established for the case of natural convection flow adjacent to a vertical plate with constant heat flux density. The importance of coupling the disturbance momentum and energy equations was demonstrated by the agreement between the coupled theoretical results and the experimental data. The magnitude and phase of the disturbance velocity and temperature were also measured.

Dring and Gebhart [8] developed a new precise method for calibrating the hot-wire anemometer. They used the carefully calibrated probe to determine the disturbance velocity and temperature profiles along a uniformly heated plate. Good agreement with their theoretical results [7] was obtained.

Lock, Gort and Pond [28], and Lloyed and Sparrow [27] plotted critical local Grashof number against angle of inclination of flat plates for natural disturbances to present the results of their experiments with air and water. It was generally noticed that an increase in the inclination from the vertical of heated plates facing upwards stimulates instability and eddying.

Using a technique developed by Baker [1] for measuring fluid velocities in the range 0-5 cm/s, Sparrow and Husar [37] discovered a row of longitudinal vortices for plates inclined to the vertical by an angle 17 degrees or more.

Motivated by the results of Eckert, Hartnett and Irvine and by those of Sparrow and Husar, Jaluria and Gebhart [21] introduced two-dimensional oscillations with transverse variations into the boundary layer adjacent to a vertical uniformly heated plate. Results confirmed that the two-dimensional effects dominate initially, and that transverse variations do not appear quickly. However, further downstream, these instabilities begin to amplify and lead to strong secondary flows in the form of a double longitudinal vortex system, through non-linear interactions. No contradiction is noticed between the results of Jaluria and Gebhart, and those of Sparrow and Husar; two dimensional oscillations precede three-dimensional longitudinal vortices to an angle of 17 degrees to the vertical. Beyond this angle, vortices dominate the flow before two-dimensional instability sets in.

CHAPTER III

ANALYSIS

The coupled Orr-Sommerfeld equations for the considered case of buoyancy-driven flow around a horizontal cylinder are derived following the steps Plapp [32] used for the case of a vertical flat plate. A thorough order of magnitude investigation is carried out to determine the terms of significance to be considered in the analysis. Asymptotic solutions for these simplified equations are obtained for the "basically stagnant" fluid region to serve as boundary conditions at the outer edge of the boundary layer. The method devised by Kaplan [22] and Mach [29] to solve instability problems is used to solve the present one.

Computations are carried out for air ($N_{Pr} = .733$), for position angles $x^+ = 30$ to 150 degrees measured from the lowermost point, and for values of the instability parameter G which is mainly a function of the local Grashof number of 0 to 200. The results are presented in two types of graphs, one of them with G versus either the dimensionless frequency β_r or wave number α_r , and with the angle x^+ as parameter. The second type shows a single flow situation as indicated by Grashof number; the stability curves are drawn on x^+ versus α_r or x^+ versus β_r planes.

To determine the effect of curvature on the critical values of the instability parameter G as given by the neutral stability curves, comparison is made between the obtained results and those for inclined plates given by Haaland [14]. A study of frequency-filtering is also carried out for the present problem.

Derivation of the Differential Equations Governing Disturbances

The considered problem would be an unsteady two-dimensional flow problem in which the energy dissipation term is neglected and the properties are taken as constants. Following Bird, Stewart and Lightfoot [3], the governing equations in polar coordinates, with body forces substituted for with normal expressions of natural convection, are: Mass balance equation and tangential momentum balance equation

$$\frac{1}{r} (\hat{r} v)_{\hat{r}} + \frac{1}{r} u_x = 0 \quad (3-1a)^*$$

$$\begin{aligned} u_t + v u_{\hat{r}} + \frac{u}{r} u_x + \frac{v u}{r} &= -\frac{1}{r} P_x^* + \hat{g} \hat{\beta} \theta \sin(x) \\ + v \left[\left\{ \frac{1}{r} (\hat{r} u)_{\hat{r}} \right\}_{\hat{r}} + \frac{1}{r^2} u_{xx} + \frac{2}{r^2} v_x \right] & \end{aligned} \quad (3-1b),$$

normal momentum balance equation

$$\begin{aligned} v_t + v v_{\hat{r}} + \frac{u}{r} v_x - \frac{u^2}{r} &= -\frac{1}{r} P_{\hat{r}}^* - \hat{g} \hat{\beta} \theta \cos(x) \\ + v \left[\left\{ \frac{1}{r} (\hat{r} v)_{\hat{r}} \right\}_{\hat{r}} + \frac{1}{r^2} v_{xx} - \frac{2}{r^2} u_x \right] & \end{aligned} \quad (3-1c)$$

and energy equation

$$\theta_t + v \theta_{\hat{r}} + \frac{u}{r} \theta_x = a \left[\frac{1}{r} (\hat{r} \theta_{\hat{r}})_{\hat{r}} + \frac{1}{r^2} \theta_{xx} \right] \quad (3-1d)$$

The coordinate system may now be changed to that of the circumferential distance s measured from the lower stagnation point and the

*Time and spatial coordinate subscripts denote differentiation with respect to the subscript.

normal distance n measured from the cylinder surface. Defining, also,

$$x = \frac{s}{r}, \quad \text{and} \quad \hat{r} = r + n \quad (3-2)$$

gives, respectively,

$$\frac{r}{r+n} u_s + v_n + \frac{v}{r+n} = 0 \quad (3-3a)$$

$$u_t + \frac{r}{r+n} u u_s + v u_n + \frac{u \cdot v}{r+n} = -\frac{1}{\rho} P_s^* \frac{r}{r+n} + \hat{g} \hat{\beta} \theta \sin\left(\frac{s}{r}\right) \\ + v \left\{ u_{nn} + \frac{1}{r+n} u_n + \left(\frac{r}{r+n}\right)^2 u_{ss} - \frac{u}{(r+n)^2} + \frac{2r}{(r+n)^2} v_s \right\} \quad (3-3b)$$

$$v_t + \frac{r}{r+n} u v_s + v v_n - \frac{u^2}{r+n} = -\frac{1}{\rho} P_n^* - \hat{g} \hat{\beta} \cos\left(\frac{s}{r}\right) \\ + v \left\{ v_{nn} + \frac{1}{r+n} v_n + \left(\frac{r}{r+n}\right)^2 v_{ss} - \frac{v}{(r+n)^2} - \frac{2r}{(r+n)^2} u_s \right\} \quad (3-3c)$$

$$\theta_t + \frac{r}{r+n} u \theta_s + v \theta_n = a \left\{ \theta_{nn} + \frac{1}{r+n} \theta_n + \left(\frac{r}{r+n}\right)^2 \theta_{ss} \right\} \quad (3-3d)$$

These equations are similar to those of Hermann [16] except for the unsteady terms u_t , v_t , and θ_t which are present here.

For disturbed flows, the situation is mathematically modeled by considering unstable flow components superimposed on the basic or "undisturbed" ones, i.e.

$$u(s, n, t) = U(s, n) + \tilde{u}(s, n, t)$$

}

$$\begin{aligned}
 v(s, n, t) &= V(s, n) + \tilde{v}(s, n, t) \\
 \theta(s, n, t) &= \Theta(s, n) + \tilde{\theta}(s, n, t) \\
 P^*(s, n, t) &= P(s, n) + \tilde{P}(s, n, t)
 \end{aligned}
 \quad \left. \vphantom{\begin{aligned} v(s, n, t) &= V(s, n) + \tilde{v}(s, n, t) \\ \theta(s, n, t) &= \Theta(s, n) + \tilde{\theta}(s, n, t) \\ P^*(s, n, t) &= P(s, n) + \tilde{P}(s, n, t) \end{aligned}} \right\} (3-4)$$

where U , V , Θ , and P are the basic flow components, while \tilde{u} , \tilde{v} , $\tilde{\theta}$, and \tilde{P} are the disturbance components. By this, the governing equations include two groups of equations; the basic equations and the disturbance equations. The basic equations were handled by Hermann [16]; they are:

$$\frac{r}{r+n^+} U_{s^+} + V_{n^+} + \frac{V}{r+n^+} = 0 \quad (3-5a)$$

$$\begin{aligned}
 \frac{r}{r+n^+} U U_{s^+} + V U_{n^+} + \frac{UV}{r+n^+} &= -\frac{1}{\rho} P_{s^+}^* \frac{r}{r+n^+} + \hat{g} \hat{\beta} \Theta \sin\left(\frac{s^+}{r}\right) \\
 + \gamma \left\{ U_{n^+ n^+} + \frac{1}{r+n^+} U_{n^+} + \left(\frac{r}{r+n^+}\right)^2 U_{s^+ s^+} - \frac{U}{(r+n^+)^2} + \frac{2r}{(r+n^+)^2} V_{s^+} \right\} & \quad (3-5b)
 \end{aligned}$$

$$\begin{aligned}
 \frac{r}{r+n^+} U V_{s^+} + V V_{n^+} - \frac{U^2}{r+n^+} &= -\frac{1}{\rho} P_{n^+}^* - \hat{g} \hat{\beta} \cos\left(\frac{s^+}{r}\right) \\
 + \gamma \left\{ V_{n^+ n^+} + \frac{1}{r+n^+} V_{n^+} + \left(\frac{r}{r+n^+}\right)^2 V_{s^+ s^+} - \frac{V}{(r+n^+)^2} - \frac{2r}{(r+n^+)^2} U_{s^+} \right\} & \quad (3-5c)
 \end{aligned}$$

$$\frac{r}{r+n^+} U \Theta_{s^+} + V \Theta_{n^+} = a \left\{ \Theta_{n^+ n^+} + \frac{1}{r+n^+} \Theta_{n^+} + \left(\frac{r}{r+n^+}\right)^2 \Theta_{s^+ s^+} \right\} \quad (3-5d)$$

An outline of Hermann's solution is given in Appendix A, it contains many quantities that are used in the present analysis.

Subtracting the basic flow equations, equations (3-5), from the overall governing equations, equations (3-3), gives the disturbance governing equations. The latters are further linearized according to the linear stability theory by neglecting terms containing multiples of disturbance quantities. The whole procedure is explained by the following example

$$u u_s = (U + \tilde{u})(U_s + \tilde{u}_s) = U U_s + \tilde{u} U_s + \tilde{u}_s U + \tilde{u} \tilde{u}_s$$

Subtracting the basic flow term $U U_s$, and neglecting the term $\tilde{u} \tilde{u}_s$, the disturbance term due to $u u_s$ left in the disturbance equations would, therefore, be $\tilde{u} U_s + U \tilde{u}_s$.

As explained later, the "+" superscript over s and n indicates the length scales used with the basic components, as distinct from those used with the disturbance components. The disturbance equations would, therefore, be

$$\frac{r}{r+n} \tilde{u}_s + \tilde{v}_n + \frac{\tilde{w}}{r+n} = 0 \quad (3-6a)$$

$$\begin{aligned} \tilde{u}_t + \frac{r}{r+n} \tilde{u} U_s + \frac{r}{r+n} U \tilde{u}_s + V \tilde{u}_n + \tilde{v} U_n + \frac{U \tilde{w}}{r+n} + \frac{V \tilde{u}}{r+n} = -\frac{1}{\rho} \tilde{p}_s \frac{r}{r+n} \\ + \hat{g} \hat{p} \tilde{\theta} \sin\left(\frac{s}{r}\right) + \nu \left\{ \tilde{u}_{nn} + \frac{1}{r+n} \tilde{u}_n + \left(\frac{r}{r+n}\right)^2 \tilde{u}_{ss} - \frac{\tilde{u}}{(r+n)^2} + \frac{2r}{(r+n)^2} \tilde{v}_s \right\} \end{aligned} \quad (3-6b)$$

$$\begin{aligned} \tilde{v}_t + \frac{r}{r+n} \tilde{u} V_s + \frac{r}{r+n} U \tilde{v}_s + \tilde{v} V_n + V \tilde{v}_n - \frac{2U \tilde{u}}{r+n} = -\frac{1}{\rho} \tilde{p}_n - \hat{g} \hat{p} \cos\left(\frac{s}{r}\right) \tilde{\theta} \\ + \nu \left\{ \tilde{v}_{nn} + \frac{1}{r+n} \tilde{v}_n + \left(\frac{r}{r+n}\right)^2 \tilde{v}_{ss} - \frac{\tilde{v}}{(r+n)^2} - \frac{2r}{(r+n)^2} \tilde{u}_s \right\} \end{aligned} \quad (3-6c)$$

$$\begin{aligned} \tilde{\theta}_t + \frac{r}{r+n} \tilde{u} \Theta_{s^+} + \frac{r}{r+n} U \tilde{\theta}_s + \Theta_{n^+} \tilde{v} + v \tilde{\theta}_n \\ = a \left\{ \tilde{\theta}_{nn} + \frac{1}{r+n} \tilde{\theta}_n + \left(\frac{r}{r+n} \right)^2 \tilde{\theta}_{ss} \right\} \end{aligned} \quad (3-6d)$$

It should be noted that the largest disturbance would acquire a size or, in other words, a length scale of order δ , the boundary layer thickness. Therefore s and n for the disturbance components are of order δ . For the basic flow, Hermann's analysis gives s^+ of order 1 and n^+ of order δ . This would give compatible time scales for both the basic flow and disturbances, where the time scale for basic flow is $s^+/U = n^+/V \approx 1$,^{*} and the time scale for the disturbance is $s/\tilde{u} = n/\tilde{v} \approx 1$.

The same result could have been obtained through the disturbance mass balance equation, equation (3-6a). Substituting $\tilde{v} \approx \tilde{u} \approx \delta$, and $n \approx \delta$ gives $s \approx \delta$.^{**}

The order of magnitude of s as associated with disturbance quantities was also analyzed by Hieber and Gebhart [17] with the same result.

A further step in the development of the final mathematical form of the problem is to replace the mass balance equation, equation (3-6a) by defining the functions $\tilde{\psi}_s$ and $\tilde{\psi}_n$ as follows

$$-\frac{r+n}{r} \tilde{u} = \tilde{\psi}_s, \quad \text{and} \quad \tilde{u} = \tilde{\psi}_n \quad (3-7)$$

As usual in boundary layer analysis, equations (3-6b and c) are cross

* The sign \approx indicates "of order of magnitude of."

** The other alternative is that \tilde{v} and \tilde{u} are negligible which means that the disturbances are one dimensional.

differentiated to cancel out the pressure term; this reduces the two momentum equations to the following single equation

$$\begin{aligned}
 & \frac{1}{r} \tilde{\psi}_{nt} + \frac{r}{r+n} \tilde{\psi}_{nnt} + \tilde{\psi}_{nn} U_{s^+} + \tilde{\psi}_n U_{s^+n^+} + U_{n^+} \tilde{\psi}_{ns} + U \tilde{\psi}_{nns} \\
 & + \frac{1}{r} V \tilde{\psi}_{nn} + \frac{r+n}{r} V_{n^+} \tilde{\psi}_{nn} + \frac{r+n}{r} V \tilde{\psi}_{nnn} - U_{n^+n^+} \tilde{\psi}_s - U_{n^+} \tilde{\psi}_{sn} + \frac{U}{(r+n)^2} \tilde{\psi}_s \\
 & - \frac{1}{r+n} U_{n^+} \tilde{\psi}_s - \frac{U}{r+n} \tilde{\psi}_{ns} + \frac{V_{n^+} \tilde{\psi}_n}{r} + \frac{V}{r} \tilde{\psi}_{nn} + \frac{r}{r+n} \tilde{\psi}_{sst} - \frac{r}{r+n} \tilde{\psi}_{ns} V_{s^+} - \frac{r}{r+n} \tilde{\psi}_n V_{s^+n^+} \\
 & + \left(\frac{r}{r+n}\right)^2 U_{s^+} \tilde{\psi}_{ss} + \left(\frac{r}{r+n}\right)^2 \tilde{\psi}_{sss} U + \frac{r}{r+n} V_{n^+} \tilde{\psi}_{ss} + \frac{r}{r+n} V_{n^+s^+} + \tilde{\psi}_s - \frac{r}{(r+n)^2} \tilde{\psi}_{ss} V \\
 & - \frac{r}{(r+n)^2} \tilde{\psi}_s V_{s^+} + \frac{r}{r+n} \tilde{\psi}_{ns} V_{s^+} + \frac{r}{r+n} \tilde{\psi}_{nss} V + \frac{2U_{s^+} \tilde{\psi}_n}{r+n} + \frac{2U}{r+n} \tilde{\psi}_{ns} = \hat{g} \hat{\beta} \tilde{\Theta}_n \sin\left(\frac{s}{r}\right) \frac{r+n}{r} \\
 & + \frac{1}{r} \hat{g} \hat{\beta} \tilde{\Theta} \sin\left(\frac{s}{r}\right) + \hat{g} \hat{\beta} \tilde{\Theta}_s \cos\left(\frac{s}{r}\right) - \frac{1}{r} \hat{g} \hat{\beta} \tilde{\Theta} \sin \frac{s}{r} + \gamma \left\{ \frac{1}{r} \tilde{\psi}_{nnn} + \frac{r+n}{r} \tilde{\psi}_{nnnn} \right. \\
 & + \frac{1}{r} \tilde{\psi}_{nnn} - \frac{r}{(r+n)^2} \tilde{\psi}_{nss} + \frac{r}{r+n} \tilde{\psi}_{nsss} + \frac{\tilde{\psi}_n}{r(r+n)^2} - \frac{\tilde{\psi}_{nn}}{r(r+n)} + \frac{4r}{(r+n)^3} \tilde{\psi}_{ss} \\
 & \left. - \frac{2r}{(r+n)^2} \tilde{\psi}_{ssn} + \frac{r}{r+n} \tilde{\psi}_{ssnn} + \frac{r}{(r+n)^2} \tilde{\psi}_{ssn} + \left(\frac{r}{r+n}\right)^3 \tilde{\psi}_{ssss} \right\} \quad (3-8a)
 \end{aligned}$$

The energy equation (3-6d) remains unchanged, namely;

$$\begin{aligned}
 & \tilde{\Theta}_t + \frac{r}{r+n} \tilde{\psi}_n \Theta_{s^+} + \frac{r}{r+n} U \tilde{\Theta}_s - \frac{r}{r+n} \tilde{\psi}_s \Theta_{n^+} + V \tilde{\Theta}_n \\
 & = a \left\{ \tilde{\Theta}_{nn} + \frac{1}{r+n} \tilde{\Theta}_n + \left(\frac{r}{r+n}\right)^2 \tilde{\Theta}_{ss} \right\} \quad (3-8b)
 \end{aligned}$$

Order of Magnitude Analysis

With the previous discussion of the order of magnitude of n , n^+ , s and s^+ kept in mind; together with Hermann's analysis, the following could

be concluded

$$\left. \begin{array}{lll}
 U \approx 1 & \tilde{u} \approx \delta & \nu \approx \delta^2 \\
 V \approx \delta & \tilde{v} \approx \delta & a \approx \delta^2 \\
 n^+ \approx \delta & \tilde{\psi} \approx \delta^2 & t \approx 1 \\
 s^+ \approx 1 & \tilde{\theta}/\Delta T \approx \delta & \\
 H = \theta/\Delta T \approx 1 & n \approx \delta & \\
 & s \approx \delta &
 \end{array} \right\} \quad (3-9)$$

The order of magnitude of the terms of equation (3-8) are derived and listed in Appendix B.

In equations (3-8), n may be neglected with respect to r , terms of order δ or smaller may be neglected in equation (3-8a), and those of order δ^2 and smaller may be also neglected in equation (3-8b). Further using the basic mass balance equation, $U_{s^+} + V_{n^+} = 0$, reduce equations (3-8a and b) to

$$\begin{aligned}
 & \tilde{\psi}_{nnt} + \tilde{\psi}_n U_{s^+ n^+} + U \tilde{\psi}_{nns} + V \tilde{\psi}_{nnn} - U_{n^+ n^+} \tilde{\psi}_s - \frac{1}{r} U_{n^+} \tilde{\psi}_s + \frac{1}{r} U \tilde{\psi}_{sn} + \tilde{\psi}_{sst} + U \tilde{\psi}_{sss} \\
 & + V \tilde{\psi}_{sss} = \hat{g} \hat{\beta} \tilde{\theta}_n \sin\left(\frac{x}{r}\right) + \hat{g} \hat{\beta} \tilde{\theta}_s \cos\left(\frac{x}{r}\right) + \gamma \left\{ \tilde{\psi}_{nnnn} + 2 \tilde{\psi}_{nnss} + \tilde{\psi}_{ssss} \right\} \quad (3.10a)
 \end{aligned}$$

$$\tilde{\theta}_t + \tilde{\psi}_n \Theta_{s^+} + U \tilde{\theta}_s - \tilde{\psi}_s \Theta_{n^+} + V \tilde{\theta}_n = a \left\{ \tilde{\theta}_{nn} + \tilde{\theta}_{ss} \right\} \quad (3-10b)$$

These disturbance equations are rendered dimensionless by using equations (A-20 to 24) together with the following dimensionless variables

$$\left. \begin{array}{l}
 x = \frac{s}{r}, \quad y = \frac{n}{r}, \quad \bar{z} = \frac{t}{\nu^2}, \quad \psi^* = \tilde{\psi}/\gamma, \\
 \text{and} \quad \theta^* = \tilde{\theta}/\Delta T
 \end{array} \right\} \quad (3-11)$$

The dimensionless form of these disturbance equations, equations (3-10)

would then be

$$\begin{aligned}
 & \psi_{yy}^* \bar{\epsilon} + \psi_y^* \frac{1}{\delta^3} (F'' - F''' \eta) + F' U^* \psi_{yx}^* - \frac{1}{\delta} (3F - F' \eta) \psi_{yyy}^* \\
 & - F''' \frac{U^4}{\delta^2} \psi_x^* - F'' \frac{U^3}{\delta} \psi_x^* + F' U^* \psi_{yx}^* + \psi_{xx}^* \bar{\epsilon} + F' U^* \psi_{xxx}^* \\
 & - \frac{1}{\delta} (3F - F' \eta) \psi_{yxx}^* = N_{Gr,r} (\theta_y^* \sin(x) + \theta_x^* \cos(x)) + \psi_{yyy}^* \\
 & + 2 \psi_{yy}^* \psi_{xx}^* + \psi_{xxx}^* \psi_{xx}^*
 \end{aligned} \tag{3-12a}$$

$$\begin{aligned}
 & \theta_{\bar{\epsilon}}^* - \psi_y^* H' \eta \frac{1}{\delta^2 U^*} + F' U^* \theta_x^* - \psi_x^* H' \frac{1}{\delta} - \frac{1}{\delta} (3F - F' \eta) \theta_y^* \\
 & = \frac{1}{N_{Pr}} \{ \theta_{yy}^* + \theta_{xx}^* \}
 \end{aligned} \tag{3-12b}$$

where F , F' , F'' , F''' , H , H' , and η are defined in Appendix A, and N_{pr} is the fluid Prandtl number.

Substitution for Disturbance Quantities

Generally, two-dimensional disturbances seem to be the first unstable mode to appear. That was theoretically proved by Squire [38] for forced flow, and by Knowles and Gebhart [24] for natural convection instability for flat plates. Experiments of Eckert, Hartnett and Irvine [9], together with those of Jaluria and Gebhart [21] show that two dimensional waves are the first mode of instability to appear. However, three dimensional longitudinal vortices dominate the field for plates inclined more than 17 degrees to the vertical as found by Sparrow and Husar [37], Iyer and Kelley [20], and Khawita and Meroney [23]. This inclination corresponds, in the present case to position angles beyond 107 degrees. For the

case of horizontal cylinders, two-dimensional waves are, therefore, expected to be the first unstable mode to appear.

The assumed two-dimensional waves are given after Nachtshein [30] from

$$\psi^* = \bar{\phi}(y) e^{i\bar{\alpha}(x - \bar{c}\bar{\tau})} \quad (3-13a)$$

where $\bar{\alpha}$ and \bar{c} are complex quantities. Similarly, it is usual to express the temperature oscillations in the same form, with the same frequency and amplification, namely:

$$\theta^* = \bar{\zeta}(y) e^{i\bar{\alpha}(x - \bar{c}\bar{\tau})} \quad (3-13b)$$

The following dimensionless quantities may now be defined

$$\left. \begin{aligned} \eta = y/\delta, \quad \xi = x/\delta, \quad \tau = \bar{c}U^*/\delta, \quad \phi(\eta) = \bar{\phi}(y)/(\delta U^*), \\ \bar{\zeta}(\eta) = \bar{\zeta}(y), \quad c = \bar{c}/U^*, \quad \text{and} \quad \alpha = \bar{\alpha}\delta \end{aligned} \right\} \quad (3-14)$$

substitution from these relations into expressions (3-13) gives:

$$\left. \begin{aligned} \psi^* &= \phi \delta U^* e^{i\alpha(\xi - c\tau)} = \phi \delta U^* e^{i(\alpha\xi - \beta\tau)} \\ \theta^* &= \zeta e^{i\alpha(\xi - c\tau)} = \zeta e^{i(\alpha\xi - \beta\tau)} \end{aligned} \right\} \quad (3-15)$$

where $\beta = \alpha c$ is also complex. It should be noted that the quantity $\bar{\alpha}_r x$, where the subscript r denotes the real part of $\bar{\alpha}$, indicates the phase angle that would be acquired by the disturbance due to streamwise travel for a distance x . In this expression we can characterize the wave by some wave

length L through the relation $\bar{\alpha}_r = 2\pi/L$. The term $e^{-i\bar{\alpha}_i x}$, where the subscript i denotes the imaginary part of $\bar{\alpha}$, implies amplification ($\bar{\alpha}_i < 0$) or damping ($\bar{\alpha}_i > 0$) due to streamwise travel. Naturally $\bar{\alpha}_i = 0$ indicates no amplification or damping due to streamwise travel. The quantity $\beta_r \tau$ indicates a phase shift with β_r being the angular velocity of wave propagation. The term $e^{i\beta_i \tau}$ denotes amplification (for $\beta_i > 0$) or damping (for $\beta_i < 0$) with time, whereas $\beta_i = 0$ stands for locally stable oscillations. It should be noted from above that neutrally stable oscillations require that $\alpha_i = \beta_i = 0$.

Substituting into equations (3-12), and using equations (A-15, 25, and 26), give:

$$(\phi'''' - 2\alpha^2\phi'' + \alpha^4\phi) + (\zeta' + i\alpha\zeta \cot(x)) = i\alpha G \{ (F'-c)(\phi'' - \alpha^2\phi) - F'''\phi - F''\phi\delta + F'\phi'\delta \} + \{ F'' - F'''\eta \} \phi' - (\phi''' - \alpha^2\phi') (3F - F'\eta) \quad (3-16a)$$

$$(\zeta'' - \alpha^2\zeta) = i\alpha N_{Pr} G [(F'-c)\zeta - H'\phi] + N_{Pr} [-H'\eta\phi' - (3F - F'\eta)\zeta'] \quad (3-16b)$$

$$\text{where } G = f(x) N_{Gr,r}^{1/4} \quad (3-17)$$

Equations (3-16) are the coupled Orr-Sommerfeld equations for the case of natural convection flow around horizontal cylinders. They constitute a sixth order complex problem, with ϕ , ϕ' , ϕ'' , ϕ''' , ζ , ζ' as variables and α , G , N_{Pr} , and β as parameters.

Method of Solution

Equations (3-16) have solution only for certain combined values of the parameters α , G , N_{Pr} , and β . These constitute eigenvalues for the problem to be determined as outlined below. An "asymptotic solution" is then obtained for the domain outside the boundary layer where there is no basic streamwise flow while oscillations still exist. This asymptotic solution is finally used as a boundary condition for the solution within the boundary layer.

The Eigenvalue Problem

Following Kaplan [22] and Mach [29], for given values of G and N_{Pr} , values are assumed for α_i and β_i whereas α_r and β_r are left to be determined as eigenvalues. It should be noted that while N_{Pr} is a fluid property, G depends on the temperature difference and position angle. The zero values of α_i and β_i stand for points on the neutral stability curves where instabilities are neither amplified nor damped.* As β_r represents the dimensionless frequency, results can be displayed in the form of a position angle versus frequency graph for neutrally stable oscillations.

In Kaplan's method, a step-by-step integration method is used; it starts at the outer edge of the boundary layer, with the asymptotic solutions serving as starting values for this integration.

* Since, in the present problem, instabilities are induced into a time steady basic flow, they are not expected to acquire any time amplification rates. β_i is, therefore, taken zero in the analysis. This assumption is supported by the experimental results of Gebhart and his coworkers for vertical flat plates and also by the present experimental results.

The Asymptotic Solution

At large distances from the cylinder ($\eta \geq \eta_e$), basic flow quantities F , F' , F'' , F''' , H and H' acquire constant values and some terms drop from the governing equations, while others acquire constant coefficients. The resulting "asymptotic" equations are linear differential equations with constant coefficients; for which methods of solutions are readily available in classical mathematical references. Because the tangential velocity component and the temperature difference diminish together with their derivatives beyond the edge of the boundary layer, i.e. for $\eta \geq \eta_e$, we must have $F' = F'' = F''' = H = H' = 0$. The normal velocity component acquires a constant value F_e in this region, hence $F = F_e$. Substitution of these values into equations (3-16) gives, for the region outside the boundary layer,

$$\begin{aligned} \phi'''' + 3F_e \phi''' + (iG\beta - 2\alpha^2) \phi'' - 3F_e \alpha^2 \phi' + (\alpha^4 - i\alpha^2 G\beta) \phi \\ = -(\zeta' + i\alpha \zeta \cot(x)) \end{aligned} \quad (3-18a)$$

$$\text{and } \zeta'' + 3F_e N_p \zeta' + (iN_p G\beta - \alpha^2) \zeta = 0 \quad (3-18b)$$

The solution of the above equations is obtained following conventional mathematical procedures as given in Appendix C, where the solution is obtained as equations (C-12a and b), namely:

$$\phi = C_1 e^{\gamma_1 \eta} + C_2 e^{\gamma_2 \eta} + C_3 e^{\gamma_3 \eta} \quad (3-19a)$$

and
$$\zeta = -C_3 \left[\frac{\gamma_3^2 + 3F_e \gamma_3^2 + (iG\beta - 2\alpha^2)\gamma_3^2 - 3F_e \alpha^2 \gamma_3 + (\alpha^4 - i\alpha^2 G\beta)}{\gamma_3 + i\alpha \cot(x)} \right] \quad (3-19b)$$

In these equations

$$\gamma_1 = -|\alpha_r| + i\alpha; \quad (3-20a)$$

$$\gamma_2 = -3/2 F_e \pm 1/2 \left[9.0 F_e^2 + 4(\alpha^2 - iG\beta) \right]^{1/2} \quad (3-20b)$$

$$\gamma_3 = -3/2 F_e N_{Pr} \pm 1/2 \left[9.0 F_e^2 N_{Pr}^2 + 4(\alpha^2 - iG\beta N_{Pr}) \right]^{1/2} \quad (3-20c)$$

Only roots with negative real parts should be chosen for the γ values to give the actual case of "damped solution" outside the boundary layer.

Solution Within the Boundary Layer

The method outlined by Kaplan [22] for solving the Orr-Sommerfeld equations and by Mach [29] for solving the coupled equations is used. Starting by assuming $C_1 = 1$ and $C_2 = C_3 = 0$ and $\eta = \eta_e$, an assumption of α_r and β_r would give, from equations (3-19 and 20) values of $\phi_{I,e}$ and $\zeta_{I,e}$ at the edge of the boundary layer. Using their values and a fourth order Runge-Kutta integration method, a solution of equations (3-16) for ϕ_I and ζ_I within the boundary layer is obtained. This gives also the derivatives ϕ_I' , ϕ_I'' , ϕ_I''' and ζ_I' from which the values of the functions ϕ_I and ζ_I and their derivatives are determined at the surface ($\eta = 0$). This is repeated to determine ϕ_{II} and ζ_{II} for $C_2 = 1$ and $C_1 = C_3 = 0$; and ϕ_{III} and ζ_{III} for $C_3 = 1$ and $C_1 = C_2 = 0$ and their respective derivatives.

The next step is to determine the constants C_1 , C_2 and C_3 . This could be obtained from the values of the functions and derivatives at the surface from the following boundary conditions that denote, respectively, the absence of the tangential and normal disturbance velocities, and of the temperature disturbance at the surface, namely:

$$\phi(0) = C_1 \phi_I + C_2 \phi_{II} + C_3 \phi_{III} = 0 \quad (3-21a)$$

$$\phi'(0) = C_1 \phi_I' + C_2 \phi_{II}' + C_3 \phi_{III}' = 0 \quad (3-21b)$$

$$\zeta(0) = 0 \quad (3-21c)$$

The last expression is evaluated from the values ζ_I , ζ_{II} and ζ_{III} calculated through the relatively complex expression of equation (3.19b).*

However, a simultaneous solution of the above three equations for C_1 , C_2 and C_3 would give zero values to these constants. To have a non-trivial solution a normalizing condition is used to replace one of the above homogeneous equations, namely:

$$\phi(\eta_e) = C_1 e^{\gamma_1 \eta_e} + C_2 e^{\gamma_2 \eta_e} + C_3 e^{\gamma_3 \eta_e} = 1 \quad (3-22)$$

Equations (3-21a,b) and (3-22) would then be used to determine the unknown coefficients. A check on the validity of the solution, and hence on the

* It should be noted that whereas $\zeta_I = \zeta_{II} = 0$ at the edge of the boundary layer, they have finite values at the surface.

correctness of the initial assumption of the eigenvalues α_r and β_r , is the verification of the deleted relation, equation (3-21c).

For computations initial guessing for α_r and β_r is made, and an iterative technique is used to obtain their correct values that correspond to the assumed values of the other parameters, namely, G , N_{Pr} , α_i , and β_i . The standardized Quasi Newton subroutine of the C.D.C. computer was used for this iteration; fast convergence was always achieved with convergence criterion taken to be $|\zeta(0)| \leq 10^{-4}$. Computer program is given in Appendix I.

Computational Results

Neutral stability curves were computed for position angles x^+ ranging from 30 to 150 degrees and the instability parameter G going up to 200. This range of position angles was chosen because Hermann's solution is not very accurate outside this range as described in Appendix A. Indeed, the flow at $x^+ < 30$ degrees is highly stable under normal conditions and there seems to be no point in considering it in an instability analysis. On the other hand, highly unstable separated flow is expected at positions of $x^+ > 150$ degrees.

Since instability for the considered range of position angles x^+ starts at values of the instability parameter G less than 200, the instability information sought is obtained in the range of G from 0 - 200. Also, highly unstable flow is expected for values of G larger than 200 due to disturbance amplification and the assumptions of linear stability theory are no longer valid.

Results for the considered range are shown in Figures (3-1 and 2). These curves show the trend noted by Hieber and Gebhart [17], namely that two modes of neutral stability exist and merge to give the nose shaped curves shown. The upper part of the curve is attributed to the hydrodynamically amplified oscillations, i.e., oscillations that would be amplified has the temperature oscillations been negligible. For this reason this part represents the "hydrodynamic instability mode." The lower curve is obtained because of temperature instability effects, and this part is, therefore, called the "thermal instability mode."

Present results are compared with those of Haaland [14] for inclined plates. It should be noted that the comparison bears no physical significance. This is because flow over a cylinder is actually a flow over a surface of varying inclination angle. The comparison is held, therefore, between the neutral stability curves obtained by solving the governing equations for fixed angles for both cases. It was found, however that flow around horizontal cylinders gives more unstable "solutions," and that the difference is more pronounced for the hydrodynamically amplified oscillations as shown by Figure (3-3). This increased instability is due to the added centrifugal force on the fluid.

Results for a physical flow situation, given by $N_{Gr,r} = 2.5 \times 10^6$, are shown in Figures (3-4 and 5). In Figure (3-4) the Neutral Stability curve and constant α_i curves are shown on the $x^+ - \beta_r$ plane. Constant frequency lines are also drawn; they are determined from equations (3-11, 14, and 15) as follows:

$$\beta_r \frac{vU^*}{r^2 \delta} = 2\pi \hat{f}$$

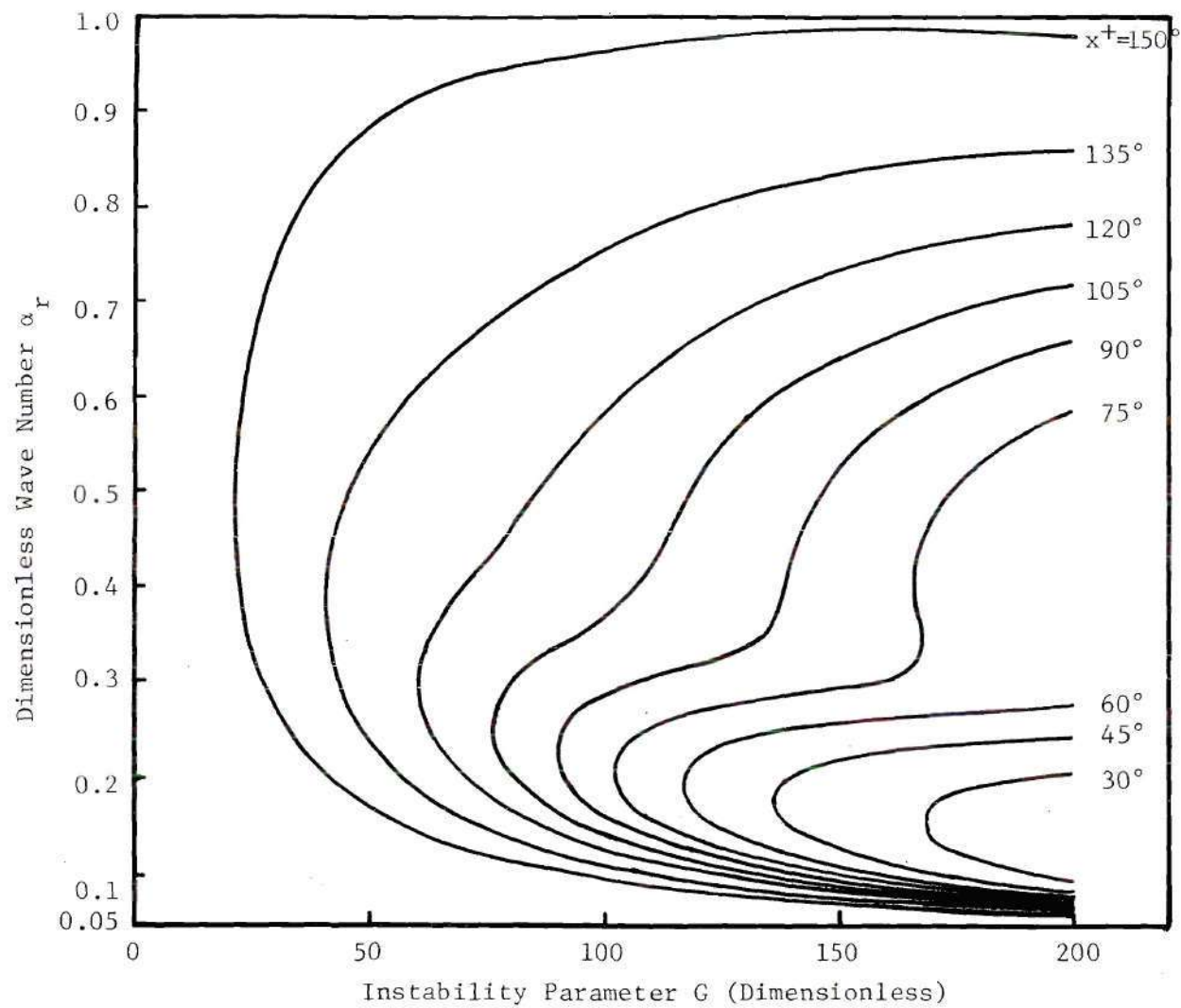


Figure 3.1 Neutral Stability Curves for Natural Convection Around Horizontal Cylinders in Air; $N_{Pr} = 0.733$.

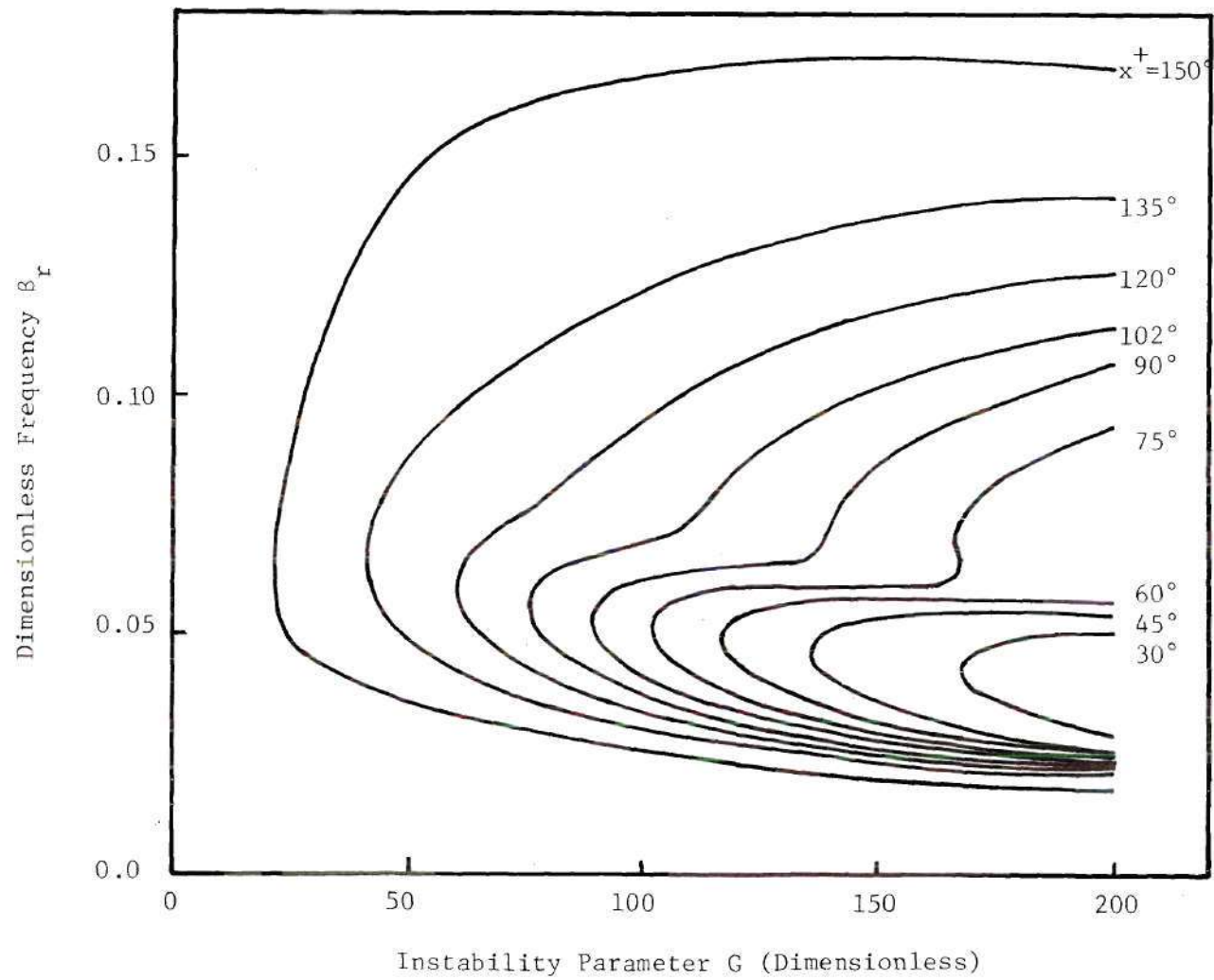


Figure 3-2 . Neutral Stability Curves for Natural Convection Around Horizontal Cylinders in Air; $N_{Pr} = 0.733$.

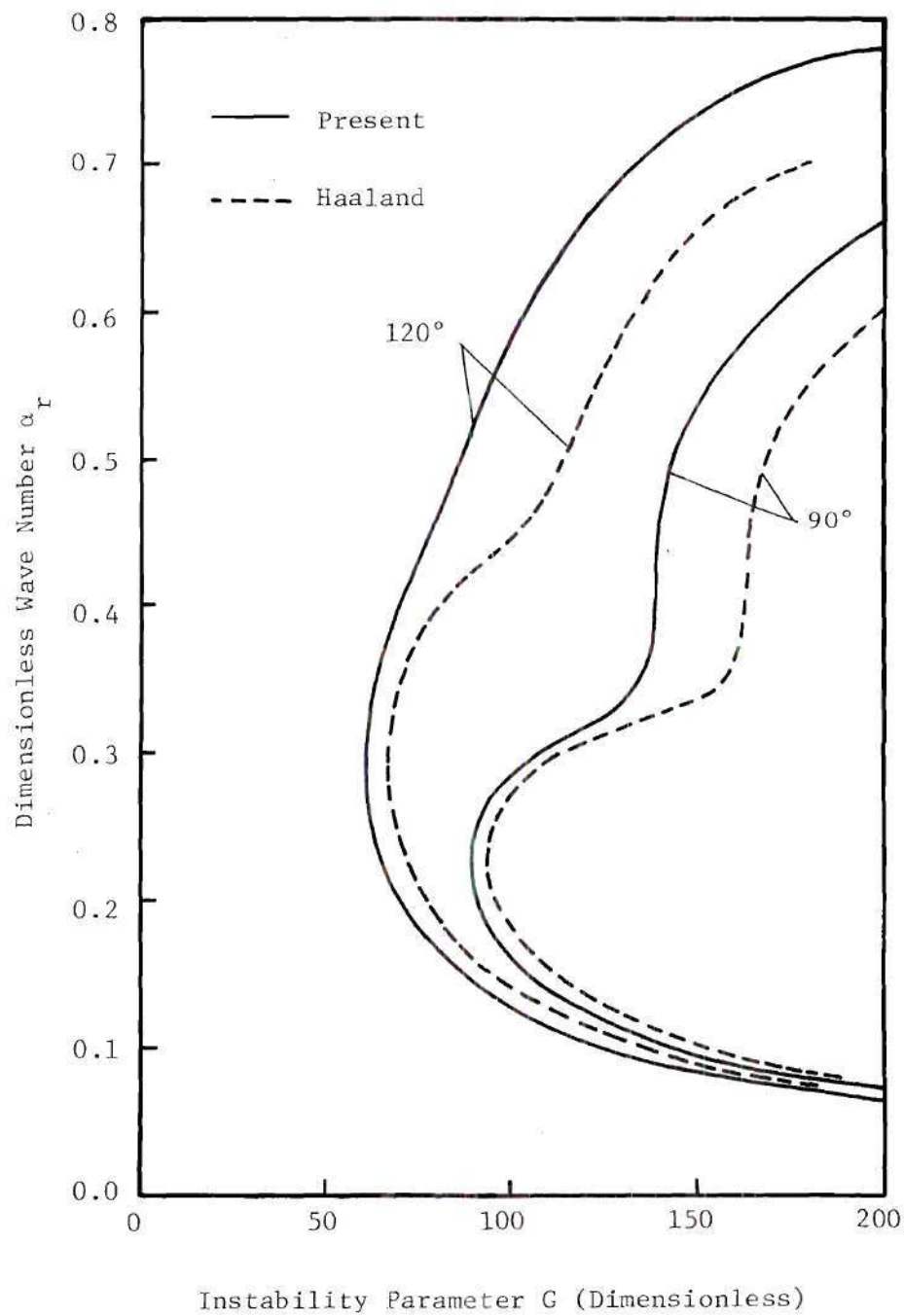


Figure 3-3 . Comparison of the Present Results and Those of Haaland [14] for Inclined Plates.

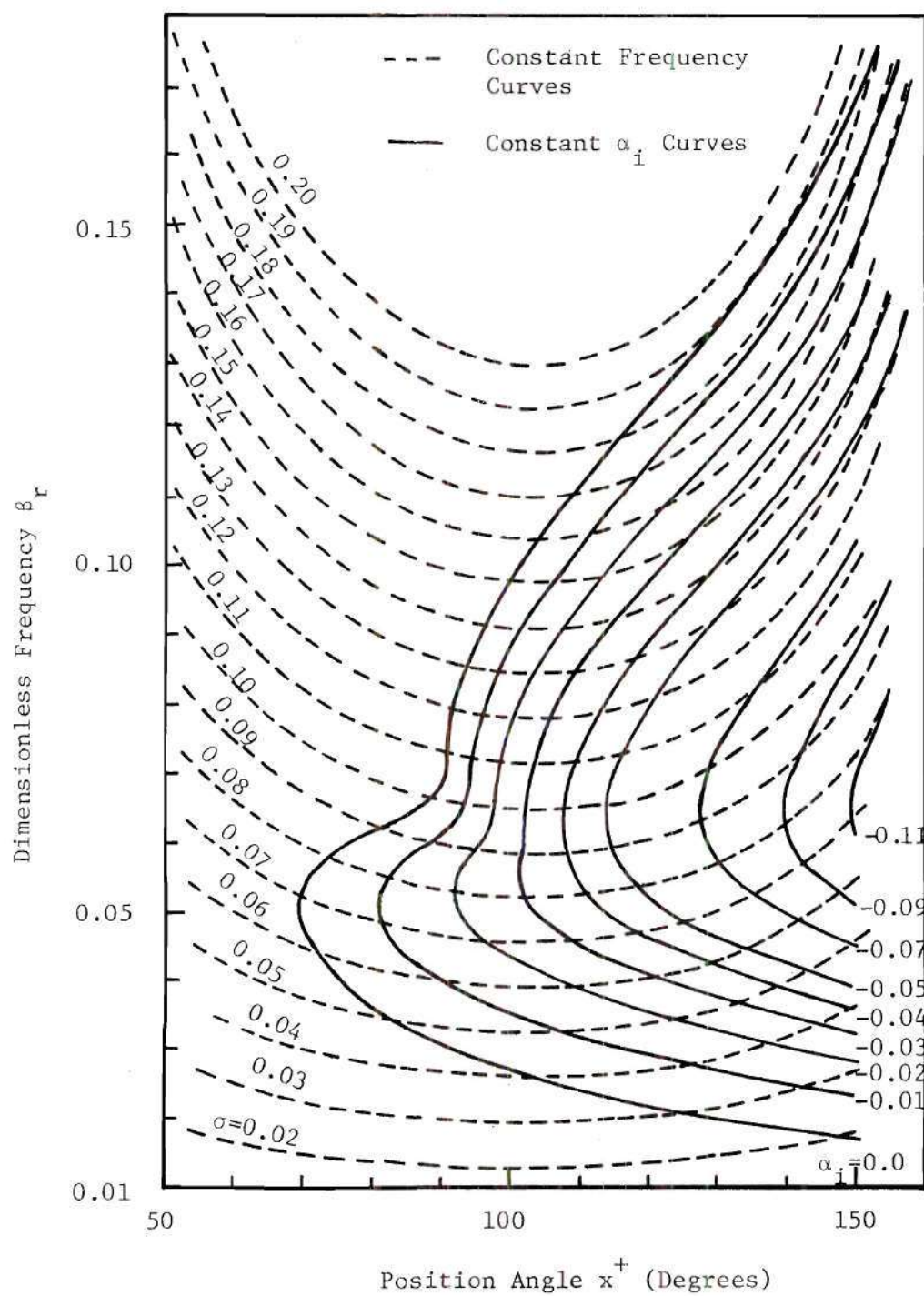


Figure 3-4 . Instability Curves for Horizontal Cylinders;
 $N_{Pr} = 0.733$, and $N_{Gr,r} = 2.5 \times 10^6$.

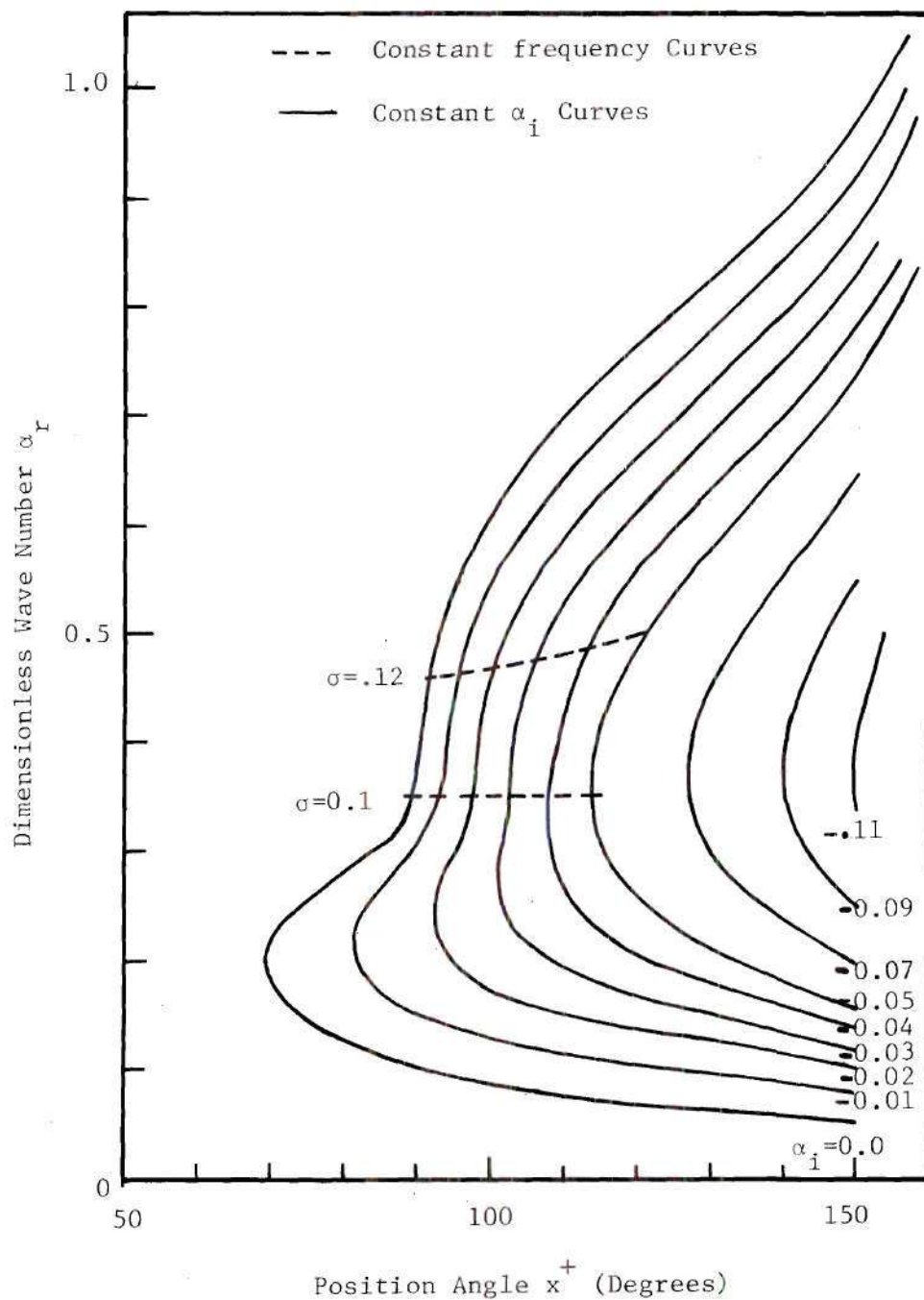


Figure 3-5 . Instability Curves for Horizontal Cylinders;
 $N_{Pr} = 0.733$, and $N_{Gr,r} = 2.5 \times 10^6$.

Here \hat{f} is the frequency in Hz, hence using equations (A-15, 25, and 26) gives

$$\frac{2\pi \hat{f} r^2}{\gamma N_{Gr,r}^{3/4}} \beta_r = \frac{1}{\delta \sin(x)} \quad (3-23)$$

Taking

$$\sigma = \frac{2\pi r^2 \hat{f}}{\gamma N_{Gr,r}^{3/4}} \quad (3-24)$$

gives $\beta_r = \frac{\sigma}{\delta \sin(x)} \quad (3-25)$

Equation (3-25) is used to draw the constant reduced frequency, σ , lines which represents to scale the physical frequency \hat{f} .

Some of these lines are further mapped into the $x^+ - \alpha_r$, plane of Figure (3-5) which shows that constant frequency disturbances would propagate at an approximately constant wave number α_r and hence at a wavelength

$$L = 2\pi / \alpha_r = 2\pi \delta / \alpha_r$$

This wavelength L is, therefore, proportional to the boundary layer thickness δ , a fact which supports the initial assumption that s and n are of order δ .

Figure (3-4) is further mapped into the $x^+ - \hat{f}$ plane of Figure (3-6) It could be seen from these two figures that some of the constant-frequency lines of high values intersect the neutral stability curve and the constant

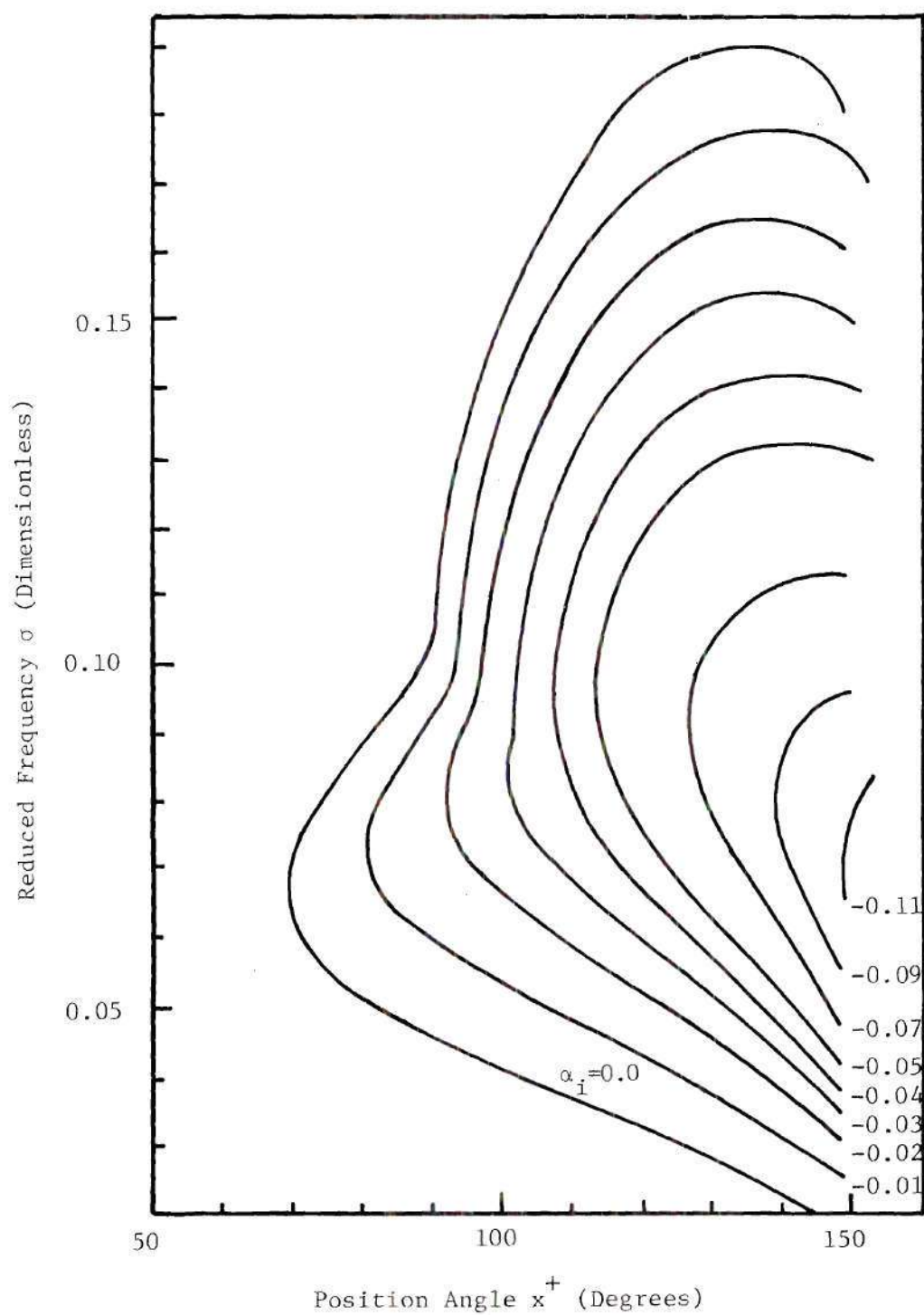


Figure 3-6 . Frequency Response of Natural Convection Flow Around Horizontal Cylinders;
 $N_{Pr} = 0.733$, $N_{Gr,r} = 2.5 \times 10^6$.

α_i lines twice; they clear the amplifying region beyond some angle further downstream. This may be difficult to understand physically and may be attributed to the invalidity of Hermann's solution at large angular positions, as explained in Appendix A.

Amplification rates are calculated for oscillations of different frequencies, where

$$\hat{A}/\hat{A}_N = e^{i\bar{\alpha} \Delta x} \quad (3-26)$$

In this relation \hat{A}_N denotes the amplitude at point x_N of neutral stability, and \hat{A} the amplitude at a point x downstream of x_N and a distance Δx from it. Taking the limit as Δx vanishes, the above relation gives

$$\hat{A}/\hat{A}_N = \text{Exp} \left(\int_{x_N}^x \bar{\alpha}_i dx \right) \quad (3-27)$$

Amplification with position angle x^+ are computed from equation (3-27) and plotted in Figures (3-7a and b) for different frequencies, i.e., different values of reduced frequency σ . As could be seen, oscillations with $\sigma = 0.08$ to 0.09 have the highest amplification rates in the considered case, all others have less amplification rates. This is shown more clearly in Figure (3-8) which is a plot of the relative amplitude \hat{A}/\hat{A}_N at an angle of 150 degrees versus the reduced frequency σ . The conclusion is that the frequency filtering phenomenon exists in the present case of natural convection around horizontal cylinders.

It is noted that the reduced frequency σ is a function of the total Grashof number $N_{Gr,r}$, the cylinder radius r and the kinematic viscosity ν

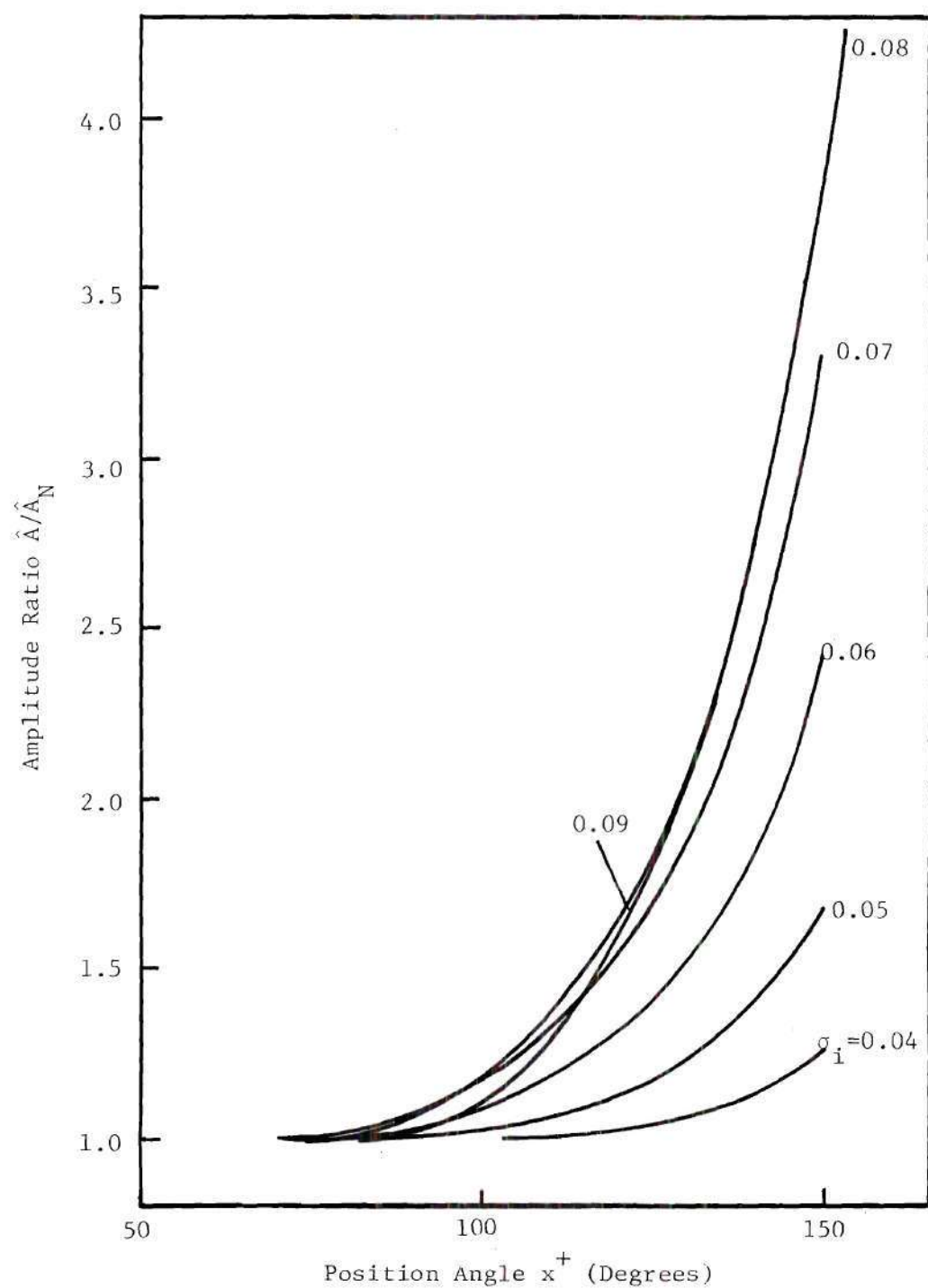


Figure 3-7a . Amplification Rates for Disturbances of Different Frequencies [(a) $\sigma = 0.04$ to 0.09];
 $N_{Pr} = 0.733$, $N_{Gr,r} = 2.5 \times 10^6$.

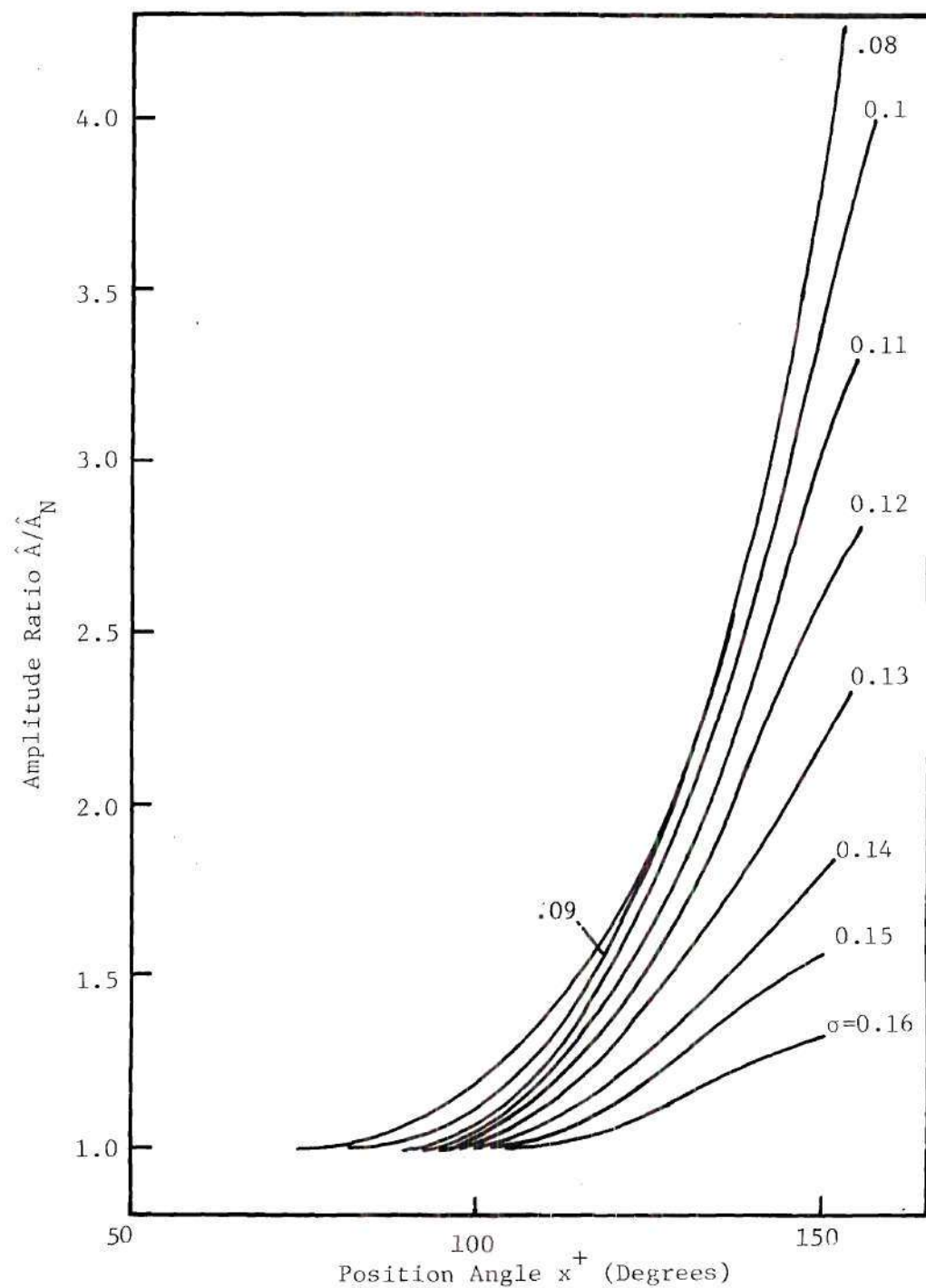


Figure 3-7b . Amplification Rates for Disturbances of Different Frequencies [(b) $\sigma=0.08-0.16$]; $N_{Pr} = 0.733$, $N_{Gr,r} = 2.5 \times 10^6$.

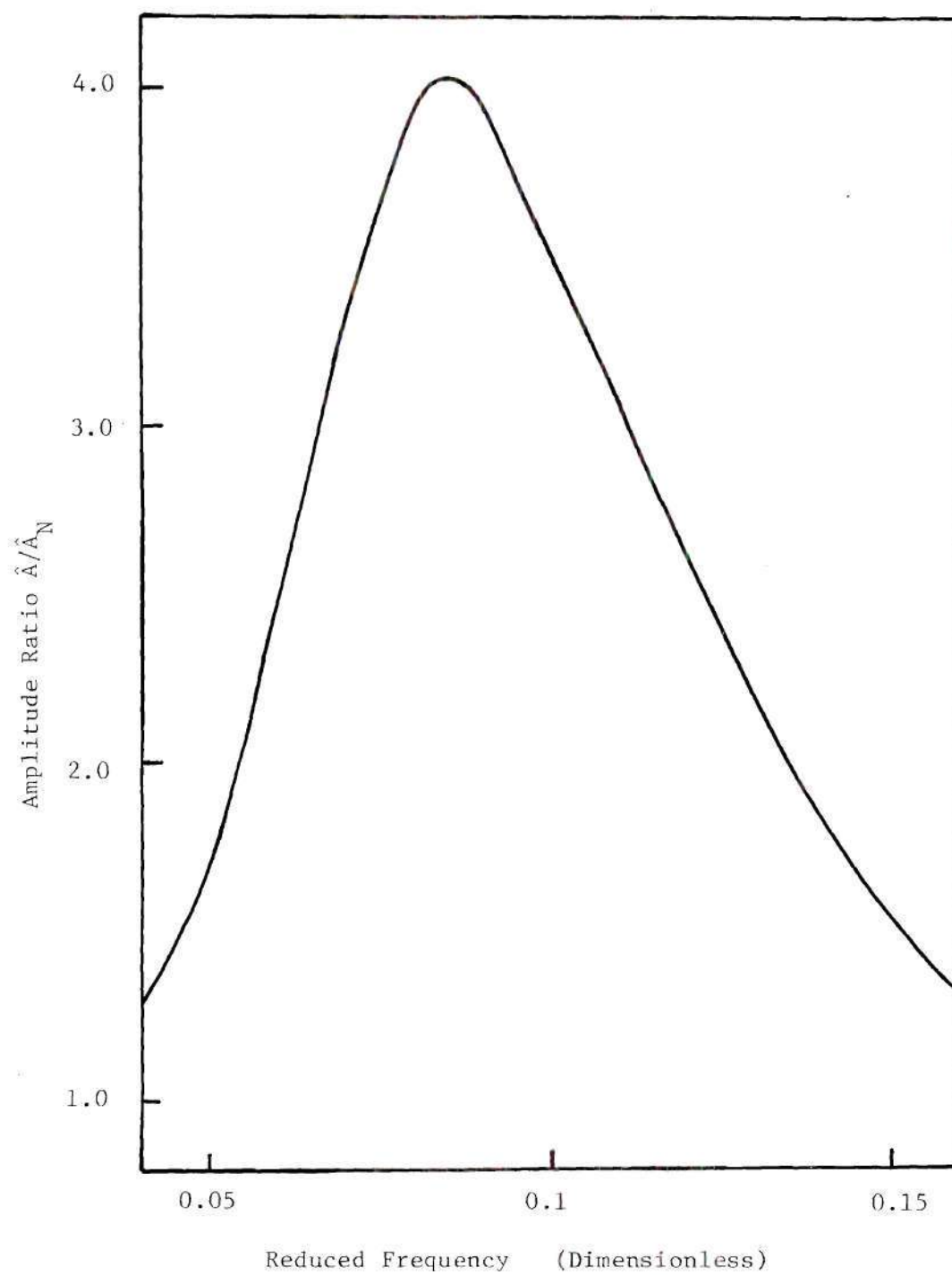


Figure 3-8 . Distribution Curve for the Amplitude Ratio \hat{A}/\hat{A}_N at a Position Angle $x^+ = 150^\circ$;
 $N_{Pr} = 0.733$, $N_{Gr,r} = 2.5 \times 10^6$.

as could be seen from equation (3-24). The favorite frequency band is, therefore, a function of the cylinder radius and the temperatures of the surface of the cylinder and the surrounding fluid. Since $N_{Gr,r}$ tends to infinity gives $\sigma = 0$, a unique value for the dominant frequency would be expected in this particular case. Indeed, this would be the case of a flat plate already worked out by Gebhart and his coworkers.

CHAPTER IV

EXPERIMENTAL APPARATUS

Experiments were carried out to determine the neutral stability curve of a natural convection flow around a horizontal cylinder in air to compare it with the theoretically determined one.

The experimental cylinder used is made of aluminum; it is 152 mm (6 in.) diameter and 280 mm (11 in.) long. Hot water of practically constant temperature was used to heat this experimental cylinder. A hot wire probe with a 5μ wire was used for velocity and temperature measurements.* Two traverse mechanisms were used to adjust accurately the position of the hot wire sensor, both tangentially and radially. A $12.7\mu\text{m}$ (0.0005 in.) diameter alumel heating wire was placed in the boundary layer and used to introduce controlled temperature oscillations. An enclosure was built around the experimental cylinder to isolate it from the uncontrolled disturbances of the room air. The details of the experimental set up are given below.

Experimental Cylinder

An aluminum tube 152 mm (6 in.) diameter and 9.5 mm. ($3/8$ in.) thick was used. Aluminum was preferred, being a good conductor, cheap, and readily available. A copper sheet is rolled, soldered, and placed as

* The hot wire was preferred to other methods such as dust particle trajectories [10] or quartz fibre anemometer [40], being a method for measuring both temperature and velocity and because it gives an electrical signal that can be easily recorded.

a core for the aluminum cylinder as shown in Figure (4-1). The resulting 6.4 mm (1/4 in.) annulus forms the conduit for the heating water. This design results in high hot water velocity and, hence, the high heat transfer coefficient necessary for the uniformity of surface temperature; it further requires a small flow rate of heating water. This design together with the thick cylinder wall, succeeded in maintaining the surface temperature variation within $\pm 0.08^\circ\text{C}$ ($\pm 0.15^\circ\text{F}$) with reasonable hot water flow rates.

Sixteen thermocouples are used to measure the surface temperature of the cylinder. Eight thermocouples are introduced in the cylinder wall from each side. They could be moved in the axial direction of the cylinder to within 38 mm (1.5 in.) from the mid cross section. Copper constantan thermocouples were cemented with 2.4 mm (3/32 in.) outside diameter brass tubes that can slide within corresponding 3.2 mm (1/8 in.) outside diameter similar tubes that are embedded in the cylinder wall. Seven thermocouples are placed 30 degrees apart, covering the 180 degrees of the circumference of one side of the cylinder. An eighth thermocouple is placed on the other side of the cylinder to check the symmetry of the flow.

Hot Wire Probe

A subminiature, boundary layer type probe was used to measure both velocity and temperature. It has curved supports to minimize conduction through them which is very important for the accurate measurements of temperature. The probe has a pin that protrudes 0.153 mm (0.06 in.) from the wire as shown in Figure (4.2). This allows an accurate measurement of distance from the cylinder surface. With the pin touching the cylinder

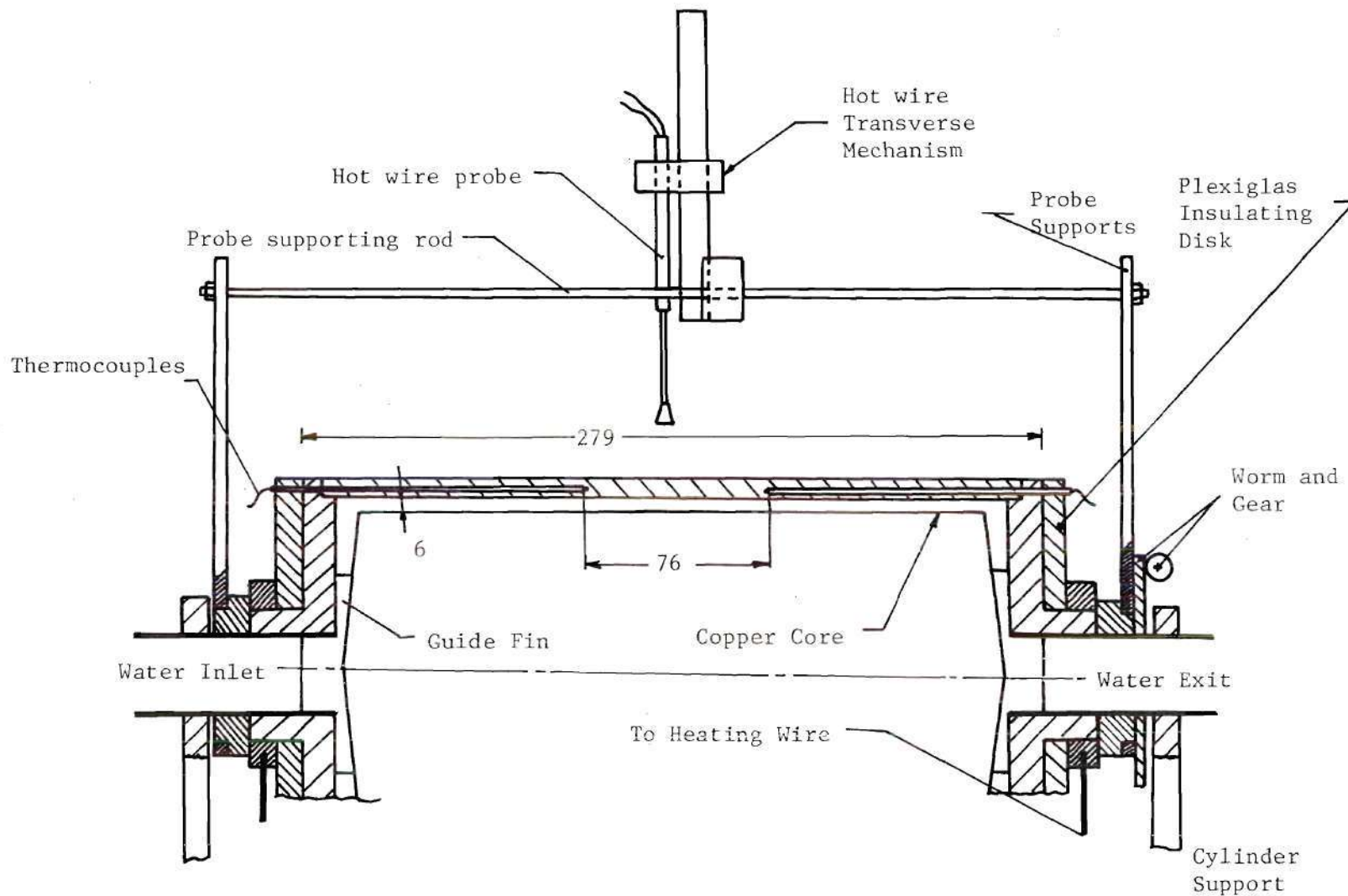


Figure 4-1 . Plan of Cylinder Assembly
(Dimensions in mm)

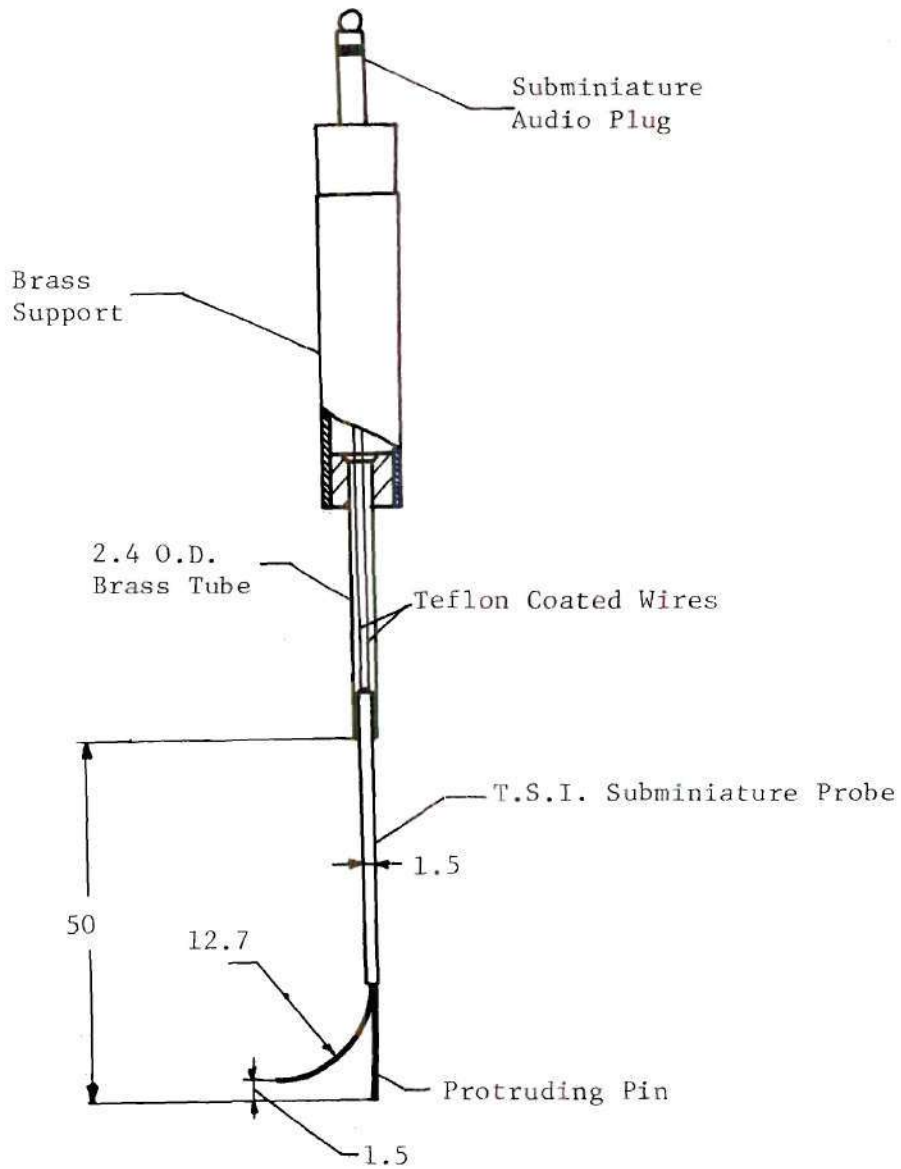


Figure 4-2 . Hot Wire Probe.
(Dimensions in mm)

surface, the wire is calculated to be at 0.5 mm (0.02 in.) from the surface. The distance from the tip of the pin to the wire was measured by a traversing microscope with an accuracy of 0.005 mm. The sensor is a tungsten wire 5 μ m diameter and 8 mm long. These dimensions were calculated to maintain the wire at practically uniform temperature and such that its frequency response would be much higher than needed for the experiments. These calculations are given in Appendix D. The probe support is made of two brass tubes of different diameters matched to each other by a small brass sleeve soldered to both tubes. The sensor stem is centered and cemented to the smaller tube. The electric leads are connected to a subminiature audio plug cemented to the outer end of the larger tube.

The probe was controlled and monitored by a T.S.I. model 1503A bridge in combination with a variable decade resistor, a monitor and power supply, and a signal conditioner. A digital voltmeter was used to take readings for velocity measurements.

Traverse Mechanism

A worm and gear of reduction ratio 180:1 are used for accurately placing the wire in the required angular position. An accuracy of 0.02 degree could be achieved in determining this position. A vernier with a resolution of 0.25 mm (0.01 in.) was used for accurately locating the wire in the radial direction. The movement in this direction is obtained through a threaded rod moving through a fixed nut; as shown in Figure (4-3).

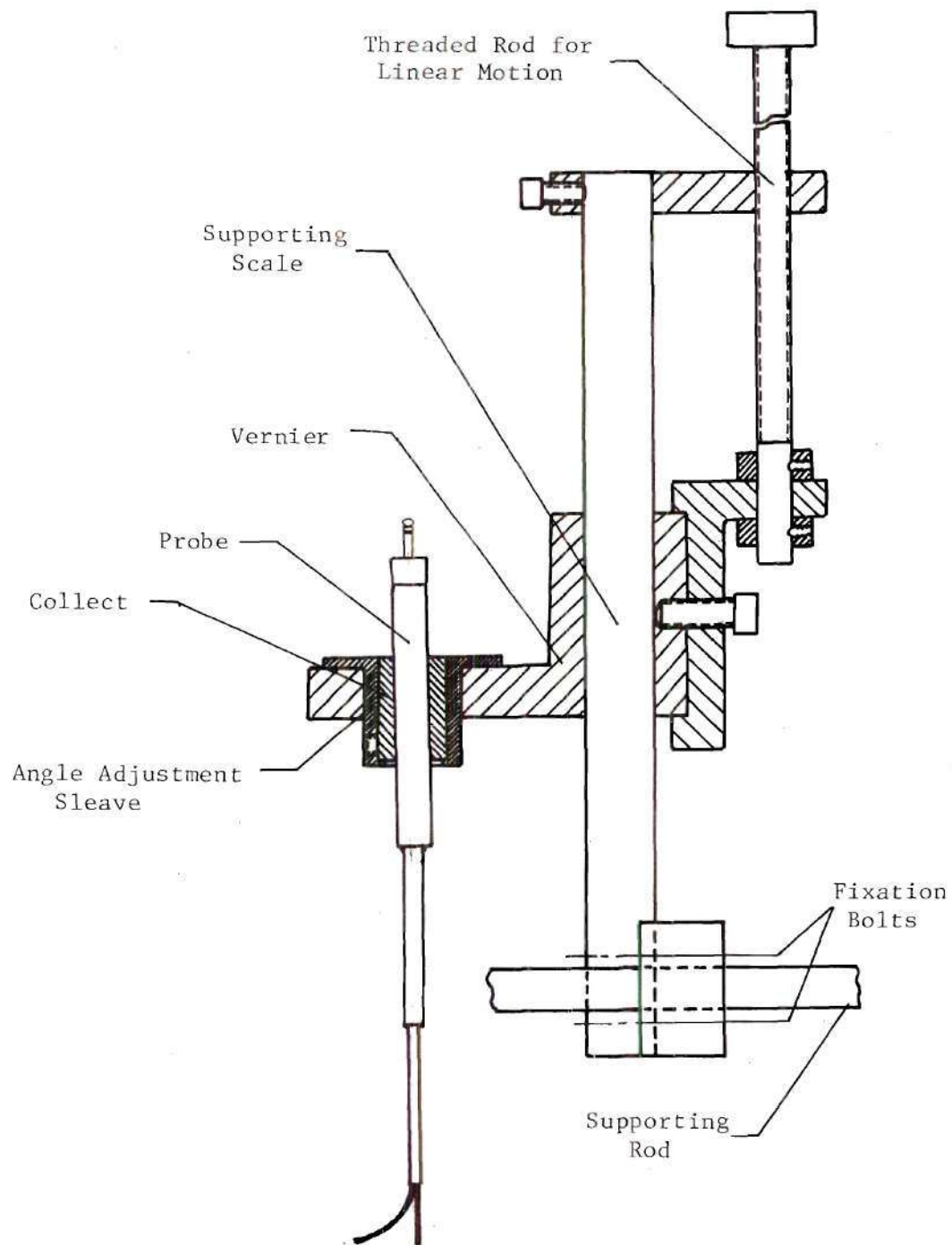


Figure 4-3 . Probe Traversing Mechanism.

Heating Wire

An alumel heating wire 12.7 μ (0.0005 in.) diameter is used to induce temperature oscillations of controlled amplitude and frequency in the boundary layer. The wire is 240 mm (9 1/2 in.) long and placed parallel to the cylinder axis. Rough control of the radial and tangential location are only available. Since the exact location of the wire was believed, and proved, to be of little importance. The wire is coupled to an HP-3310 function generator which is capable of generating sinusoidally oscillating voltage of controlled frequency in the range from 5×10^{-4} to 5×10^6 Hz. This wire was calculated to respond, with very small damping, to frequencies in the needed range of 0 - 4 Hz. These calculations are given in Appendix H. A sketch showing the cylinder, the traverse mechanism, the hot wire and the heating wire support are given in Figure (4-1).

Enclosure

An enclosure 75 x 90 x 180 cm high is built using steel angles, plywood, carton boards and plexyglass in which the experimental cylinder was centered, 120 cm above the floor. The enclosure top is completely covered to isolate the experimental space from the rest of the room air. Two transverse openings 15 cm high are left at the bottom of the two sides to allow air to enter and circulate in the enclosure. The use of this enclosure, together with the closing of the air conditioning and ventilation room grills were necessary to practically eliminate uncontrolled instabilities.

Air temperature in the enclosure was measured by a copper-constantan thermocouple placed about 22 cm from the cylinder surface.

Calibration of the Hot Wire Probe

The hot wire probe was calibrated for both temperature and velocity measurements, the following procedures were followed.

Temperature Calibration

The hot wire was calibrated as a resistance thermometer in a water bath of constant temperature against a copper constantan thermocouple. The results are shown in Figure (4-4). Its sensitivity was found to be $0.0475 \times (1 \pm 0.01)$ ohm/F.

Velocity Calibration

The hot wire was placed on a rotating disk attached to a variable speed motor as shown in Figure (4-5). The anemometer was placed such that the wire was set radially at 10 cm (4 in.) from the center of the disk. The disk and the probe were placed in an enclosure to isolate them from the air currents in the room, and those due to the motor movement and heat dissipation. The rotational speed of the disc could be varied in the range of 0 to 50 rpm, and was measured by a stop watch. A voltage velocity curve was obtained and is given in Figure (4-6). Except for three extreme points, the reproducibility of these results was found to be within ± 2 percent.

The hot wire was set at a constant temperature difference of $71 \pm 0.1^\circ\text{C}$ from the surrounding. This was done by increasing the wire resistance by 6.07 ohm above its cold value. With the temperature difference between the wire and surroundings set constant at each reading, the power dissipation from the wire would indicate the velocity. By this method, one calibration curve would be enough for velocity measurements in a non-isothermal flow, had the variation in properties be negligible.

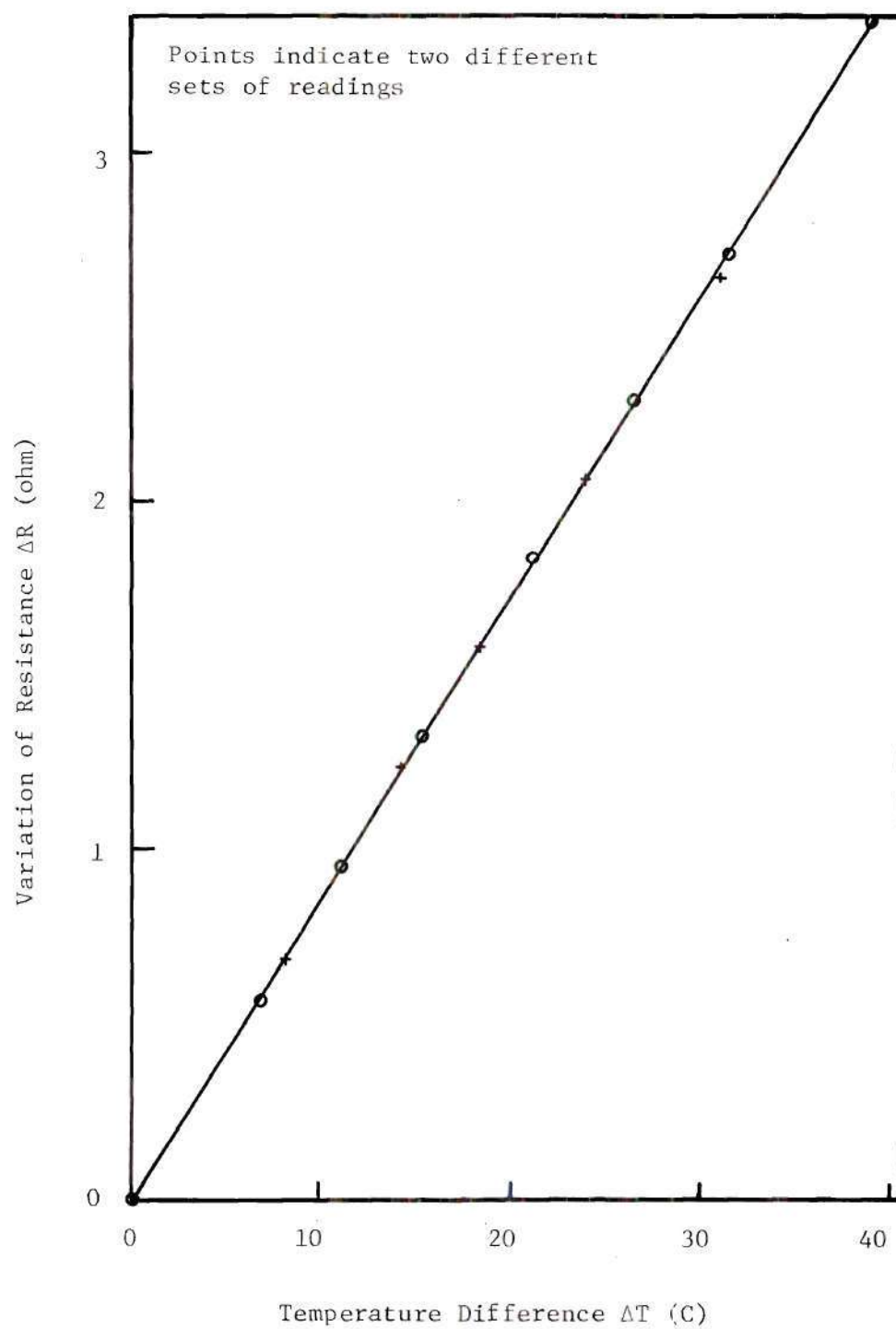


Figure 4-4 . Temperature Calibration of Sensor in the Range 20 to 60°C.

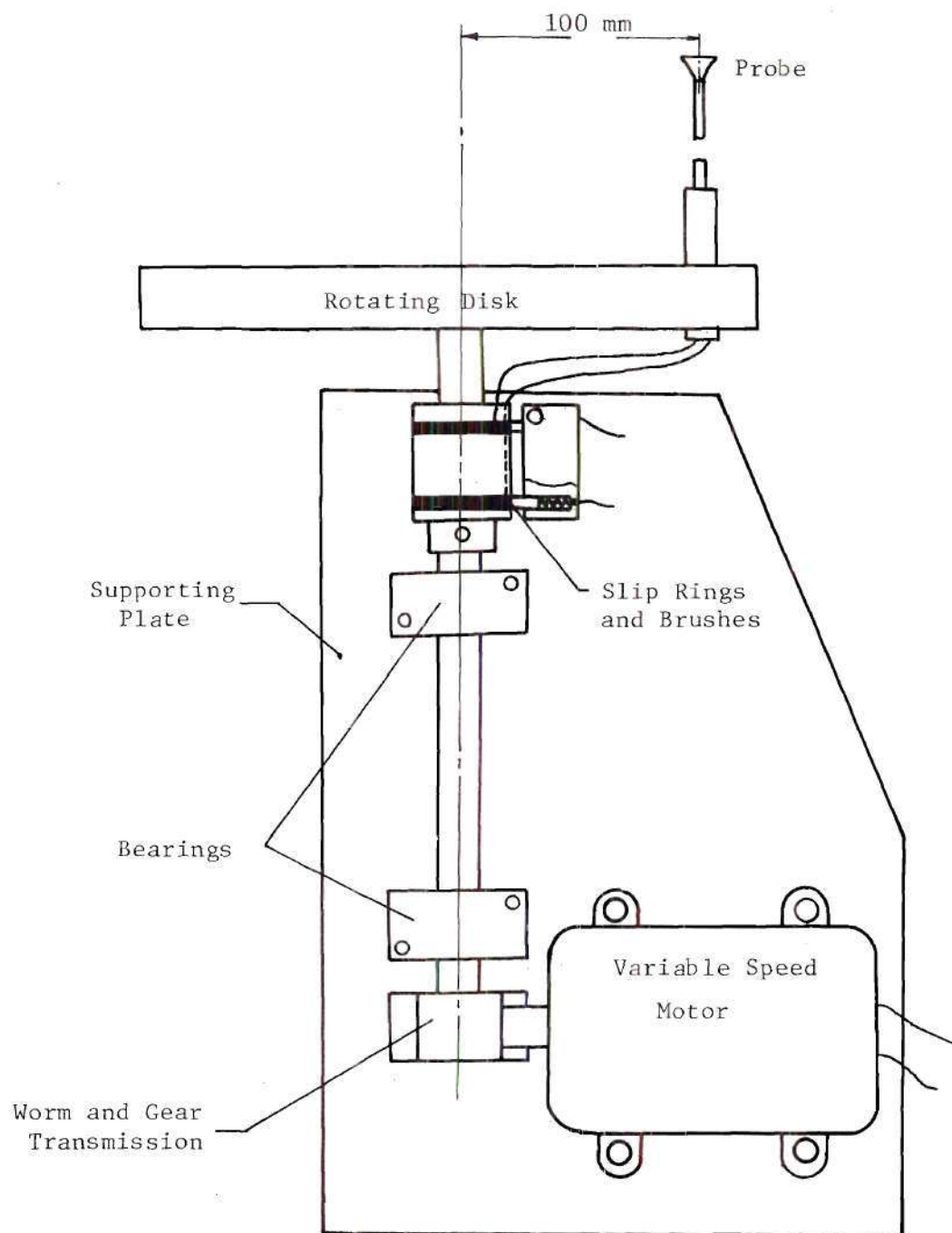


Figure 4-5 . Elevation of Velocity Calibration Apparatus.

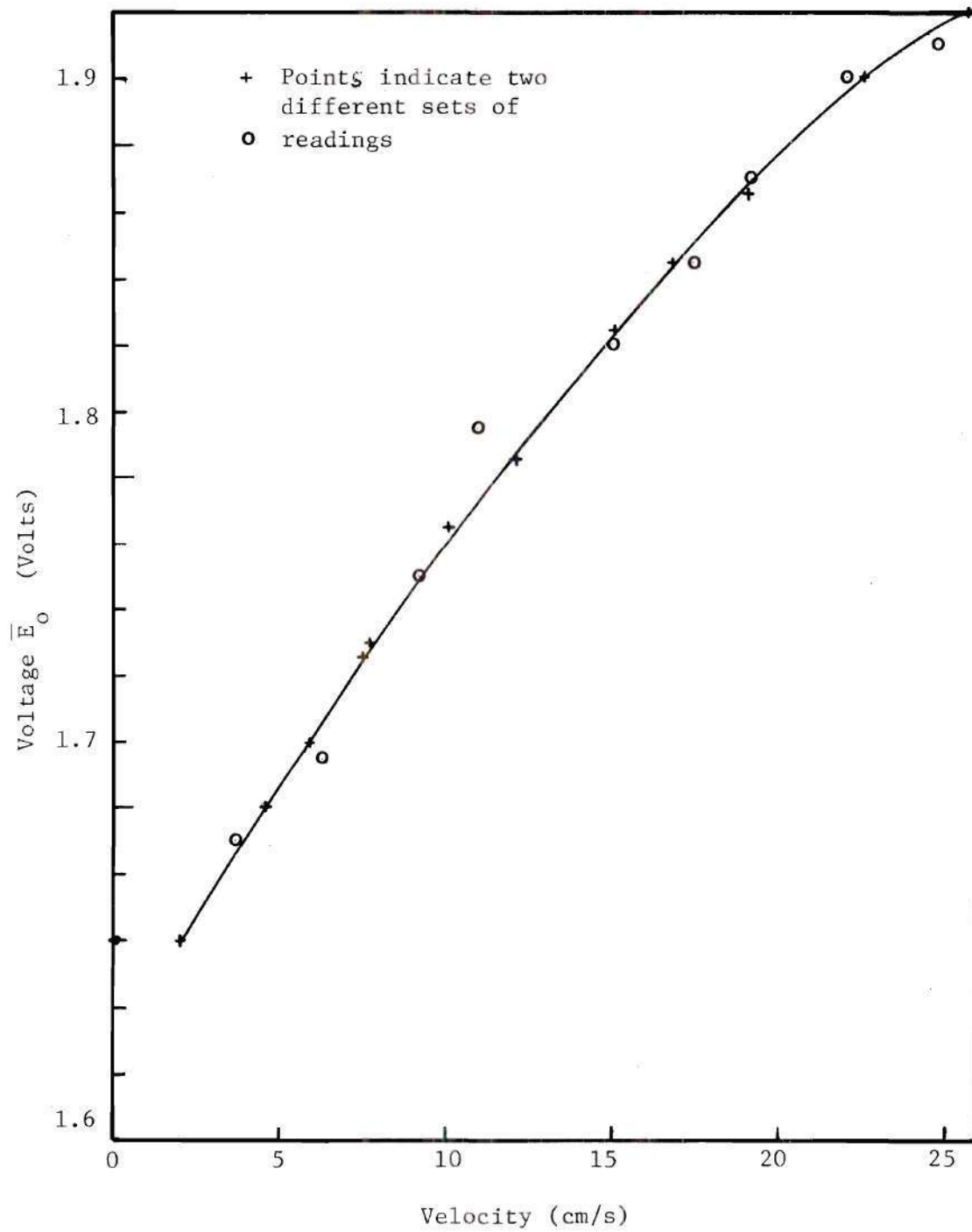


Figure 4-6 Velocity Calibration of Sensor.

According to Dring and Gebhart [8], natural convection from the wire would have a negligible effect on the hot wire reading if $N_{Gr} < .04N_{Re}^2$ for the wire.* According to this, natural convection effects could be neglected in the present case for measured velocities larger than 1.6 cm/s. As could be noted from the calibration curve, Figure (4-6), the zero velocity voltage and the voltage corresponding to a velocity of 2 cm/s are the same. This is attributed to the interaction between forced and natural convection from the wire. This limit of 2 cm/s was taken, therefore, to represent the experimental lower limit of velocity measurement for the use of this probe.

* Diameter of the wire is taken to be the characteristic length.

CHAPTER V

EXPERIMENTAL RESULTS

Two groups of measurements were carried out. The first was to determine the basic temperature and velocity profiles; the other was to determine the neutral stability curve. The results showed reasonable agreement with theory. Details of the procedure and the obtained results are given below.

Steady State Measurements

Measurements were taken for temperature and velocity fields at position angles of 50 to 130 every 20 degrees. For each of these position angles, a profile was determined from readings at about 24 positions across the boundary layer.

During any experiment, air and water temperatures were constant within $\pm 0.1^\circ\text{C}$ ($\pm 0.2^\circ\text{F}$). The surface temperature varied within $\pm 0.08^\circ\text{C}$ ($\pm 0.15^\circ\text{F}$). Consequently, the error in temperature difference measurements is within a maximum of $\pm 0.275^\circ\text{C}$ ($\pm 0.55^\circ\text{F}$). This corresponds to an error in the total Grashof number of less than ± 1.5 percent.

The error in angle measurements is taken to be half the resolution, i.e. ± 0.02 degrees. The corresponding errors in the functions $f(x^+)$ and $g(x^+)$ are negligible.

The dimensionless normal distance η is calculated from the expression

$$\eta = \frac{n}{r} N_{Gr,r}^{1/4} g(x^+) \quad (5-1)$$

and the error in η due to errors in n , $N_{Gr,r}$, and $g(x^+)$ could be calculated from

$$\Delta\eta = \Delta n + \frac{1}{4} \Delta N_{Gr,r} + \Delta g \quad (5-2)$$

The error in the normal distance n , is taken to be half the resolution, i.e., ± 0.127 mm (± 0.005 in.). This gives an error of ± 0.8 percent of the boundary layer thickness. Hence,

$$\Delta\eta = \pm(0.008 + \frac{1}{4} \times 0.015 + 0) = \pm 0.012 = \pm 1.2\%$$

Local Temperature Measurements

The wire cold resistance was measured at each location. It was used, together with the reading of the air thermocouple and the results of the sensor temperature calibration to determine the local air temperature. The air in temperature measurements due to end effects on wire temperature was estimated in Appendix D to be -1.3 percent of the total temperature difference across the boundary layer. Resistances could be measured to within 0.01 ohm which leads to an error of ± 0.2 percent. Uncertainty of wire temperature calibration was found to be of the order ± 1 percent, and that of air and surface temperature to be of the order of ± 1.5 percent. Total error in temperature measurements would, therefore, be

$$\Delta T = -1.3 \pm .2 \pm 1 \pm 1.5 = -1.3 \pm 2.7 \text{ percent.}$$

The dimensionless temperature profiles $H(\eta)$ are calculated from the relation

$$H(\eta) = \frac{T - T_{\infty}}{T_c - T_{\infty}}$$

where T_{∞} is the air temperature outside the boundary layer and T_c is the surface temperature.

Dimensionless temperature profiles $H(\eta)$ are plotted versus η in Figure (5-1). Results are compared to the theoretical curve of Hermann and good agreement could be seen. The points are, however, slightly below the theoretical curve, this is the trend found experimentally by Jodlbauer* [42].

Velocity Measurements

A constant resistance of 6.07 ohm, corresponding to a temperature difference of $71 \pm 0.1^\circ\text{C}$ between the wire and the surrounding air, is added to the measured resistance at each location. The wire voltage is taken to indicate the local velocity; however, a correction for variation in the wire resistance and air properties from those of the velocity calibration curve, Figure (4-6) was made. This correction is explained in Appendix E.

It should be noted that the hot wire actually reads the vectorial sum of the tangential and radial velocities U and V . A correction is carried out for that using Hermann's expressions, namely

$$U = \frac{\gamma}{r} N_{Gr,r}^{1/2} f g F' \quad (5-3)$$

$$V = - \frac{\gamma}{r} N_{Gr,r}^{1/4} \left\{ f' F + \frac{f g'}{g} \eta F' \right\} \quad (5-4)$$

*In Hermann [16].

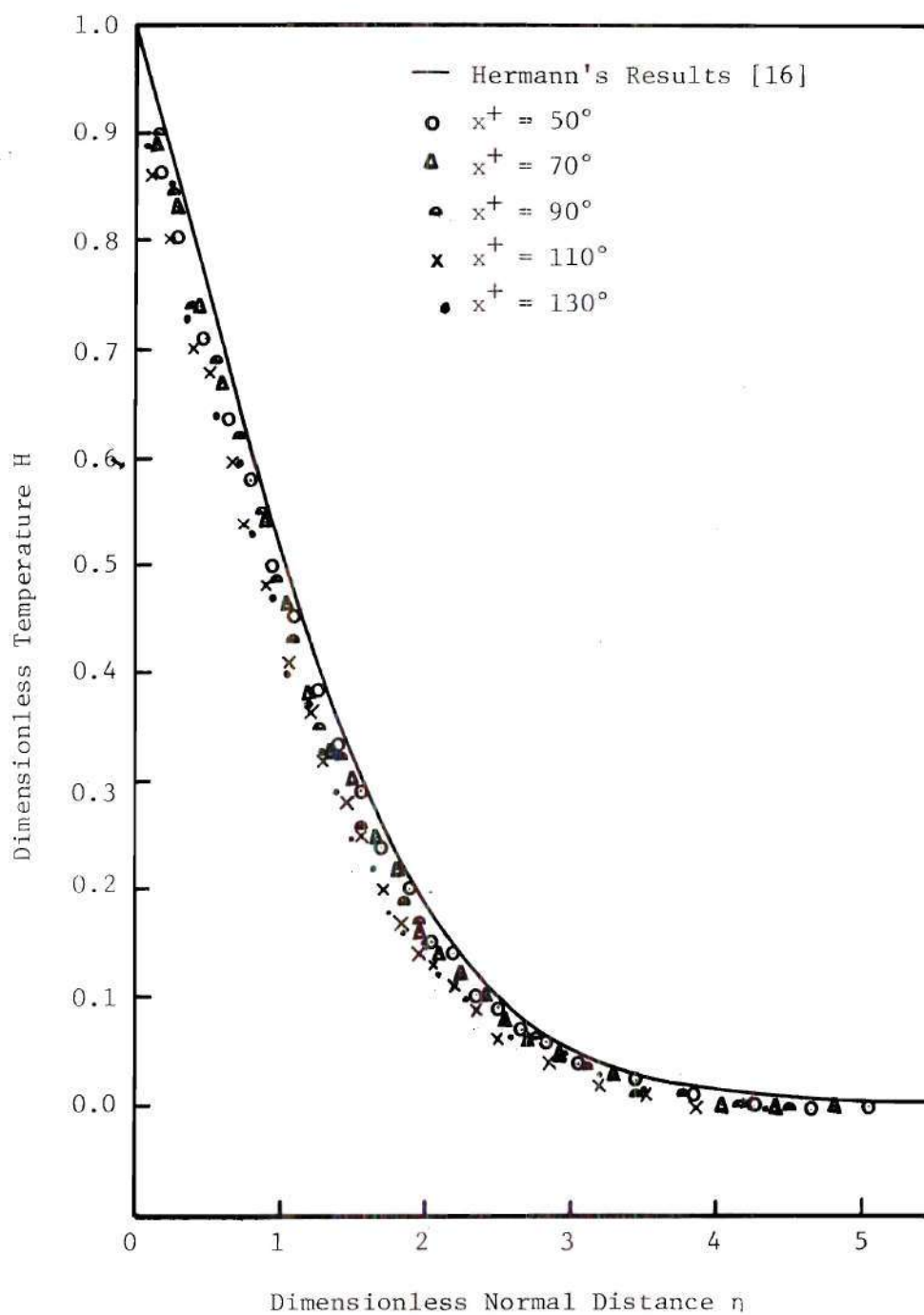


Figure 5-1 . Basic Temperature Profiles.

The ratio $U/\sqrt{U^2 + V^2}$ is calculated at each location using the above expressions and used as a correction factor to obtain the value of U from the measured value, $\sqrt{U^2 + V^2}$. Further, the value of the dimensionless velocity F' could be obtained by using equation (5-3).

The error in measuring U is determined from the reproducibility of the velocity calibration curve; it was found to be within ± 2 percent. The error in F' would, therefore, be given from equation (5-3) by

$$\begin{aligned}\Delta F' &= \Delta U - \frac{1}{2} \Delta N_{Gr,r} - \Delta F - \Delta g \\ &= \pm 2 - \frac{1}{2} (\pm 1.5) - 0 - 0 \\ &= \pm 2.75 \text{ percent}\end{aligned}$$

Measured values of F' are plotted versus η in Figure (5-2) together with Hermann's theoretical solution. Experimental results for $F'(\eta)$ are higher than the theoretical values, a trend that was also found by Jodlbauer [42].

The present results are generally in good agreement with Hermann's and Jodlbauer's results.

Determination of the Neutral Stability Curve

Temperature oscillations of controlled frequency and amplitude were induced at a point in the boundary layer by placing a heating wire in it and subjecting the wire to sinusoidal voltage oscillations by a function generator. The positioning of the heating wire was not critical. Sometimes, however, it was necessary to move it downstream when the probe failed to distinguish variations in amplitude due to excessive damping.

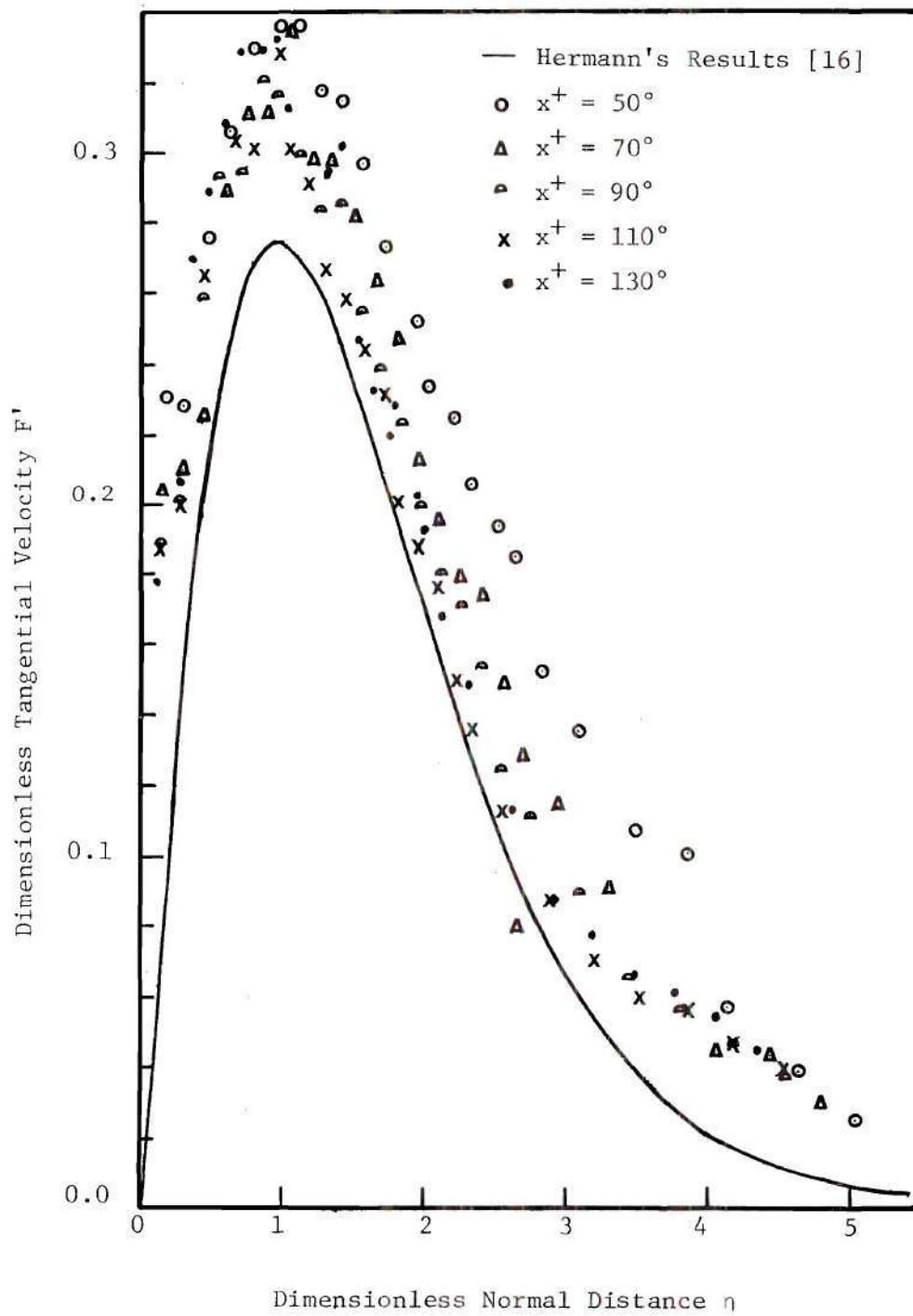


Figure 5-2 Basic Velocity Profiles.

For each reading, the probe was moved in the radial direction to locate the point of maximum local disturbance amplitude changing the position angle at which the probe is set, other readings were taken for the same frequency. A local maximum amplitude was determined for each of these position angles. The minimum of these local maxima was used to designate the point sought for this frequency on the neutral stability curve.

Hot Wire Response to Small Oscillations

It was shown in Appendix D that the wire has a negligible heat capacity; the energy balance of the hot wire sensor is given by

$$hA\theta = \frac{E^2}{R} \quad (5-5)$$

Due to the oscillatory flow situation, h , θ , and E are replaced in the above relation by a steady component plus an oscillatory one, namely

$$\left. \begin{aligned} h &= \bar{h} + \tilde{h} \\ \theta &= \bar{\theta} + \tilde{\theta} \\ E &= \bar{E} + \tilde{e} \end{aligned} \right\} \quad (5-6)$$

In the above the bar stands for the basic components while the wiggle stands for the oscillatory components. Substituting equation (5-6) into equation (5-5), and neglecting second order terms in oscillatory quantities gives

$$\bar{h}A\bar{\theta} + \bar{h}A\tilde{\theta} + \tilde{h}A\bar{\theta} = (\bar{E}^2 + 2\bar{E}\tilde{e})/R \quad (5-7)$$

Here the steady electric power \bar{E}^2/R is the wire response for the "basic" term $\bar{h}A\bar{\theta}$. The oscillatory voltage, \tilde{e} , therefore, indicates

$$\tilde{e} = \frac{R \bar{h} A \bar{\theta}}{2 \bar{E}} \left(\frac{\tilde{\theta}}{\bar{\theta}} + \frac{\tilde{h}}{\bar{h}} \right) \quad (5-8)$$

The term in parentheses is the sum of the relative temperature oscillations $\tilde{\theta}/\bar{\theta}$ and the relative velocity oscillations as indicated by \tilde{h}/\bar{h} . It should be noticed, however, that there exists a variable phase angle between the two.* To achieve reliable measurements, one of the two terms should be made negligible with respect to the other.

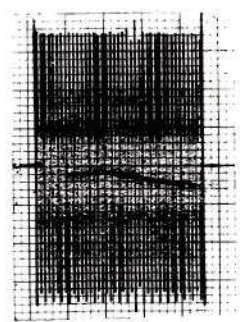
For $(\tilde{\theta}/\bar{\theta})$ to be negligible, $\bar{\theta}$ should be taken very large. In this case natural convection currents from the wire itself would have appreciable effects on the basic velocity and temperature in the vicinity of the wire. On the other hand, one can reduce the effect of the term \tilde{h}/\bar{h} by reducing $\bar{\theta}$ to a negligible value. It was therefore, decided to take the temperature oscillations as a measure of instability. The temperature difference $\bar{\theta}$ was reduced to almost zero by taking an overheat resistance $\Delta R \approx 0$. Equation (5-8) would then give

$$\left(\frac{\tilde{e}}{\bar{h}} \right) = \frac{R A}{2 \bar{E}} \tilde{\theta} \quad (5-9)$$

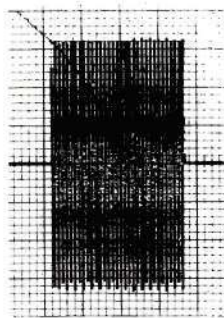
A correction for variation of \bar{h} with streamwise travel, due to variations in the mean velocity U is carried out in Appendix G. The corrected amplitude of the sinusoidal voltage output is then used to determine points of neutral stability.

A sample of the hot wire response to temperature oscillations of a frequency of 1.8 Hz is shown in Figure (5-3). Oscillations were practically sinusoidal as could be seen from the recording at $x^+ = 135$ degrees on extended time scale. The relative amplitudes were corrected for

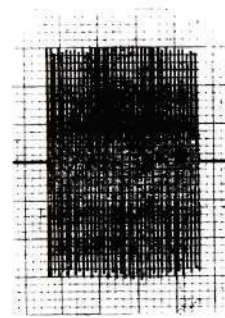
* This could be seen from the theoretical results of Knowles and Gebhart [24].



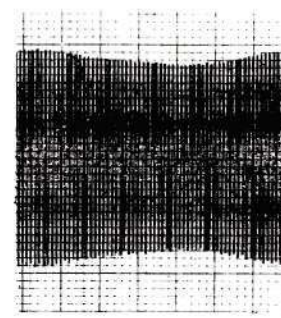
$x^+ = 65$



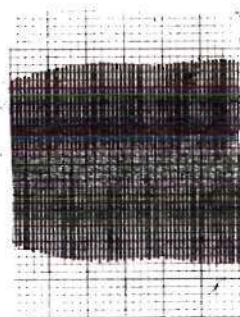
$x^+ = 75$



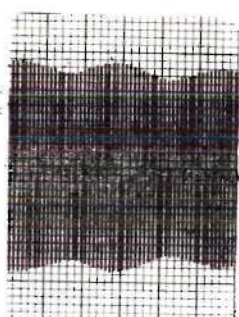
$x^+ = 85$



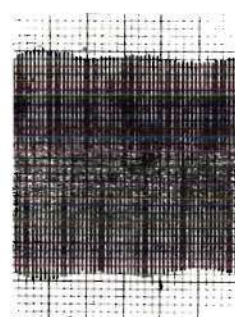
$x^+ = 95$



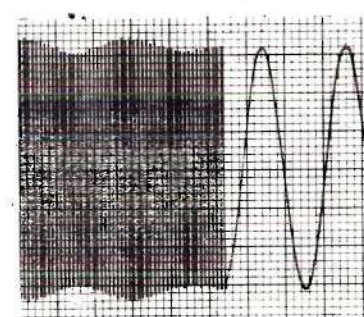
$x^+ = 105$



$x^+ = 115$



$x^+ = 125$



$x^+ = 135$

Figure 5-3 . Temperature Response of Probe at $N_{Gr,r} = 1.04 \times 10^6$ and 1.8 Hz at Different Position Angles x^+ in Degrees.

variations of \bar{h} and the corrected results are given as an angle versus amplitude graph in Figure (5-4) for this particular frequency.

Results of Stability Measurements

Frequency Lower Limit: At a frequency of 0.8 Hz a second harmonic appeared in the probe output, and increased with the downstream travel as shown in Figure (5-5). The fact that a frequency of 1.6 Hz was sustained through the flow indicates that the latter frequency is more rapidly amplified than that of 0.8 Hz. This is in accordance with the filtering phenomenon found theoretically. It also sets a lower limit for the experimental points. The amplification rates of these lower frequencies are small, and only scattered readings of practically constant amplitude are obtained at different values of the position angle x^+ . The presence of second harmonics in the output of the probe was also noticed by Dring and Gebhart [7]. For these reasons, points of the lower branch of the neutral stability curves are extremely difficult to locate experimentally, as could be seen from the results of Polymeropolous and Gebhart [34] and of Knowles and Gebhart [25] for the case of vertical uniformly heated plates.

Results: In the stability measurements, the position angle x^+ was changed by steps of 10 degrees. The error in measuring the position angle was previously estimated as 0.02 degrees; it is of negligible effect on the determination of the position angle. Error in frequency determination was found, from counting the number of cycles per centimeter on the chart paper, to be negligible. It was noticed that the mean flow fluctuates with time at large values of the position angle x^+ . These fluctuations appear as variations in the envelope of the sinusoidal disturbances $\tilde{\theta}_e$ as

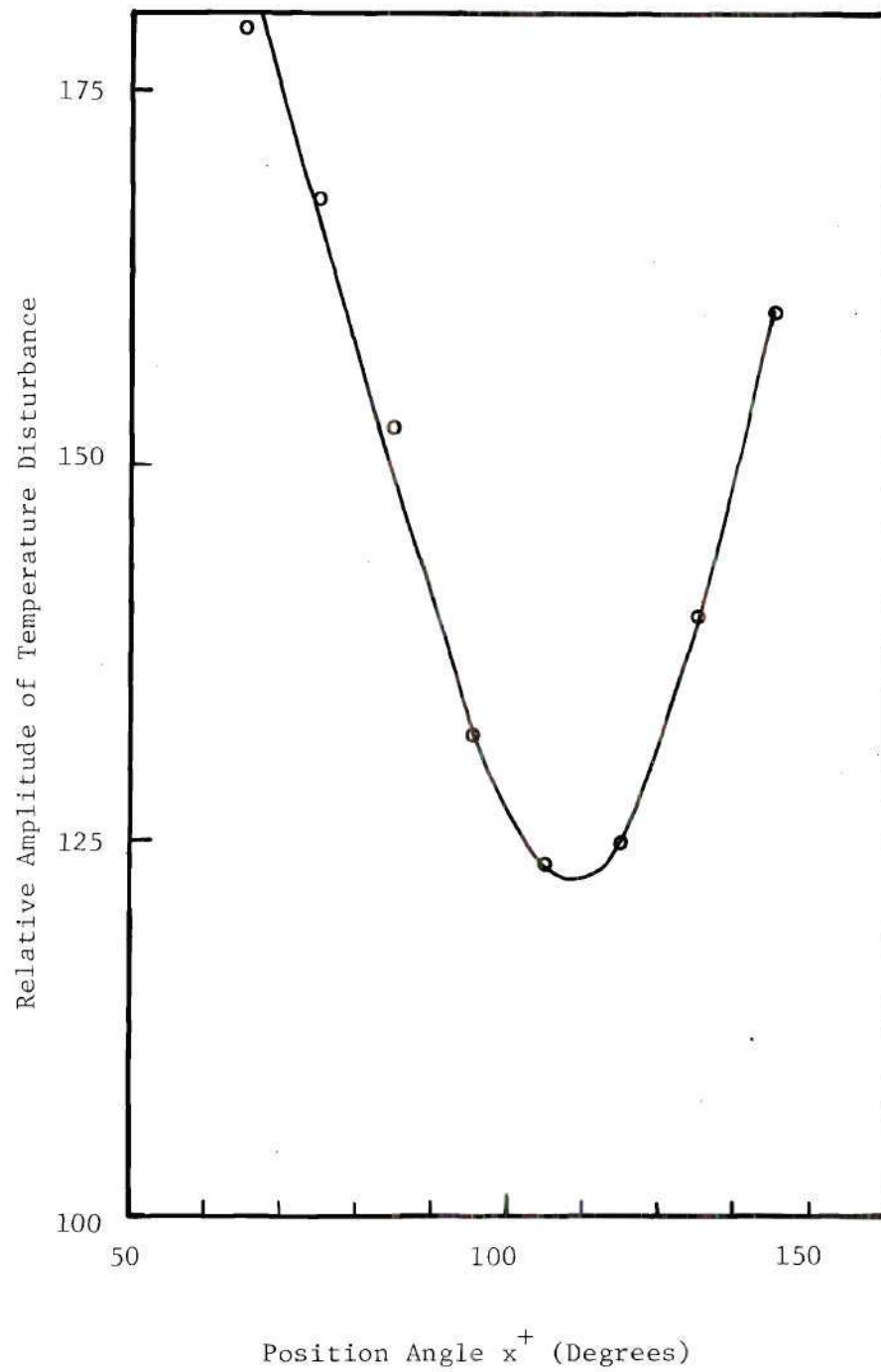
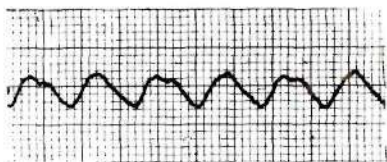
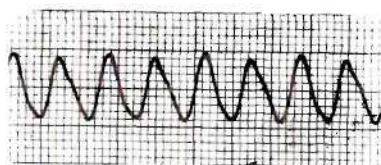


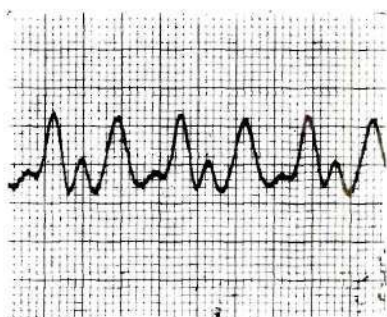
Figure 5.4 Relative Amplitude of Temperature Oscillations
 $(N_{Gr,r} = 1.04 \times 10^6, \hat{f} = 1.8 \text{ Hz}, \text{ and } N_{Pr} = 0.733)$.



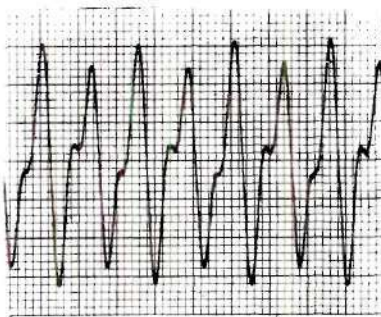
0.6 Hz, Near the
Heating Wire



0.8 Hz, Near the
Heating Wire



0.6 Hz, Far from the
Heating Wire



0.8 Hz, Far from the
Heating Wire

Figure 5-5 . Appearance of Second Harmonics in the Hot Wire Response for Small Frequencies.

could be seen from Figure (5-3). They may be attributed to the existence of some "natural" sources of instability that cannot be removed. These "natural" instabilities would amplify with streamwise travel, and their influence distinguishably appears at large position angles. It was noticed that these perturbations are irregular ones and generally acquire larger wavelengths. The maximum deviation in the values of $\tilde{\theta}_e$ due to these perturbations are of the order of ± 7.5 percent of $\tilde{\theta}_{e,av}$, the average value of $\tilde{\theta}_e$. However, the error in determining the position angle for neutral stability due to these perturbations is expected to vanish as explained in Appendix F.

Experimental results are plotted in Figure (5-6) and compared with the present analytic results as obtained for the case of $N_{Gr,r} = 1.05 \times 10^6$ which is approximately equivalent to the average total Grashof number for the different runs. It could be seen that the highest frequency on the experimental neutral stability curve is lower than the theoretically computed one. The flow encountered experimentally at these frequencies was found to be more stable than expected from analysis. This may be attributed to the fact that energy is transferred to the amplified perturbations, previously mentioned, depriving the two dimensional oscillations from some energy and hence rendering them more stable.

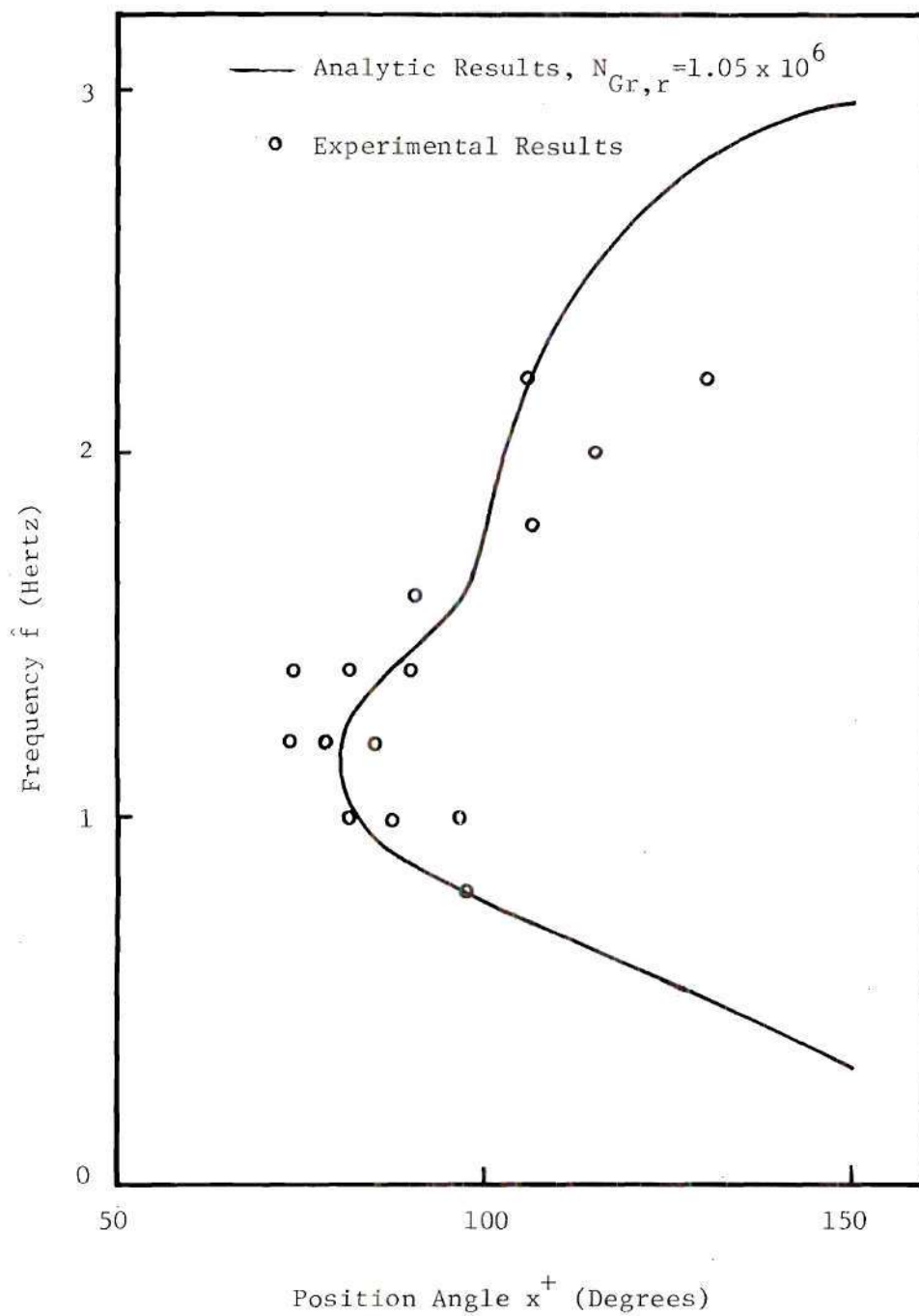


Figure 5-6 . Neutral Stability Experimental Points, Compared to Present Analytic Results.

CHAPTER VI

CONCLUSIONS

The governing coupled Orr-Sommerfeld equations for small, two dimensional disturbances were derived for the present case of natural convection around horizontal cylinders. The solution of these equations was carried out, using the method devised by Kaplan [22] and Mach [29]. Computations were made for air for the instability parameter G going up to 200. Neutral stability curves are presented graphically as relations between G and either the dimensionless frequency β_r or the wave number α_r with the position angle x^+ as parameter. Values of x^+ were taken from 30 to 150 degrees excluding the vicinities of the stagnation points, irrelevant to the present study.

Comparison of the present results with the previous data for an inclined plate showed that curvature stimulates instability; its effect is more appreciable on the hydrodynamic instability mode than on the thermal instability mode.

The flow was found as in the case of natural convection flow adjacent to a vertical flat plate, to be sensitive only to disturbances within a small band of frequencies, i.e. these disturbances are the ones that are amplified. Further, this band is filtered to a more favorite band because some frequencies acquire larger amplification rates than the others and dominate the flow as they propagate downstream. In the case of vertical flat plates, this favorite frequency band was found, by Gebhart and

Mahajan [46] to be a function of the fluid Prandtl number only. By comparison, in the present case, it was found that the favorite frequency or frequency band is function of the overall Grashof number, the cylinder radius and the value of kinematic viscosity ν as could be seen from equation (3-24) that shows the dependence of the value of the reduced frequency σ on these factors.

Experiments were carried out to check the analysis. Measurements were carried out to determine the basic temperature and velocity profiles using a hot wire probe. These profiles showed good agreement with the available theoretical and experimental data.

A Neutral Stability curve was obtained by determining the points of least temperature oscillation amplitudes. It was compared to the present theoretical results for the same values of N_{Pr} and $N_{Gr,r}$; good agreement was found.

Proposed Further Work

The favorite frequency which dominates a natural convection flow around a horizontal cylinder was found to be function of the local Grashof number, the cylinder radius and the kinematic viscosity ν , i.e. the physical dimensionless frequency as given by $\hat{f}r^2/\nu$ is a function of $N_{Gr,r}$. Further investigation is suggested to correlate the relation between the two and to study its possible applications.

APPENDIX A

BASIC VELOCITY AND TEMPERATURE PROFILES

Basic velocity and temperature profiles of natural convection flow around horizontal cylinders were given by Hermann [16], and are needed here to compute the stability curves. Some details of Hermann's analysis are also needed in the derivation of the disturbance equations. Hermann's analysis is, therefore, outlined in this appendix.

The governing equations for natural convection around horizontal cylinders, as given by Hermann, are:

Mass balance equation:

$$\frac{r}{r+n^+} U_{s^+} + V_{n^+} + \frac{V}{r+n^+} = 0 \quad (\text{A-1})$$

Tangential momentum balance equation:

$$\begin{aligned} \frac{r}{r+n^+} U U_{s^+} + V U_{n^+} + \frac{UV}{r+n} = & -\frac{1}{\rho} P_{s^+}^* + \hat{g} \hat{\beta} \Theta \sin\left(\frac{s^+}{r}\right) \\ & + \gamma \left\{ U_{n^+n^+} + \frac{1}{r+n^+} U_{n^+} + \left(\frac{r}{r+n^+}\right)^2 U_{s^+s^+} - \frac{U}{(r+n^+)^2} + \frac{2r}{(r+n^+)^2} V_{s^+} \right\} \end{aligned} \quad (\text{A-2})$$

Normal momentum balance equation:

$$\begin{aligned} \frac{r}{r+n^+} U V_{s^+} + V V_{n^+} - \frac{U^2}{r+n^+} = & -\frac{1}{\rho} P_{n^+}^* - \hat{g} \hat{\beta} \Theta \cos\left(\frac{s^+}{r}\right) \\ & + \gamma \left\{ V_{n^+n^+} + \frac{1}{r+n^+} V_{n^+} + \left(\frac{r}{r+n^+}\right)^2 V_{s^+s^+} - \frac{V}{(r+n^+)^2} - \frac{2r}{r+n^+} U_{s^+} \right\} \end{aligned} \quad (\text{A-3})$$

Energy balance equation:

$$\frac{r}{r+n^+} U \Theta_{s^+} + V \Theta_{n^+} = a \left\{ \Theta_{n^+ n^+} + \frac{1}{r+n^+} \Theta_{n^+} + \left(\frac{r}{r+n^+} \right)^2 \Theta_{s^+ s^+} \right\} \quad (\text{A-4})$$

The above equations represent the mathematical model of a steady, two-dimensional flow with constant properties.

The plus sign over s and n indicates the finite length scale used in steady-state calculations as distinct from the much smaller distances that have to be considered in connection with disturbances. This is explained more fully in Chapter III.

Following the order of magnitude analysis given by Hermann, we have*

$$\begin{array}{lll} U \approx 1 & S^+ \approx r \approx 1 & n \approx \delta \\ V \approx \delta & \Theta \approx 1 & P \approx \delta \end{array}$$

where δ is the boundary layer thickness. Neglecting terms of order δ with respect to those of order 1, equations (A-1 to 4) become

$$U_{s^+} + V_{n^+} = 0 \quad (\text{A-5})$$

$$U U_{s^+} + V U_{n^+} = \nu U_{n^+ n^+} + \hat{g} \hat{\beta} \Theta \sin\left(\frac{S^+}{r}\right) \quad (\text{A-6})$$

$$-\frac{U^2}{r} = -\frac{1}{\rho} P_{n^+} - \hat{g} \hat{\beta} \Theta \cos\left(\frac{S^+}{r}\right) \quad (\text{A-7})$$

$$U \Theta_{s^+} + V \Theta_{n^+} = a \Theta_{n^+ n^+} \quad (\text{A-8})$$

*The \approx sign indicates order of magnitude.

It should be noted that equation (A-7) is not necessary for the general solution of the problem, its only use is in obtaining the pressure gradient in the radial direction. It is, therefore, dropped in the following analysis. To render the remaining equations dimensionless, the following substitutions were used by Hermann:

$$\left. \begin{aligned} x^+ &= \frac{s^+}{r} \quad , \quad y^+ = \frac{n^+}{r} N_{Gr,r}^{1/4} \quad , \quad u = \gamma \psi_{n^+} N_{Gr,r}^{1/4} \quad , \\ v &= -\gamma \psi_{s^+} N_{Gr,r}^{1/4} \quad , \quad N_{Gr,r} = \hat{g} \hat{\beta} \Delta T r^3 / \gamma^2 \quad , \quad \Theta = H \Delta T \end{aligned} \right\} \quad (A-9)$$

In these expressions x^+, y^+, ψ, H are of order unity. With these, the continuity equation (A-5) drops out and equations (A-6) and (A-8) become

$$\psi_{y^+} \psi_{x^+ y^+} - \psi_{x^+} \psi_{y^+ y^+} = \psi_{y^+} \gamma^+ \gamma^+ + H \sin(x^+) \quad (A-10)$$

$$\psi_{y^+} H_{x^+} - \psi_{x^+} H_{y^+} = \frac{1}{N_{Pr}} H_{y^+} \gamma^+ \quad (A-11)$$

Following Hermann, a similarity solution was obtained by defining

$$\left. \begin{aligned} \eta &= y^+ g(x^+) \\ \psi &= F(\eta) f(x^+) \\ H &= H(\eta) \end{aligned} \right\} \quad (A-12)$$

Substitution of these quantities into equations (A-10) and (A-11) gives

$$F'^2 \{ f^2 g g' + g^2 f f' \} - F F'' (f f' g^2) = F'' (f g^3) + H \sin(x) \quad (A-13)$$

$$H'' + N_{Pr} F H' \frac{f'}{g} = 0 \quad (A-14)$$

To achieve a similarity solution compatible with the original solution of Pohlhausen* for vertical flat plates, Hermann set the following equations

$$f' = a g \quad (\text{A-15a})$$

$$f^2 g g' = b \sin(x) \quad (\text{A-15b})$$

$$g^2 f f' = c \sin(x) \quad (\text{A-15c})$$

$$f g^3 = d \sin(x) \quad (\text{A-15d})$$

where $a = 3$, $b = -1$, $c = 3$, and $d = 1$. This gives

$$F''' + 3 F F'' - 2 F'^2 + H = 0 \quad (\text{A-16})$$

$$H'' + 3 N_F F H' = 0 \quad (\text{A-17})$$

These are the well-known Pohlhausen equations, solutions for which are readily available. In particular, later accurate numerical evaluations obtained with computer by Ostrach [31] are used here.

Solution of equations (A-15a to d) was carried out by Hermann, and gives the following expression for $f(x^+)$ and $g(x^+)$

$$f(x^+) = 3.4284 \left\{ 1 + 0.581 \bar{\Phi} - 0.05626 \bar{\Phi}^2 - 0.01412 \bar{\Phi}^3 - 0.00165 \bar{\Phi}^4 - 0.00066 \bar{\Phi}^5 \right\} \quad (\text{A-18a})$$

$$\text{where } \bar{\Phi} = (x^+ - 90) \pi / 180 \quad (\text{A-18b})$$

* Part of Schmidt and Beckman work [35].

and
$$g(x^+) = \left\{ \frac{\sin(x^+)}{f(x^+)} \right\}^{1/3} \quad (A-19)$$

It should be noted that three independent equations, namely equations (A-15b,c and d),* are used to determine the functions f and g . A second expression could be obtained for g from the relation $f' = ag$, this differs from the present expression of equation (A-19) only near the lower stagnation point. At the upper stagnation point, the function $g(x^+)$ equals zero, which physically means that the boundary layer thickness goes to infinity. The situation could be interpreted as a representation of separation with all assumptions of boundary layer flow invalid. Hermann's solution is, therefore, considered valid throughout the flow domain except near the two stagnation points.

The basic quantities that are necessary for the solution of the disturbance equations are listed below. They were originally derived by Hermann

$$U = \frac{\gamma}{r} F' U^* \quad (A-20)$$

$$U_{n^+} = \gamma F'' U^* / (\delta r^2) \quad (A-21)$$

$$U_{n^+n^+} = \gamma F''' U^* / (\delta^2 r^3) \quad (A-22)$$

$$U_{s^+n^+} = \gamma (F'' - F''' \eta) / (\delta^3 r^3) \quad (A-23)$$

$$V = -\gamma (3F - F' \eta) / (\delta r) \quad (A-24)$$

*Equation (A-15a) could be obtained from equations (A-15c and d).

where $U^* = f g N_{G,r}^{1/2}$ (A-25)

and $\delta = 1 / (g N_{G,r}^{1/4})$ (A-26)

APPENDIX B

ORDER OF MAGNITUDE ANALYSIS OF TERMS OF THE
DISTURBANCE EQUATION

Based on the order of magnitude of the terms of equation (3-9), analysis of different terms of equations (3-8a and b) is carried out.

Equations (3-9) are

$$\left. \begin{array}{lll}
 U \approx 1 & \tilde{u} \approx \delta & v \approx \delta^2 \\
 V \approx \delta & \tilde{v} \approx \delta & a \approx \delta^2 \\
 n^+ \approx \delta & \tilde{\psi} \approx \delta^2 & t \approx 1 \\
 s^+ \approx 1 & \tilde{\theta}/\Delta T \approx \delta & \\
 H = \Theta/\Delta T \approx 1 & n \approx \delta & \\
 & s \approx \delta &
 \end{array} \right\} \quad (3-9)$$

The order of magnitude of terms of equations (3-8a and b) are given by the following:

$$\tilde{\psi}_{nt} \approx \frac{\tilde{\psi}}{n \times t} \approx \frac{\delta^2}{\delta \times 1} \approx \delta$$

$$\tilde{\psi}_{nn} \approx \frac{\delta^2}{\delta \times \delta \times 1} \approx 1$$

$$\tilde{\psi}_{nn} U_{s^+} \approx \frac{\delta^2}{\delta \times \delta} \times \frac{1}{1} \approx 1$$

$$\tilde{\psi}_n U_{s^+ n^+} \approx \frac{\delta^2}{\delta} \times \frac{1}{1 \times \delta} \approx 1$$

$$U_{n^+} \tilde{\psi}_{ns} \approx \frac{1}{\delta} \times \frac{\delta^2}{\delta \times \delta} \approx 1/\delta$$

$$U \tilde{\psi}_{nns} \approx 1 \times \frac{\delta^2}{\delta \times \delta \times \delta} \approx 1/\delta$$

$$V \tilde{\psi}_{nn} \approx \delta \times \frac{\delta^2}{\delta \times \delta} \approx \delta$$

$$V_n + \tilde{\psi}_{nn} \approx \frac{\delta}{\delta} \times \frac{\delta^2}{\delta \times \delta} \approx 1$$

$$V \tilde{\psi}_{nnn} \approx \delta \times \frac{\delta^2}{\delta \times \delta \times \delta} \approx 1$$

$$U_{n+n} \tilde{\psi}_s \approx \frac{1}{\delta \times \delta} \times \frac{\delta^2}{\delta} \approx 1/\delta$$

$$U_n + \tilde{\psi}_{sn} \approx \frac{1}{\delta} \times \frac{\delta^2}{\delta \times \delta} \approx 1/\delta$$

$$U \tilde{\psi}_s \approx 1 \times \frac{\delta^2}{\delta} \approx \delta$$

$$U_n + \tilde{\psi}_s \approx \frac{1}{\delta} \times \frac{\delta^2}{\delta} \approx 1$$

$$U \tilde{\psi}_{ns} \approx 1 \times \frac{\delta^2}{\delta \times \delta} \approx 1$$

$$V_n + \tilde{\psi}_n \approx \frac{\delta}{\delta} \times \frac{\delta^2}{\delta} \approx \delta$$

$$V \tilde{\psi}_{nn} \approx \delta \times \frac{\delta^2}{\delta \times \delta} \approx \delta$$

$$\tilde{\psi}_{sst} \approx \frac{\delta^2}{\delta \times \delta \times 1} \approx 1$$

$$\tilde{\psi}_{ns} V_{s+} \approx \frac{\delta^2}{\delta \times \delta} \times \frac{\delta}{1} \approx \delta$$

$$\tilde{\psi}_n V_{s+s+} \approx \frac{\delta^2}{\delta} \times \frac{\delta}{1 \times 1} \approx \delta^2$$

$$U_s + \tilde{\psi}_{ss} \approx \frac{1}{1} \times \frac{\delta^2}{\delta \times \delta} \approx 1$$

$$U \tilde{\psi}_{SSS} = 1 \times \frac{\delta^2}{\delta \times \delta \times \delta} \approx 1/\delta$$

$$V_n^+ \tilde{\psi}_{SS} \approx \frac{\delta}{\delta} \times \frac{\delta^2}{\delta \times \delta} \approx 1$$

$$V_{n+S}^+ \tilde{\psi}_S \approx \frac{\delta}{\delta \times 1} \times \frac{\delta^2}{\delta} \approx \delta$$

$$\tilde{\psi}_{SS} V \approx \frac{\delta^2}{\delta \times \delta} \times \delta \approx \delta$$

$$\tilde{\psi}_S V_{S^+} \approx \frac{\delta^2}{\delta} \times \frac{\delta}{1} \approx \delta^2$$

$$\tilde{\psi}_{nS} V_{S^+} \approx \frac{\delta^2}{\delta \times \delta} \times \frac{\delta}{1} \approx \delta$$

$$\tilde{\psi}_{nSS} V \approx \frac{\delta^2}{\delta \times \delta \times \delta} \times \delta \approx 1$$

$$U_{S^+} \tilde{\psi}_n \approx \frac{1}{1} \times \frac{\delta^2}{\delta} \approx \delta$$

$$U \tilde{\psi}_{nS} \approx 1 \times \frac{\delta^2}{\delta \times \delta} \approx 1$$

$$g\beta \tilde{\Theta}_n \sin\left(\frac{S}{r}\right) \approx \frac{\delta}{\delta} \approx 1$$

$$g\beta \tilde{\Theta}_S \cos\left(\frac{S}{r}\right) \approx \frac{\delta}{\delta} \approx 1$$

$$\gamma \tilde{\psi}_{nnn} \approx \delta^2 \times \frac{\delta^2}{\delta \times \delta \times \delta} \approx \delta$$

$$\gamma \tilde{\psi}_{nnnn} \approx \delta^2 \times \frac{\delta^2}{\delta \times \delta \times \delta \times \delta} \approx 1$$

$$\gamma \tilde{\psi}_{nnn} \approx \delta^2 \times \frac{\delta^2}{\delta \times \delta \times \delta} \approx \delta$$

$$\gamma \tilde{\psi}_{nSS} \approx \delta^2 \times \frac{\delta^2}{\delta \times \delta \times \delta} \approx \delta$$

$$\gamma \tilde{\psi}_{nnss} \approx \delta^2 \times \frac{\delta^2}{\delta \times \delta \times \delta \times \delta} \approx 1$$

$$\gamma \tilde{\psi}_n \approx \delta^2 \times \frac{\delta^2}{\delta} \approx \delta^3$$

$$\gamma \tilde{\psi}_{nn} \approx \delta^2 \times \frac{\delta^2}{\delta \times \delta} \approx \delta^2$$

$$\gamma \tilde{\psi}_{ss} \approx \delta^2 \times \frac{\delta^2}{\delta \times \delta} \approx \delta^2$$

$$\gamma \tilde{\psi}_{ssn} \approx \delta^2 \times \frac{\delta^2}{\delta \times \delta \times \delta} \approx \delta$$

$$\gamma \tilde{\psi}_{ssnn} \approx \delta^2 \times \frac{\delta^2}{\delta \times \delta \times \delta \times \delta} \approx 1$$

$$\gamma \tilde{\psi}_{ssss} \approx \delta^2 \times \frac{\delta^2}{\delta \times \delta \times \delta \times \delta} \approx 1$$

$$\tilde{\theta}_t \approx \frac{\delta}{1} \approx \delta$$

$$\tilde{\psi}_n \otimes_{s+} \approx \frac{\delta^2}{\delta} \times \frac{1}{1} \approx \delta$$

$$\cup \tilde{\theta}_s \approx 1 \times \frac{\delta}{\delta} \approx 1$$

$$\tilde{\psi}_s \otimes_{n+} \approx \frac{\delta^2}{\delta} \times \frac{1}{\delta} \approx 1$$

$$\vee \tilde{\theta}_n \approx \delta \times \frac{\delta}{\delta} \approx \delta$$

$$\alpha \tilde{\theta}_{nn} \approx \delta^2 \times \frac{\delta}{\delta \times \delta} \approx \delta$$

$$\alpha \tilde{\theta}_n \approx \delta^2 \times \frac{\delta}{\delta} \approx \delta^2$$

$$\alpha \tilde{\theta}_{ss} \approx \delta^2 \times \frac{\delta}{\delta \times \delta} \approx \delta$$

APPENDIX C

SOLUTION OF THE ASYMPTOTIC EQUATIONS

The asymptotic equations govern the instabilities outside the boundary layer; they are equations (3-18a and b), namely

$$\begin{aligned} \phi'''' + 3F_e \phi''' + (iG\beta - 2\alpha^2) \phi'' - 3F_e \alpha^2 \phi' + (\alpha^4 - i\alpha^2 G\beta) \phi \\ = -(\zeta' + i\alpha \zeta \cot(x^*)) \end{aligned} \quad (C-1)$$

$$\text{and} \quad \zeta'' + 3F_e N_p \zeta' + (iN_p G\beta - \alpha^2) \zeta = 0 \quad (C-2)$$

An outline of their solution is given in this appendix. The auxiliary form for equation (C-1) is obtained by replacing the derivatives of ϕ with respect to η by the symbol D , and omitting the right hand side which would be used to obtain its particular solution.

The resulting auxiliary equation is

$$D^4 + 3F_e D^3 + (i\alpha G\beta - 2\alpha^2) D^2 - 3F_e \alpha^2 D + (\alpha^4 - i\alpha^2 G\beta) = 0 \quad (C-3)$$

The roots of the above equation are:

$\hat{\gamma}_1, \hat{\gamma}_2, \hat{\gamma}_3$ and $\hat{\gamma}_4$ where

$$\hat{\gamma}_1 = +\alpha \quad (C-4a)$$

$$\hat{\gamma}_2 = -\alpha \quad (C-4b)$$

$$\hat{\gamma}_3 = 0.5 \left[-3F_e + \left\{ 9F_e^2 + 4(\alpha^2 - iG\beta) \right\}^{1/2} \right] \quad (C-4c)$$

$$\hat{\gamma}_4 = 0.5 \left[-3F_e - \left\{ 9F_e^2 + 4(\alpha^2 - iG\beta) \right\}^{1/2} \right] \quad (C-4d)$$

Following the same procedure, the auxiliary form for equation (C-2) is given by

$$D^2 + 3F_e N_{Pr} D + (i N_{Pr} G\beta - \alpha^2) = 0 \quad (C-5),$$

and its roots are

$$\hat{\gamma}_5 = 0.5 \left[-3F_e N_{Pr} + \left\{ 9F_e^2 N_{Pr}^2 + 4(\alpha^2 - i N_{Pr} G\beta) \right\}^{1/2} \right] \quad (C-6a)$$

$$\hat{\gamma}_6 = 0.5 \left[-3F_e N_{Pr} - \left\{ 9F_e^2 N_{Pr}^2 + 4(\alpha^2 - i N_{Pr} G\beta) \right\}^{1/2} \right] \quad (C-6b)$$

Solution of the simultaneous equations (C-1 and 2) would, therefore, be

$$\phi = \sum_{j=1}^6 \hat{C}_j e^{\hat{\gamma}_j \eta} \quad (C-7)$$

$$\zeta = \hat{C}_7 e^{\hat{\gamma}_5 \eta} + \hat{C}_8 e^{\hat{\gamma}_6 \eta} \quad (C-8)$$

It should be noted that the terms $C_5 e^{\gamma_5 \eta}$ and $C_6 e^{\gamma_6 \eta}$ are included in the solution of equation (C-1) being its particular solution as obtained after the evaluation of ζ by solving equation (C-2).

Out of the six exponents $\hat{\gamma}_j$, three have negative real parts. These are only considered because oscillations diminish far from the cylinder, a condition that can be only satisfied by such terms. Solutions of equations (C-1) and (C-2) are, therefore, given by

$$\phi = c_1 e^{\gamma_1 \eta} + c_2 e^{\gamma_2 \eta} + c_3 e^{\gamma_3 \eta} \quad (C-9)$$

$$\zeta = c_4 e^{\gamma_3 \eta} \quad (C-10)$$

where γ_1 , γ_2 and γ_3 are the roots having negative real parts among the $\hat{\gamma}_j$'s. The constant c_4 could be further estimated in terms of the other constants c_1 , c_2 , and c_3 by substituting equation (C-9 and 10) into equation (C-1); this gives

$$c_4 = -c_3 \left[\frac{\gamma_3^4 + 3F_e \gamma_3^3 + (iG\beta - 2\alpha^2) \gamma_3^2 - 3F_e \alpha^2 \gamma_3 + (\alpha^4 - i\alpha^2 G\beta)}{\gamma_3 + i\alpha \cot(x^*)} \right] \quad (C-11)$$

By this, the asymptotic solutions would be given by

$$\phi = c_1 e^{\gamma_1 \eta} + c_2 e^{\gamma_2 \eta} + c_3 e^{\gamma_3 \eta} \quad (C-12a)$$

$$\zeta = -c_3 \left[\frac{\gamma_3^4 + 3F_e \gamma_3^3 + (iG\beta - 2\alpha^2) \gamma_3^2 - 3F_e \alpha^2 \gamma_3 + (\alpha^4 - i\alpha^2 G\beta)}{\gamma_3 + i\alpha \cot(x^*)} \right] e^{\gamma_3 \eta} \quad (C-12b)$$

APPENDIX D

DESIGN OF PROBE

The hot wire probe was used to measure both temperature and velocity. Its response as a thermometer is discussed in this appendix. As such, the probe is required to measure the local temperature accurately in a field with rather steep gradient. An error is expected because the wire supports would be affected by temperatures in adjacent parts of the field and, therefore, attain a temperature different from the local one to be measured. This would heat (or cool) the ends of the wire sensor.

The probe should also follow the local temperature fluctuations within the expected range of frequencies, and appropriately indicate them. For this, the wire should have the least possible heat capacity.

Error in Temperature Measurements Due to End Effects of the Wire

The wire sensor of the probe is used to measure the fluid temperature T_a while its supports are assumed to be at some other temperature T_∞ . The wire would, therefore, act as a fin, and there would be a temperature distribution along its length. The reading obtained from the wire would, accordingly, indicate some average value in the range T_∞ to T_a .

Assuming half the wire length to be a fin with insulated tip, the temperature distribution over it would be given by [11]

$$\theta = \frac{T - T_a}{T_\infty - T_a} = \cosh(ml) - \sinh(ml) \tanh(mL) \quad (D-1)$$

$$\text{where } m = (h\hat{P}/kA)^{1/2} \quad (D-2)$$

and ℓ is the variable distance measured from the wire support. Integrating over the length of the wire gives

$$\bar{\theta} = \frac{\tanh(mL)}{mL} \quad (D-3)$$

or

$$(\bar{T} - T_a) = (T_{\infty} - T_a) \frac{\tanh(mL)}{mL} \quad (D-4)$$

Naturally, the relative error $\bar{\theta}$ increases as the heat transfer coefficient, or the fluid velocity, decreases. To limit the error to less than 10 percent at a velocity of 2 cm/s, it was found that for a tungsten wire 5 μ m diameter, a length of 7 mm or more should be used. Actually the wire used is 8 mm long. Further, curved supports were used for the probe. This further reduces the temperature range $(T_{\infty} - T_a)$ over the last 5 mm of the support length to about 3C. This, in turn, reduces the error $\bar{T} - T_a$ to about -.27C or -1.3 percent of the total temperature difference across the boundary layer.

Frequency Response of Probe Sensor

A study of the frequency response of a hot wire probe was carried out to determine its ability to detect the highest frequencies encountered in the experiment.

Calculations are based on the use of a tungsten wire 5 μ m diameter placed at a point of 2 cm/s velocity, the minimum detectable value. In the following analysis, it was assumed that the wire operates in air at about 300°K.

In measurements of temperature oscillations, the wire temperature was set at a constant value approximately equal to that of the mean temperature of the air at the wire location. In other words, the wire was operated as anemometer with an overheat resistance $\Delta R \approx 0$. However, for estimating the frequency response of the wire to temperature oscillations, it was assumed that the control circuit is relaxed. By this, the wire temperature is expected to follow the sinusoidally varying air temperature except for some damping factor; calculations of that damping factor are given below.

Under the above velocity and temperature condition, the value of the wire Reynolds number would be about 0.005. According to Collis and Williams [41], the heat transfer coefficient would be given by

$$h = \frac{k}{d} \left(\frac{T_m}{T_\infty} \right)^{0.17} / (1.18 - 1.1 \log(N_{Re})) = 1577 \text{ W/m}^2 \text{ K}$$

For the tungsten hot wire used, the Biot number would be about 5×10^{-5} . Infinite thermal conductivity in the radial direction can, therefore, be assumed for the wire; i.e. that its temperature is practically uniform throughout its cross-section. For this case the energy balance gives

$$h \hat{p} L (T_a - T_w) = \rho C_p A L \frac{dT_w}{dt} \quad (D-5)$$

where T_a is the surrounding air temperature, T_w is the wire temperature, \hat{p} the perimeter, and A the cross sectional area. Assuming air temperature to fluctuate sinusoidally with a mean value \bar{T}_a , it could be represented by

$$T_a = \bar{T}_a + \tilde{\Theta}_A \sin \omega t \quad (D-6)$$

And due to velocity oscillations, h will vary sinusoidally,* around its mean value \bar{h} ; as given by following relation

$$h = \bar{h} + \tilde{h}_A \sin \omega t \quad (D-7)$$

The same frequency was assumed for both temperature and velocity oscillations in equations (D-6 and 7).

Substituting equations (D-6 and 7) in equation (D-5) and neglecting disturbance quantities of second order gives

$$\frac{d\bar{\Theta}}{dt} = -M \left\{ \bar{\Theta} - \tilde{\Theta}_A \sin(\omega t) + (\bar{\Theta} \tilde{h}_A / \bar{h}) \sin(\omega t) \right\} \quad (D-8)$$

where

$$M = \frac{\hat{P} \bar{h}}{\rho C_p A} \quad \text{and} \quad \bar{\Theta} = T_W - \bar{T}_A \quad (D-9)$$

For the considered case of using the hot wire for measuring the temperature oscillations, the difference between the wire temperature T_W and the mean air temperature \bar{T}_A is expected to be very small. The term $\bar{\Theta} \tilde{h}_A \sin \omega t$ would, therefore, be negligible and equation (D-9) becomes

$$\frac{d\bar{\Theta}}{dt} = -M \left[\bar{\Theta} - \tilde{\Theta}_A \sin(\omega t) \right] \quad (D-10)$$

The solution of equation (D-10) together with the initial condition $\bar{\Theta}(0) = 0$, which denotes a zero initial temperature difference between the wire and

* Velocity - heat transfer coefficient relation is assumed linear within the small amplitude of the disturbance velocity, hence h varies sinusoidally with time.

the surrounding air, is obtained by using Laplace Transforms; this solution is given by*

$$\bar{\theta} = \tilde{\theta}_A \frac{M^2}{M^2 + \omega^2} \left[\sin(\omega t) - e^{-\frac{M}{\omega} t} \frac{\omega}{M} (1 - \cos(\omega t)) \right] \quad (D-11)$$

The conditions that would be established after a relatively long period of time would, therefore, be

$$\bar{\theta} = \tilde{\theta}_A \frac{M^2}{M^2 + \omega^2} \sin(\omega t) \quad (D-12)$$

In our case $M = \frac{hP}{\rho C_p A} = 4.8 \times 10^5 \text{ sec}^{-1}$ whereas the maximum value of ω is expected to be within 20 rad/s.

This gives $\frac{M^2}{M^2 + \omega^2} = 1$ and

$$T_w - \bar{T}_a = \tilde{\theta}_A \sin(\omega t) \quad (D-13)$$

Comparing this with equation (D-6) gives

$$T_w = T_a \quad (D-14)$$

As previously explained, in the actual measurements the wire temperature is kept constant by the anemometer controlling bridge. Consequently voltage indications would appropriately represent the temperature variations.

*Reference [15] was used to determine the solution.

APPENDIX E

CORRECTION OF VELOCITY MEASUREMENTS FOR
LOCAL TEMPERATURE EFFECTS

The hot wire anemometer was calibrated at a temperature of 24.7°C (76.4°F) and used at different temperatures depending on its position in the flow field. Although the temperature difference between the hot wire and air was maintained constant at 71°C, a correction should be made for the change of the resistance R_w of the hot wire, and for the variation of thermal conductivity k and kinematic viscosity ν of the air. A change in the wire resistance R_w , changes the bridge arm ratio $R_w/(R_w + 40)$ that represents the ratio of the wire to bridge voltage (the bridge has a constant resistance of 40 ohms in series with the wire).

The velocity-voltage calibration curve Figure (4-6) is reduced to the dimensionless form of Reynolds number N_{Re} versus Nusselt number N_{Nu} of Figure (E-1) by using the following relations

$$N_{Re} = \frac{Ud}{\nu} \quad , \quad N_{Nu} = \frac{\bar{E}^2}{R_w A \Delta T} \frac{d}{k}$$

In these relations, the properties are taken at the mean film temperature around the wire, namely $(24.7 + 71)/2 = 47.9^\circ\text{C}$. The temperature difference ΔT is taken here as 71°C which corresponds to the overheat resistance $\Delta R = 6.07$ ohm used, as mentioned in Chapter IV. A straight line approximation of the graph in the expected velocity range (2 to 17 cm/s) gives

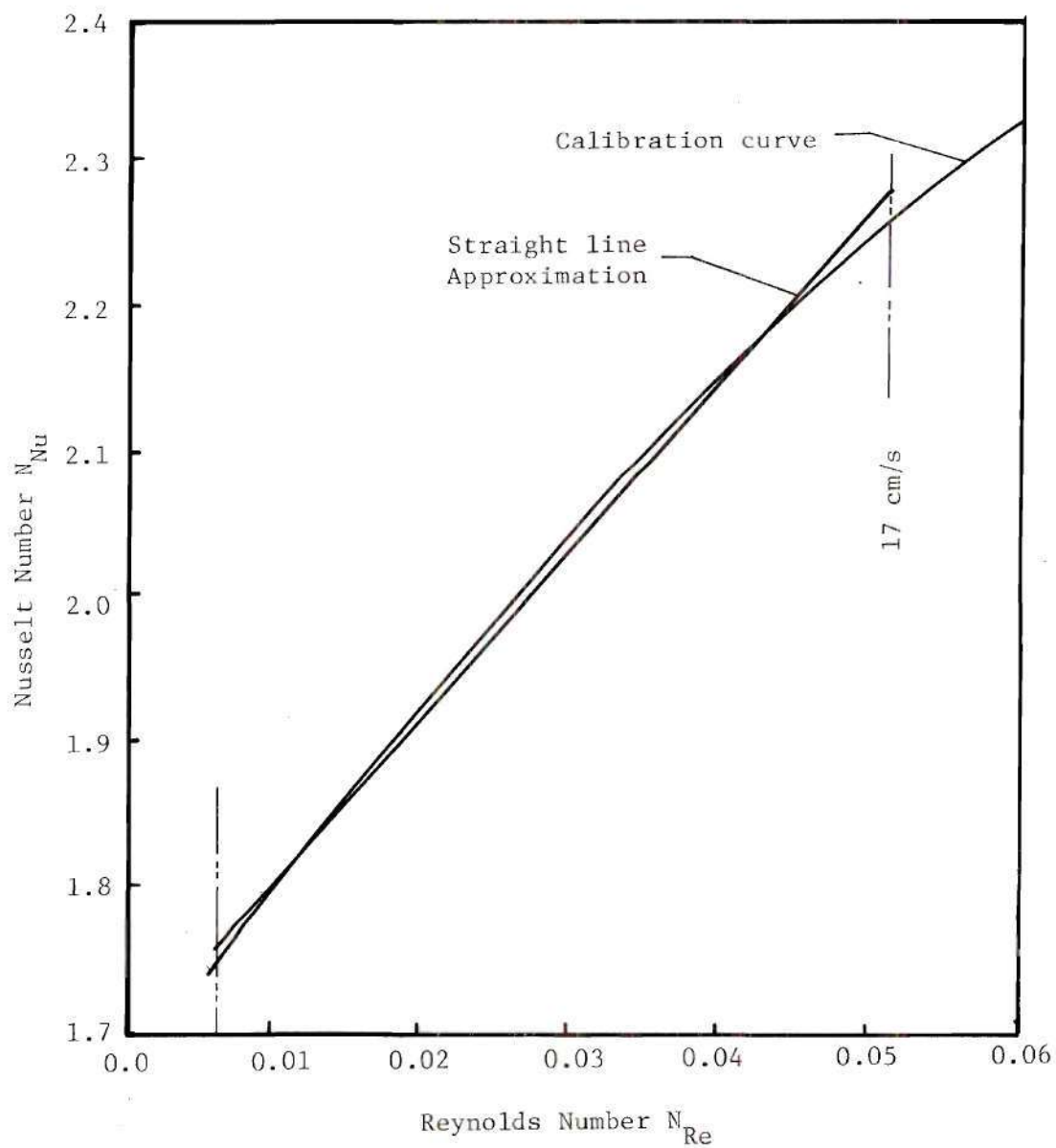


Figure E-1 . Dimensionless Velocity Calibration Curve and Its Straight Line Approximation.

$$N_{Nu} = A + B N_{Re}$$

with $A = 1.695$ and $B = 11.75$

$$\left. \begin{array}{l} \\ \\ \end{array} \right\} (E-1)$$

All other variables are linear or considered so, hence

$$R_w = R_o (1 + \alpha_1 \theta) \quad (E-2a)$$

$$(40 + R_w) = (40 + R_o) (1 + \alpha_2 \theta) \quad (E-2b)$$

$$k = k_o (1 + \alpha_3 \theta) \quad (E-2c)$$

$$\gamma = \gamma_o (1 + \alpha_4 \theta) \quad (E-2d)$$

where θ is the difference between the local air temperature and the reference temperature 24.7°C of the calibration curve. The values of α_1 through α_4 were determined and are given below

$$\left. \begin{array}{l} \alpha_1 = .0034 \text{ C}^{-1} \\ \alpha_2 = .00126 \text{ C}^{-1} \\ \alpha_3 = .0027 \text{ C}^{-1} \\ \alpha_4 = .0054 \text{ C}^{-1} \end{array} \right\} (E-3)$$

The energy balance equation for the wire is

$$\left(\frac{\bar{E} R_w}{40 + R_w} \right)^2 / R_w = h A \Delta T = k (A + B N_{Re}) \frac{A \Delta T}{d} \quad (E-4)$$

For measurements at different temperatures, substitution from equations (E-2) into equation (E-4) gives

$$\frac{\bar{E}^2 R_o}{(40 + R_o)^2} \left\{ 1 + (\alpha_1 - 2\alpha_2 - \alpha_3) \theta \right\} = k_o \left\{ A + B \frac{Ud}{\gamma_o} (1 - \alpha_4 \theta) \right\} \frac{A \Delta T}{d} \quad (E-5)$$

For measurements at the reference temperature, θ vanishes and equation (E-5) becomes

$$\frac{\bar{E}_o^2 R_o}{(40 + R_o)^2} = k_o \left(A + B \frac{Ud}{\gamma_o} \right) \frac{A \Delta T}{d} \quad (E-6)$$

For some velocity U , the wire reads \bar{E}_o at the reference temperature and \bar{E} for a change in temperature θ . The voltage \bar{E}_o would thus be the corrected value of \bar{E} to be used with the calibration curve, Figure (4-6). Manipulation of equations (E-5 and 6) gives the following relation

$$\begin{aligned} \frac{\bar{E}_o}{\bar{E}} &= 1 + \theta/2 \left\{ \alpha_1 - 2\alpha_2 - \alpha_3 + \frac{B Ud \alpha_4}{A \gamma_o + B Ud} \right\} \\ &= 1 - \mathcal{F} \theta \end{aligned} \quad (E-7)$$

The right hand side of equation (E-7) is the required correction. The values of \mathcal{F} are plotted versus the velocity U in Figure (E-2). As could be seen, the corrections in the range of velocities and temperatures used in the experiments were within 1.6 percent.

Knowing the approximate value of velocity and the temperature, the corrected velocity was obtained by trial and error.

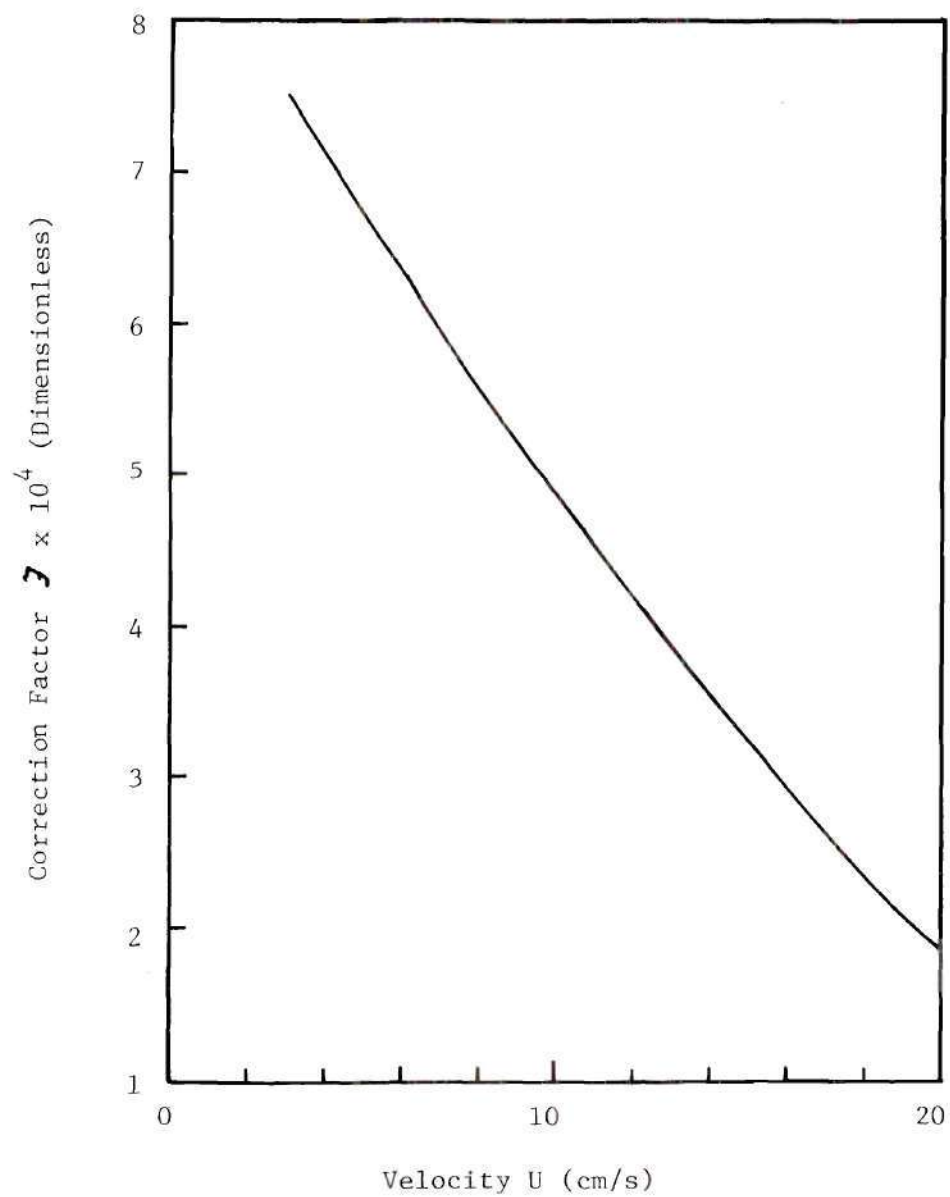


Figure E-2 . Correction for Basic Velocity Due to Temperature Variations.

APPENDIX F

ERROR IN EVALUATING POSITION ANGLES OF
POINTS OF NEUTRAL STABILITY

Temperature oscillations were measured at different position angles x^+ to determine the location of neutral stability points. As could be seen from Figure (5-3), the amplitudes $\tilde{\theta}_e$ of the recorded temperature oscillations were found to fluctuate about a mean value $\tilde{\theta}_{e,av}$ with a maximum deviation ϵ , i.e.

$$\tilde{\theta}_e = (1 \pm \epsilon) \tilde{\theta}_{e,av} \quad (F-1)$$

It was found that $\epsilon = 7.5$ percent. The error in determining the position angle for a point of neutral stability due to these perturbations is estimated in this appendix. A least square fitting to a second order curve is performed on the readings of the disturbance temperature at different position angles x^+ . The fitted curve equation is taken as

$$\tilde{\theta} = A_1 + A_2 x^+ + A_3 x^{+2} \quad (F-2)$$

According to the well-known least square algorithm, the constants A_1, A_2 , and A_3 are obtained from the following equations

$$A_1 n + A_2 \sum_{j=1}^n x_j + A_3 \sum_{j=1}^n x_j^2 = \sum_{j=1}^n \tilde{\theta}_{e,j}$$

$$\left. \begin{aligned} A_1 \sum_{j=1}^n x_j + A_2 \sum_{j=1}^n x_j^2 + A_3 \sum_{j=1}^n x_j^3 &= \sum_{j=1}^n \tilde{\theta}_{e,j} x_j \\ A_1 \sum_{j=1}^n x_j^2 + A_2 \sum_{j=1}^n x_j^3 + A_3 \sum_{j=1}^n x_j^4 &= \sum_{j=1}^n \tilde{\theta}_{e,j} x_j^2 \end{aligned} \right\} \quad (F-3)$$

where n is the number of experimental points.

The error in the left hand terms of equation (F-3) is negligible, being dependent only on the precisely determined position angles x^+ . The equation includes an error of $\pm \epsilon$ in the right hand side due to the linear expressions in $\tilde{\theta}_{e,j}$.

Solving for A_1 , A_2 and A_3 by Cramer's rule, the values of A_1 , for example is given by

$$A_1 = \frac{\begin{vmatrix} \sum_{j=1}^n \tilde{\theta}_{e,j} & \sum_{j=1}^n x_j & \sum_{j=1}^n x_j^2 \\ \sum_{j=1}^n \tilde{\theta}_{e,j} x_j & \sum_{j=1}^n x_j^2 & \sum_{j=1}^n x_j^3 \\ \sum_{j=1}^n \tilde{\theta}_{e,j} x_j^2 & \sum_{j=1}^n x_j^3 & \sum_{j=1}^n x_j^4 \end{vmatrix}}{\begin{vmatrix} n & \sum_{j=1}^n x_j & \sum_{j=1}^n x_j^2 \\ \sum_{j=1}^n x_j & \sum_{j=1}^n x_j^2 & \sum_{j=1}^n x_j^3 \\ \sum_{j=1}^n x_j^2 & \sum_{j=1}^n x_j^3 & \sum_{j=1}^n x_j^4 \end{vmatrix}} \quad (F-4)$$

In the first column of the numerator determinant, $\tilde{\theta}_{e,j} = (1 \pm \epsilon) \tilde{\theta}_{e,j,av}$, therefore

$$A_1 = (1 \pm \epsilon) \times \frac{\begin{vmatrix} \sum_{j=1}^n \tilde{\theta}_{e,j,av} & \dots & \dots \\ \sum_{j=1}^n \tilde{\theta}_{e,j,av} x_j & \dots & \dots \\ \sum_{j=1}^n \tilde{\theta}_{e,j,av} x_j^2 & \dots & \dots \end{vmatrix}}{\begin{vmatrix} \dots & \dots & \dots \\ \dots & \dots & \dots \\ \dots & \dots & \dots \end{vmatrix}} = (1 \pm \epsilon) A_{1,av} \quad (F-5a)$$

Similarly

$$A_2 = (1 \pm \epsilon) A_{2,av} \quad (F-5b)$$

$$\text{and } A_3 = (1 \pm \epsilon) A_{3,av} \quad (F-5c)$$

The value of the angle x_{\min}^+ at which the minimum value of $\tilde{\theta}_e$ occurs is calculated from

$$x_{\min}^+ = \frac{-A_2}{2A_3} = - \frac{A_{2,av}}{2A_{3,av}} \frac{(1 \pm \epsilon)}{(1 \pm \epsilon)} \quad (F-6)^*$$

$$\text{or } x_{\min}^+ = \frac{-A_{2,av}}{2A_{3,av}} (1 \pm 2\epsilon) \quad (F-7)$$

Assuming a normal distribution curve for x_{\min}^+ , an error of utmost 15% is expected with a probability of 100 percent, and an error of utmost

*Equation (F-6) is obtained by differentiation equation (F-2) with respect to x^+ and equating $\left. \frac{d\tilde{\theta}}{dx^+} \right|_{x_{\min}^+}$ by zero.

$\pm 8\%$ is expected with probability 78.8 percent.

However, as the perturbation in the experimental values $\tilde{\theta}_e$ may be attributed to a naturally existing disturbance (of very large wavelength) which amplifies with streamwise travel, the peaks and valleys of these perturbations are expected to correspond to each other, hence $\frac{1 \pm \varepsilon}{1 \pm \varepsilon}$ acquires an approximate value of unity. The error in x_{\min}^+ due to these perturbations is, therefore, expected to vanish.

APPENDIX G

CORRECTION OF THE DISTURBANCE TEMPERATURE AMPLITUDES FOR
CHANGES OF BASIC VELOCITY U WITH STREAMWISE TRAVEL

The hot wire probe is used to detect the temperature oscillations by operating it as "anemometer" with zero overheat resistance. In this case the energy balance is given by equation (5-9). The voltage read is that of the bridge; it should be further multiplied by the bridge arm ratio $R_w/(R_w + 40)$ to give the voltage across the probe, hence:

$$\tilde{\theta} = \frac{2\bar{E} \tilde{e} R_w}{(R_w + 40)^2 \pi dL \bar{h}} \quad (G-1)$$

The term $\frac{2\bar{E} R_w}{(R_w + 40)^2}$ is constant since measurements were practically taken at radial positions corresponding to the same value of η ($\approx 1.24^*$ in the present case), hence at the same basic temperature.

Equation (G-1) would then give

$$\tilde{\theta} \propto \frac{\tilde{e}}{\bar{h}} \quad (G-2)$$

A correction should, therefore, be carried out to account for the variation of \bar{h} due to variation of U, the tangential basic velocity component. This is carried out in this appendix.

* This value corresponds to locations of maximum temperature disturbances in the radial direction, as obtained from experiments.

For the specific radial location ($\eta = 1.24$) used, Ostrach's [31] numerical calculations give the dimensionless tangential velocity $F' = 0.265$. Using Hermann's [16] equation, namely

$$U = \frac{F' \nu N^{1/2}}{r Gr, r} f(x^+) g(x^+) \quad (G-3)$$

gives

$$U = .06 fg$$

and

$$Re = .018 fg \quad (G-4)$$

Using the velocity calibration curve Figure (4-6), together with equations (G-4) and (G-2), a variable correction factor should be multiplied by the resulting oscillatory voltage amplitude at different angles. This correction factor was calculated as outlined above and is given in Figure (G-1).

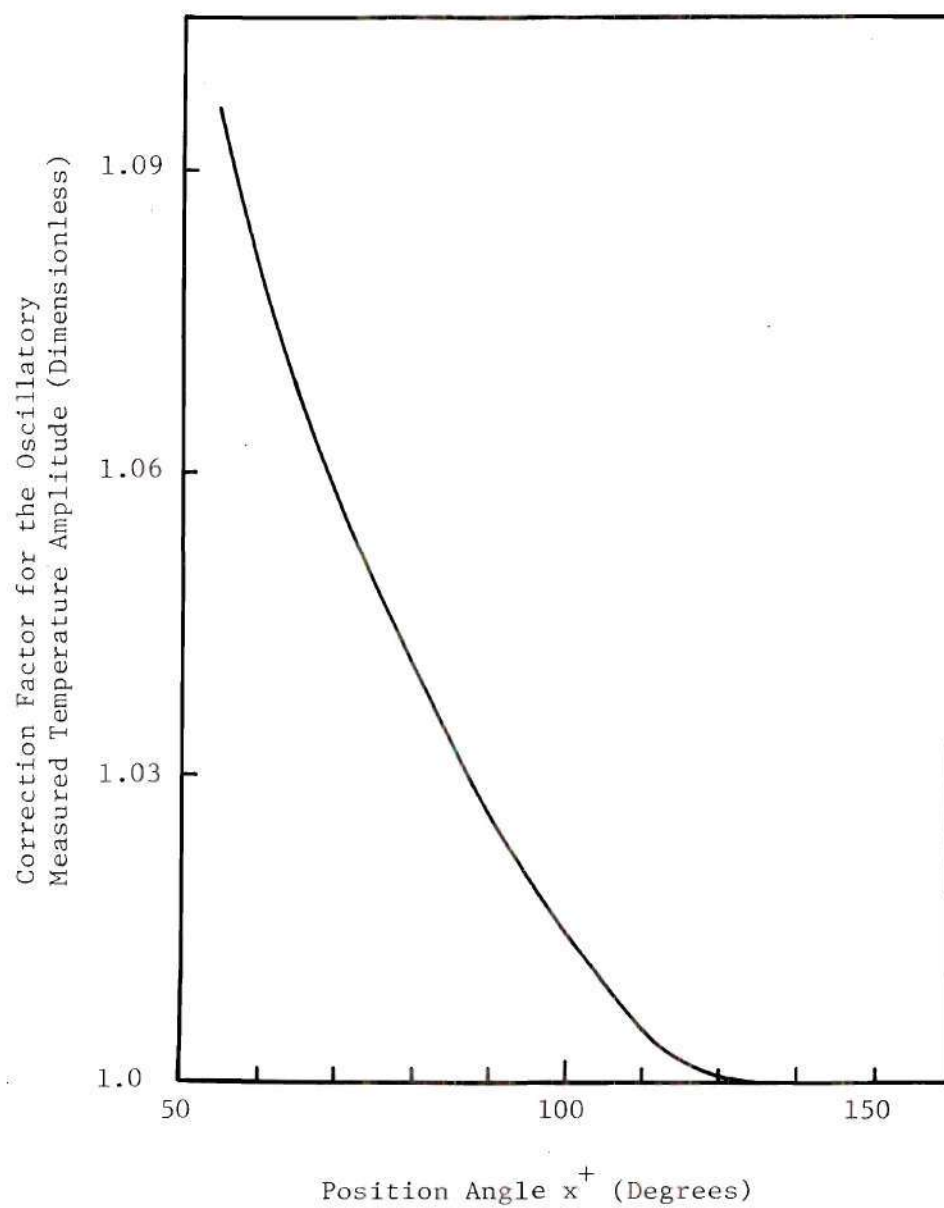


Figure G-1 . Correction for the Measured Amplitude of Oscillatory Temperature due to Variations in h .

APPENDIX H

HEATING WIRE RESPONSE TO SINUSOIDAL

ELECTRIC POWER INPUT

A heating wire is used to induce temperature oscillations of controlled frequency and amplitude. By adequately choosing the wire material and diameter, and the input voltage amplitude and frequency, the heating wire acquires sinusoidal temperature difference from the surrounding air. Calculations are carried out to choose the wire diameter such that small or no damping of sinusoidal signal is encountered.

An alumel wire of 12.7 μm (0.0005 in.) diameter was used in the experiment. It was placed at points of velocity 5 cm/s and temperature 310°K approximately. The wire Reynolds number is calculated to be 0.0374. According to Collis and Williams [41], the heat transfer coefficient is given by

$$h = \frac{k}{d} \left(\frac{T_m}{T_\infty} \right)^{0.17} [0.24 + 0.56 N_{\text{Re}}^{.45}] = 794 \text{ W/m}^2 \text{ } ^\circ\text{K}$$

For alumel wire, the Biot number would be

$$N_{\text{Bi}} = \frac{hd}{k} = 0.33 \times 10^{-3}$$

This small value of N_{Bi} indicates that infinite thermal conductivity in the radial direction could be assumed for this wire.

Energy Balance Equation

With a volumetric rate of heat generation \hat{q} , the wire (of length L and diameter d) would acquire a temperature T_w different from the environmental temperature T_a , the energy balance of the wire gives

$$\frac{d\theta}{dt} = -M\theta + \hat{q}/(\rho C_p) \quad (H-1)$$

where

$$M = 4h/(\rho C_p d), \quad \text{and} \quad \theta = T_w - T_a \quad (H-2)$$

The heat generation \hat{q} is assumed to have a steady part \hat{q}_1 and a sinusoidal part $\hat{q}_2 \sin \omega t$, i.e.

$$\hat{q} = \hat{q}_1 + \hat{q}_2 \sin(\omega t) \quad (H-3)$$

Substituting into equation (H-1) gives

$$\frac{d\theta}{dt} = -M\theta + \frac{1}{\rho C_p} \{ \hat{q}_1 + \hat{q}_2 \sin(\omega t) \} \quad (H-4)$$

Using Laplace transform to solve the above equation¹⁵ gives

$$\theta = \frac{\hat{q}_1}{\rho C_p M} (1 - e^{-Mt}) + \frac{\hat{q}_2}{\rho C_p} \frac{M^2}{M^2 + \omega^2} \left\{ \frac{1}{M} \sin \omega t - \frac{\omega}{M^2} e^{-Mt} (1 - \cos \omega t) \right\} \quad (H-5)$$

This gives the following established state solution

$$\theta = \frac{\hat{q}_1}{\rho C_p M} + \frac{\hat{q}_2}{\rho C_p M} \frac{M^2}{M^2 + \omega^2} \sin \omega t$$

or

$$T_w - T_a = \frac{\hat{q}_1 d}{4h} + \frac{\hat{q}_2 d}{4h} \frac{M^2}{M^2 + \omega^2} \sin(\omega t) \quad (\text{H-6})$$

For a sinusoidal voltage input of $E = E_A \sin \omega_1 t$, the volumetric rate of heat generation is given by

$$\hat{q} = \frac{4E^2}{R\pi d^2 L} = \frac{4E_A^2}{R\pi d^2 L} \sin^2 \omega_1 t$$

or

$$\hat{q} = \frac{2E_A^2}{R\pi d^2 L} \{1 - \cos(2\omega_1 t)\}$$

hence, except for a phase shift

$$\hat{q} = \frac{2E_A^2}{R\pi d^2 L} \{1 + \sin(\omega t)\} \quad (\text{H-7})$$

It should be noted that $\omega = 2\omega_1$, i.e. the frequency of the sinusoidal heat generation is double that of the input voltage. Substituting equation (H-7) into equation (H-6) gives

$$T_w - T_a = \frac{E_A^2}{2Rh\pi d L} \left\{ 1 + \frac{M^2}{M^2 + \omega^2} \sin(\omega t) \right\} \quad (\text{H-8})$$

To have an effective sinusoidal temperature difference without raising the wire temperature appreciably, M should be much larger than ω . In our case

$$M = \frac{4h}{\rho C_p d} \approx 5 \times 10^4$$

This should be compared to the maximum expected value of ω of about 20.

Therefore for the wire used

$$T_w - T_a \approx \frac{E_A^2}{2R \pi d h} (1 + \sin(\omega t)) \quad (H-9)$$

This means the steady state temperature rise of the wire is equal to the amplitude of its sinusoidal one. As could be seen from equation (H-8), a better situation is not attainable. It should also be noted that the power dissipated is small and would not affect the basic flow. On the other hand, the sinusoidal temperature rise would activate the required controlled disturbances.

APPENDIX I

COMPUTER PROGRAM

The computer program used to determine the stability curves in the $x^+ - \alpha_r$ or β_r planes, with α_r and β_r taken as eigenvalues is included in this appendix. Similar programs were used for different stability planes and/or different eigenvalues.

```

PROGRAM NCFCIN(INPUT,OUTPUT,TAPE5=INPUT,TAPE6=OUTPUT)
DIMENSION Y(5),YP(7,121),X(2),R(2),AJ(2,2),BL(2,4),IP(3)
EXTERNAL FUN
COMPLEX B,G,A,C,AP,CP
COMMON/WZ1/YP,MB,RE,PR,ETE,HS,MM,CTA,B,G
COMMON/WZ2/HB,DL,A,C
READ(5,1111)GR,PR
1111 FORMAT(F10.2,1X,F7.3)
READ(5,1112)CTR
1112 FORMAT(F9.1)
ETE=6.0
HS=-0.1
HB=.05
MM1=-ETE/HS+.1
MM=MM1+1
MB1=ETE/HB+0.1
MB=MB1+1
Y(1)=0.0
Y(2)=0.0
Y(3)=0.6741
Y(4)=1.0
Y(5)=-0.508
XZ=0.0
DO 111 K=1,5
111 YP(K,1)=Y(K)
YP(6,1)=-1.0
YP(7,1)=0.0
DO 10 I=2,MB
CALL RK(Y,XZ,5,HB)
DO 11 K=1,5
11 YP(K,I)=Y(K)
YP(6,I)=-3.0*Y(1)*Y(3)+2.0*Y(2)*Y(2)-Y(4)
YP(7,I)=-3.0*PR*Y(1)*Y(5)
10 CONTINUE
AP=(.06,.0)
CP=(.02,.0)
DO 3 IK=1,7
CTA=CTR*3.141592654/180.0
FY=CTA-1.570796327
FF=3.428378614*(1.0+FY*(0.581+FY*(-0.05026+FY
1 *(-0.01412+FY*(-0.00165-0.00060*FY))))))
GG=(SIN(CTA)/FF)**.3333333333333333
RE=FF*(GR**.25)
DL=FF/(GG*RE)
WRITE(6,1113)GR,PR,CTR
1113 FORMAT(8H1CASE OF/4H GR=,F10.1/4H PR=,F7.3/
1 5H CTA=,F5.1/)
A=AP
C=CP
X(1)=REAL(A)
X(2)=REAL(C)
N=2
K=2
P=0
NR=2
TOL=.0001
IP(1)=8

```



```

J=1
CALL FUN(X,N,K,R,P)
SR1=R(1)
SI1=R(2)
A=AP+.000001
X(1)=REAL(A)
CALL FUN(X,N,K,R,P)
SR2=R(1)
SI2=R(2)
A=AP
C=CP+.000001
X(1)=REAL(A)
X(2)=REAL(C)
CALL FUN(X,N,K,R,P)
SR3=R(1)
SI3=R(2)
AJ(1,1)=(SR2-SR1)*1000000.
AJ(1,2)=(SR3-SR1)*1000000.
AJ(2,1)=(SI2-SI1)*1000000.
AJ(2,2)=(SI3-SI1)*1000000.
X(1)=REAL(AP)
X(2)=REAL(CP)
CALL QNWT(X,N,NR,FUN,F,TOL,IP,J,R,RMS,AJ,BL)
IF(RMS.LT.10L)GOTO 9918
GOTO 9917
9918 WRITE(6,9915)
9916 FORMAT(21H CONVERGENCE ACHIEVED)
DIR=CIK-5.
AP=A
CP=C
3 CONTINUE
9917 CONTINUE
END

```

```

SUBROUTINE FUN(X,N,K,R,P)
COMPLEX XR,A,IC,C,B,ZA(6),ZB(6),ZG(6),G,SS,S
1  ,AJ,AJA,AJB,AJG,CC(3)
COMMON/WZ1/YP,MB,RE,PR,ETE,HS,MM,CTA,B,G
COMMON/WZ2/HB,DL,A,C
DIMENSION YP(7,121),X(N),R(K)
A=X(1)
C=X(L)
C
C COMPLEX ROOTS OF AUXILIARY EQUATIONS
C
IC=(0.0,1.0)
XR=CSQRT(9.0*YP(1,MB)*YP(1,MB)+4.0*(A*A-IC*RE*C))
B=0.5*(-3.0*YP(1,MB)-XR)
IF(REAL(B).GE. 0.0)B=0.5*(-3.0*YP(1,MB)+XR)
XR=CSQRT(9.0*YP(1,MB)*YP(1,MB)*PR*PR+4.0*(A*A-IC*PR*RE*C))
G=0.5*(-3.0*YP(1,MB)*PR-XR)
IF(REAL(G).GE. 0.0)G=0.5*(-3.0*YP(1,MB)*PR+XR)
C
C DISTURBED FLOW
C
MM1=MM-1
ZA(1)=CEXP(-ETE*A)
ZA(2)=-A*ZA(1)
ZA(3)=-A*ZA(2)
ZA(4)=-A*ZA(3)
ZA(5)=(0.0,0.0)
ZA(6)=(0.0,0.0)
XZ=ETE
DO 1003 I=1,MM1
CALL CRK(ZA,XZ,6,HS)
1003 CONTINUE
C
ZB(1)=CEXP(ETE*B)
ZB(2)=B*ZB(1)
ZB(3)=B*ZB(2)
ZB(4)=B*ZB(3)
ZB(5)=(0.0,0.0)
ZB(6)=(0.0,0.0)
XZ=ETE
DO 1004 I=1,MM1
CALL CRK(ZB,XZ,6,HS)
1004 CONTINUE
C
ZG(1)=CEXP(ETE*G)
ZG(2)=G*ZG(1)
ZG(3)=G*ZG(2)
ZG(4)=G*ZG(3)
SS=G*G*G+3.0*YP(1,MB)*G*G*G+(IC*RE*C-2.0*A*A)*G*G
1 -3.0*YP(1,MB)*A*A*G+A*A*(A*A-IC*RE*C)
SS=SS/(G+IC*A*COS(CTA)/SIN(CTA))
ZG(5)=-SS*CEXP(ETE*G)
ZG(6)=G*ZG(5)
XZ=ETE
DO 1005 I=1,MM1
CALL CRK(ZG,XZ,6,HS)
1005 CONTINUE
AJ=CEXP(-ETE*A)*(ZB(1)*ZG(2)-ZG(1)*ZB(2))

```

```

1  -C*EXP(ETE*B)*(ZA(1)*ZG(2)-ZG(1)*ZA(2))
2  +C*EXP(ETE*G)*(ZA(1)*ZB(2)-ZB(1)*ZA(2))
  AJA=ZB(1)*ZG(2)-ZG(1)*ZB(2)
  AJB=-ZA(1)*ZG(2)+ZG(1)*ZA(2)
  AJG=ZA(1)*ZB(2)-ZB(1)*ZA(2)
  CC(1)=AJA/AJ
  CC(2)=AJB/AJ
  CC(3)=AJG/AJ
  S=CC(1)*ZA(5)+CC(2)*ZB(5)+CC(3)*ZG(5)
  R(1)=REAL(S)
  R(2)=AIMAG(S)
  WRITE(6,2111)S,C,A,Re
2111 FORMAT(4H S=(,E10.4,1H,,E10.4,7H)  C=(,E13.7,1H,,E10.4,
1  7H)  A=(,E13.7,1H,,E10.4,7H)  Re=,E10.4)
  RETURN
  END

```

```

SUBROUTINE RK(F,X,M,H)
  DIMENSION F(5),P(5),Q(5),DF(5)
  DO 2001 I=1,M
2001  P(I)=F(I)
      XP=X
      CALL QQ(F,X,DF)
      DO 2002 J=1,M
        Q(J)=H*DF(J)
2002  F(J)=P(J)+0.5*DF(J)*H
        X=XP+0.5*H
        CALL QQ(F,X,DF)
        DO 2003 J=1,M
          Q(J)=Q(J)+H*DF(J)*2.0
2003  F(J)=P(J)+H*DF(J)*0.5
          CALL QQ(F,X,DF)
          DO 2004 J=1,M
            Q(J)=Q(J)+H*DF(J)*2.0
2004  F(J)=P(J)+H*DF(J)
            X=XP+H
            CALL QQ(F,X,DF)
            DO 2005 J=1,M
              Q(J)=Q(J)+DF(J)*H
              Q(J)=Q(J)/6.0
2005  F(J)=P(J)+Q(J)
      RETURN
  END

```

```

SUBROUTINE CRK(F,X,M,H)
COMPLEX F(6),P(6),Q(6),DF(6)
DO 2001 I=1,M
2001 P(I)=F(I)
XP=X
CALL EQ(P,X,DF)
DO 2002 J=1,M
Q(J)=H*DF(J)
2002 F(J)=P(J)+0.5*DF(J)*H
X=XP+0.5*H
CALL EQ(F,X,DF)
DO 2003 J=1,M
Q(J)=Q(J)+H*DF(J)*2.0
2003 F(J)=P(J)+H*DF(J)*0.5
CALL EQ(F,X,DF)
DO 2004 J=1,M
Q(J)=Q(J)+H*DF(J)*2.0
2004 F(J)=P(J)+H*DF(J)
X=XP+H
CALL EQ(F,X,DF)
DO 2005 J=1,M
Q(J)=Q(J)+DF(J)*H
Q(J)=Q(J)/0.3
2005 F(J)=P(J)+Q(J)
RETURN
END

```



```

SUBROUTINE EQ(F,X,DF)
COMMON/WZ1/YP,MB,RE,PR,ETE,HS,MH,CTA,B,G
COMMON/WZ2/HB,DL,A,C
DIMENSION YP(7,121)
COMPLEX F(6),DF(6),C,A,B,G,IC
DF(1)=F(2)
DF(2)=F(3)
DF(3)=F(4)
LN=X/HB+1.1
IC=(0.0,1.0)
DF(4)=2.0*A*A*F(3)-A*A*A*A*F(1)-(F(6)+IC*A*F(5)*COS(CTA)/SIN(CTA))
1  +1.0*RE*((YP(2,LN)*A-C)*(F(3)-A*A*F(1))-A*
2  (YP(6,LN)*F(1)+YP(3,LN)*F(1)*DL-YP(2,LN)*F(2)*DL))
3  +(YP(3,LN)-YP(6,LN)*X)*F(2)-(3.0*YP(1,LN)-YP(2,LN)*X)*
4  (F(4)-A*A*F(2))
DF(5)=F(6)
DF(6)=A*A*F(5)+IC*PR*RE*((YP(2,LN)*A-C)*F(5)-YP(5,LN)*F(1)*A)
1  +PR*(-YP(5,LN)*X*F(2)-(3.0*YP(1,LN)-YP(2,LN)*X)*F(6))
RETURN
END

```

```
SUBROUTINE QQ(F,X,DF)
  DIMENSION F(5),DF(5)
  PR=0.733
  DF(1)=F(2)
  DF(2)=F(3)
  DF(3)=-3.0*F(1)*F(3)+2.0*F(2)*F(2)-F(4)
  DF(4)=F(5)
  DF(5)=-3.0*PR*F(1)*F(5)
  RETURN
END
```

BIBLIOGRAPHY

1. Baker, D. J., "A Technique for Precise Measurement of Small Fluid Velocities," J. Fluid Mech., 26, 573-575 (1966).
2. Birch, W. D., "On the Stability of Free Convection Boundary Layers on a Vertical Flat Plate," M.S. Thesis, Air University, Wright-Patterson Air Force Base, 1959.
3. Bird, R. B., Stewart, W. E. and Lightfoot, E. N., "Transport Phenomena," John Wiley and Sons, Inc., New York, 1960.
4. Colak-Antic, P., Jahrb. Wiss Ges Luft-Raumfahrt, 172, 1964.
5. Colak-Antic, P., Sitzungsber, Heidelberg Akad. Wiss., Math.-Naturwiss. Kl. Jahrgang 1962/64, 315, Heidelberg:Springer-Verlag OHG, 1964.
6. Dring, R. P. and Gebhart, B., "A Theoretical Investigation of Disturbance Amplification in External Laminar Natural Convection," J. Fluid Mech., 34, 551-564, 1968.
7. Dring, R. P. and Gebhart, B., "An Experimental Investigation of Disturbance Amplification in External Laminar Natural Convection Flow," J. Fluid Mech., 36, 447-463, 1969.
8. Dring, R. P. and Gebhart, B., "Hot Wire Anemometer Calibration for Measurement at Very Low Velocity," J. Heat Transfer, Trans. ASME, Series C, Vol. 91, N. 2, 241-244, 1969.
9. Eckert, E. R. G., Hartnett, J. P. and Irvine, T. F., "Flow Visualization Studies of Transition to Turbulence in Free Convection Flow," ASME Paper, n. 60-Wa-260, 1960.
10. Eichhorn, R., "Measurement of Low Speed Gas Flows by Particle Trajectories: A New Determination of Free Convection Velocity Profiles," Int. J. Heat Mass Transfer, 5, 9 15-928, 1962.
11. Kreith, F., "Principles of Heat Transfer," International Text Book Company, Scranton, Pennsylvania, 1965.
12. Gartrell, H. E., "On the Oscillations of Free Convection Layers," M.S. Thesis, Air University, Wright-Patterson Air Force Base, 1959.
13. Gill, A. D. and Davy, A., "Instability of a Buoyancy Driven System," J. Fluid Mech., 35, 775-798, 1969.

14. Haaland, S. E., "Contributions to Linear Stability Theory of Nearly Parallel Flows," Ph.D. Thesis, Fluid Mechanics Program, University of Minnesota, Minneapolis, Minn., 1972.
15. Spiegel, M. R., "Laplace Transforms," McGraw-Hill Book Company, New York, 1965.
16. Hermann, R., "Heat Transfer by Free Convection from Horizontal Cylinder in Diatomic Gases," NACA TM 1366, 1954.
17. Hieber, C. A. and Gebhart, B., "Stability of Vertical Natural Convection Boundary Layers: Some Numerical Results," J. Fluid Mech., 48, 625-645, 1971.
18. Hieber, C. A. and Gebhart, B., "Stability of Vertical Natural Convection Boundary Layers at Large Prandtl Numbers," J. Fluid Mech., 49, 557-591, 1971.
19. Holman, J. P., Gartrell, H. E. and Soehngen, E. E., "A Study of Free Convection Boundary Layer Oscillations and Their Effects on Heat Transfer," WADD Technical Report 59-3, Nov. 1959.
20. Iyer, P. A. and Kelley, R. E., "The Stability of the Laminar Free Convection Flow Induced by a Heated Inclined Plate, Int. J. Heat Mass Transfer 17, 517-525, 1974.
21. Jaluria, Y. and Gebhart, B., "An Experimental Study of Nonlinear Disturbance Behaviour in Natural Convection," J. Fluid Mech., 61, 337-365, 1973.
22. Kaplan, R. E., "The Stability of Laminar Incompressible Boundary Layers in the Presence of Compliant Boundaries," ASRL-TR 116-1, 1964.
23. Khawita, R. A. and Meroney, R. N., "The Vortex Mode of Instability in Natural Convection Flow Along Inclined Plates," Int. J. Heat Mass Transfer, 17, 541-548, 1974.
24. Knowles, C. P. and Gebhart, B., "The Stability of the Laminar Natural Convection Boundary Layer," J. Fluid Mech., 34, 657-686, 1968.
25. Knowles, C. P. and Gebhart, B., "An Experimental Investigation of the Stability of Laminar Natural Convection Boundary Layers," Progress in Heat and Mass Transfer, Vol. 2, 99, New York, Pergamon, 1969.
26. Kurtz, E. F., Jr. and Crandall, S. H., "Computer Aided Analysis of Hydrodynamic Stability," J. Math. Phys. 41, 264-279, 1962.
27. Lloyed, J. R. and Sparrow, E. M., "On the Instability of Natural Convection Flow on Inclined Plates," J. Fluid Mech., 42- 465-470, 1970.

28. Lock, G. S. H., Gort, C. and Pond, G. R., "A Study of Instability in Free Convection from an Inclined Plate," Appl. Sci. Res., 171-182, 1967.
29. Mach, L. M., "Computation of the Stability of the Laminar Compressible Boundary Layer," Methods in Computation Physics, Vol. 4, Academic Press, 1965.
30. Nachtsheim, P. R., "Stability of Free Convection Boundary-Layer Flows," NASA Tech Note D-2089, 1963.
31. Ostrach, S., "An Analysis of Laminar Free Convection Flow and Heat Transfer About a Flat Plate Parallel to the Direction of the Generating Body Force," NACA Report 1111, 1953.
32. Plapp, J. E., "I-Laminar Boundary Layer Stability in Free Convection. II-Laminar Free Convection with Variable Fluid Properties," Ph.D. Thesis C.I.T., 1957.
33. Polymeropoulos, C. E. and Gebhart, B., "Stability of Free Convection Flow Over a Vertical Uniform Flux Plate," AIAA Journal, 4, 11, 2066-2068, Nov. 1966.
34. Polymeropoulos, C. E. and Gebhart, B., "Incipient Instability in Free Convection Laminar Boundary Layers," J. Fluid Mech., 30, 225-239, 1967.
35. Schmidt, E., Beckmann, W., Das Temperatur-und Geschwindigkeitfeld von einer Wärme Abgebenden senkrechter Platte bei Natürlicher Konvektion Tech. Mech. und Thermodynamic 1, 341-349, 391-406 (1930).
36. Schubauer, G. B. and Skramstad, H. K., "Laminar Boundary Layer Oscillation and Stability of Laminar Flow," Journal of the Aeronautical Science, 14, 69-78, 1947.
37. Sparrow, E. M. and Husar, R. B., "Longitudinal Vortices in Natural Convection Flow on Inclined Plates," J Fluid Mech., 37, 251-255, 1969.
38. Squire, H. B., Proc. Roy. Soc. A, 142, 621, 1933.
39. Szewczyk, A. A., "Stability and Transition of the Free Convection Layer Along a Vertical Flat Plate," Int. J. Heat Mass Transfer, 5, 903-914, 1962.
40. Tritton, D. J., "The Use of Fibre Anemometer in Turbulent Flow," J. Fluid Mech., 16, 269-281, 1963.
41. Collis, D. C., and Williams, M. J., "Two-Dimensional Convection from Heat Wires at Low Reynolds Numbers," J. Fluid Mech. 6, 357-384, 1959.

42. Joalbauer, K., Forsch. Ing. wes., Bd. 4, 1933, p. 157.
43. Chiang, T. and Kaye, J. "On Laminar Free Convection from a Horizontal Cylinder," Proceedings Fourth National Congress of Applied Mechanics, 1213-1219, 1962.
44. Saville, D. A., and Churchill, S. W., "Laminar Free Convection in Boundary Layers Near Horizontal Cylinders and Vertical Axisymmetric Bodies, J. Fluid Mech., 29, 391-399, 1967.
45. Lin, F. N., and Chao, B. T., "Laminar Free Convection over Two Dimensional and Axisymmetric Bodies of Arbitrary Contour, J. Heat Transfer, 96, 435-441, 1974.
46. Gebhart, B., and Mahajan, R., "Characteristic Disturbance Frequency in Vertical Natural Convection Flow," Int. J. Heat Mass Transfer, 18, 1143-1148, 1975.

VITA

Kadry A. F. Fathalah was born in Cairo, Egypt, on December 6, 1944. He entered Cairo University in 1961 for his undergraduate education and received his BSME in 1966.

He worked as a demonstrator at Cairo University, where he continued his graduate education and obtained his MSME in 1970.

He has continued his work in pursuit of the Ph.D. degree in the School of Mechanical Engineering, Georgia Institute of Technology, since September 1973.

Mr. Fathalah was married in August, 1973, to the former Boshra A.M. Hussien, an electrical engineer, also a graduate of Cairo University and a native of Egypt.